KU LEUVEN

ARENBERG DOCTORAL SCHOOL
Faculty of Science

The effect of solar illumination on ion outflow from the polar ionosphere.

Lukas Maes

Supervisors:
Prof. dr. Stefaan Poedts
Dr. ir. Johan De Keyser
Dr. Romain Maggiolo

Dissertation presented in partial fulfillment of the requirements for the degree of Doctor of Science (PhD): Mathematics

May 2017

The effect of solar illumination on ion outflow from the polar ionosphere.

Lukas MAES

Examination committee:
Prof. dr. Hans Van Winckel, chair
Prof. dr. Stefaan Poedts, supervisor
Dr. ir. Johan De Keyser, supervisor
Dr. Romain Maggiolo, supervisor
Prof. dr. ir. Giovanni Lapenta
Prof. dr. Rony Keppens
Dr. Stein Haaland
(University of Bergen, Max-Planck Institute for Solar Systems Research)
Dr. Benoit Hubert
(University of Liege)

Dissertation presented in partial fulfillment of the requirements for the degree of Doctor of Science (PhD): Mathematics

May 2017

aeronomie·be

Royal Belgian Institute for Space Aeronomie

Ringlaan 3, 1180 Brussels, Belgium.

Ackowledgements

The work in this thesis was made possible by the support of the Interuniversity Attraction Pole Planet TOPERS initiated by the Belgian Science Policy Office. This project supports and brings together experts from across many fields and many institutes and universities to tackle the interdisciplinary problem of habitability of planets.
http://iuap-planet-topers.oma.be/

Further I would like to thank many people.

I owe a great deal of gratitude to Romain Maggiolo for guiding me into the world of space physics. For helping me understand the many aspects of this fascinating field and teaching me the subtleties of data analysis. Thank you for always being patient during our discussions, even in those where it must have been completely obvious from the beginning how wrong I was. Without your help, this thesis would not have been.

The same can be said about Johan De Keyser, who was always available for helping with any study and paper. Both Johan and Romain acted as the perfect co-supervisors by always being accessible and open to discuss my work.

I thank Stefaan Poedts for supervising my thesis and always helping when necessary.

I would also like to express my gratitude to the members of the jury, Hans Van Winckel, Giovanni Lapenta, Rony Keppens, Stein Haaland, and Benoit Hubert, for their critical assessment and helping with the improvement of the manuscript.

Stein Haaland I would like to thank additionally for helping me already during my PhD and introducing me to many interesting projects.

All my colleagues at the Royal Belgian Institute for Space Aeronomy, thank you for making the working place a place to enjoy. Thanks for the many

nice conversations, the lunchtime football games, the drinks after work, ... Especially, Hervé, Marius, Sylvain, and Cédric. It was a pleasure sharing the office with you. Thank you for the uncountable coffees together, because without coffee, no science! Thank you for all the help and advice. I hope I didn't annoy you with too many difficult questions, especially late in the day.

Of course my friends, Wim and Jeroen, and all the friends I go running, or climbing, or MTB'ing with, my Awesomesauce friends to play music with, ... thank you for making life so interesting.

A very big thank you to my parents and my family for supporting me and my studies in science and always nurturing my amazement. And to little Charlot for springing into existence.

And finally of course: thank you, Sharo. For being there for me, for understanding me, for making these last years so special, for giving me a reason to not stay too late at work. And for sharing this exciting future with me.

Abstract

The goal of this thesis is to analyze how the fluxes of ions that flow out of the ionosphere in Earth's polar regions are affected by solar illumination. An atmosphere constantly leaks particles into space under the influence of a constant input of energy from the Sun. This energy comes in two forms: solar illumination and the solar wind. Solar illumination heats and ionizes the atmosphere. The solar wind can impact its kinetic energy on the atmosphere. At a planet with an internal magnetic field, like Earth, the interaction with the solar wind leads to the formation of a magnetosphere. The magnetosphere shields the atmosphere for a large part from the solar wind, however, it also indirectly transmits energy from the solar wind to the atmosphere by creating a magnetic connection. These outflows erode the atmosphere. Thus if we want to know the evolution of atmospheres, a good understanding of these outflow processes and the mechanisms driving them is crucial. The ion outflows can also affect the magnetospheric dynamics and are thus important for space weather.

The polar ionosphere is a special region for ion outflows, since the magnetic field there is directly connected to the solar wind. However, the most important source of energy there is solar illumination (apart from in the small region of the cusp). The main outflow mechanism from the polar ionosphere, the polar wind, is notoriously difficult to measure due to spacecraft charging. We therefore first focus on another type of outflow from the polar ionosphere, and later use an alternative technique.

First we study the ionospheric outflow above small-scale polar cap arcs. These are arcs similar to the discrete auroral arcs, but occur across the magnetic polar cap and when the interplanetary magnetic field is directed northward. They are also more stable an typically much less intense. The ions are accelerated upwards by the quasi-static electric field parallel to the magnetic field that is associated with these arcs. The results show that the outflow basically has two regimes: outflow above a sunlit ionosphere and outflow above a dark ionosphere. For H^+ ions from the sunlit side of the ionosphere flux density is on average

almost double that from the dark side. For O^+ ions it is more than 7 times higher. The transition is found the be at a solar zenith angle larger than 90°. The potential drop of the quasi-static electric field is also found to be affected by solar illumination: no small potential drops occur above a dark ionosphere implying a feedback effect of the ionosphere on the magnetospheric system. The H^+ flux densities are similar in magnitude to polar wind fluxes found in literature. This fact, together with the solar illumination control of the outflow and the relatively small energy input, suggests that the fluxes above polar cap arcs are not different from polar wind fluxes, merely accelerated.

In a second part, we start from that final suggestion of the first part and extrapolate the flux densities above polar cap arcs and their solar illumination dependence to the whole magnetic polar cap. With a very simple and conceptual model we look how the total outflow flux from the whole polar cap varies due to Earth's rotation and orbit, which causes the magnetic polar caps to rotate in and out of the sunlight. We find that the resulting flux of one polar cap exhibits daily and seasonal variations, but also the combined flux from both hemispheres still has daily and seasonal variations, due to the transition lying at a solar zenith angle larger than 90°. A large part of the ion outflow above the polar cap may end up in the plasma sheet where it might affect magnetospheric dynamics. Since the plasma sheet is located on closed field lines, the combined flux represents to some extend the total flow to the plasma sheet. Interestingly, the combined flux peaks during the equinoxes, which coincides with the bi-annual peaks in occurrence frequency of geomagnetic storms. Including the north-south asymmetry in the magnetic field of the Earth, more variations and also asymmetries in the outflow from both hemispheres are found.

Finally measurements of polar wind observed at high altitudes are analyzed to investigate the effect of solar illumination on the outflow. Because of the difficulties to measure polar wind ions at high altitudes, an alternative method is used, exploiting the wave created behind a charged spacecraft. This method cannot differentiate between ion species, but we find very similar behaviour of the flux densities to that of the H^+ ion flux densities above polar cap arcs: similar in magnitude and similar in dependence on solar illumination. Both the density and velocity are found the be affected. This shows how important solar illumination is for the polar wind, but it also corroborates the finding that flux densities of polar wind and outflow above polar cap arcs are not significantly different. A seasonal variation in the outflow was also found, as predicted in the second part, however, apart from a preliminary north-south asymmetry, more subtle predictions could not be confirmed due to limitations in accuracy of the data.

Beknopte samenvatting

Het doel van deze thesis is te analyseren hoe bestraling door de zon de fluxen van ionen die uit de ionosfeer in de polaire regio's van de aarde stromen, beïnvloedt. Een atmosfeer lekt voortdurend deeltjes naar de ruimte onder invloed van de niet aflatende toevoer van energie door de zon. Deze energie komt in twee vormen: zonlicht (elektromagnetische straling) en de zonnewind. Zonlicht warmt en ioniseert de atmosfeer. De zonnewind kan zijn kinetische energie doorgeven aan de atmosfeer. Op een planeet met een intern magnetisch veld, zoals de aarde, leidt de interactie met de zonnewind tot de vorming van een magnetosfeer. De magnetosfeer beschermt de atmosfeer voor een groot deel van de zonnewind, maar brengt indirect ook veel energie van de zonnewind over naar de atmosfeer door te zorgen voor een magnetische verbinding. Deze ontsnappende deeltjes eroderen de atmosfeer. Als we de evolutie van atmosferen willen verstaan is een goed begrip van deze uitstroomprocessen en de mechanismes die ze aandrijven dus van cruciaal belang. De uitstromende ionen kunnen bovendien de dynamica van de magnetosfeer beïnvloeden en zijn dus belangrijk voor ruimteweer.

De polaire ionosfeer is een speciale regio voor ionenuitstromen omdat het magnetisch veld daar direct verbonden is met de zonnewind. De grootste energie input daar is echter zonlicht (op een kleine regio, de cusp genaamd, na). Het belangrijkste uitstroommechanisme daar, de poolwind genaamd, is berucht omdat het zo moeilijk te meten is door de oplading van satellieten. Daarom focussen we eerst om een ander mechanisme in de polaire ionosfeer, en passen later een alternatieve techniek toe.

We beginnen met het onderzoeken van ontspannende ionen boven kleinschalige poolkap auroras. Deze zijn gelijkaardig aan de gewone discrete auroras, behalve dat ze voorkomen over de poolkappen en wanneer het interplanetaire magnetische veld noordwaarts is. Ze zijn ook stabieler en typisch veel minder intens. De ionen worden versneld door het quasi-statisch elektrisch veld parallel met het magnetisch veld dat geassocieerd is met poolkap auroras. De resultaten tonen aan dat de uitstroom ruwweg twee regimes heeft: uitstroom boven een

verlichte ionosfeer en boven een donkere ionosfeer. Voor H^+ ionen is de flux dichtheid gemiddeld bijna dubbel zo hoog boven een verlichte ionosfeer als boven een donkere ionosfeer. Voor O^+ ionen is dat meer dan 7 keer zo hoog. De overgang tussen beide regimes heeft een zonzenithhoek van meer dan 90°. Het potentiaal verschil van het quasi-statische elektrisch veld wordt ook beïnvloedt door het zonlicht: er komt geen klein potentiaalverschil voor boven een donkere ionosfeer, wat een feedback effect van de ionosfeer op het magnetosferische systeem suggereert. De H^+ flux dichtheden zijn zeer gelijkaardig aan die van de poolwind gegeven in de literatuur. Dit feit, samen met de invloed van het zonlicht en de relatief kleine energie input, suggereert dat de fluxen boven poolkap auroras niet zo verschillend zijn van die in de poolwind, enkel versneld.

In een tweede deel starten we van deze laatste implicatie en extrapoleren de flux dichtheden boven poolkap auroras en de afhankelijkheid van zonlicht naar de hele magnetische poolkap. Met een simpel en conceptueel model onderzoeken we hoe de totale flux van de hele poolkap varieert door de baan en de rotatie van de aarde, die magnetische poolkap in en uit het zonlicht doet roteren. We vinden dat de resulterende flux van een poolkap dagelijkse en seizoensgebonden variaties vertoont, en dat de gecombineerde flux van twee hemisferen ook dergelijke variaties heeft. Een groot deel van de uitstromende ionen kan terecht komen in het plasmablad (plasma sheet) van de magnetosfeer, waar ze dynamica van de magnetosfeer kunnen beïnvloeden. Aangezien het plasmablad op gesloten veldlijnen ligt, stelt de gecombineerde flux in zekere zin de toevoer naar het plasmablad voor. Interessant is dat die flux piekt rond de equinoxen, wat samenvalt met de halfjaarlijkse pieken in de frequentie van geomagnetische stormen. Met de noord-zuid asymmetrie van het magnetisch veld meegrekend, vinden we nog meer variaties en ook een noord-zuid asymmetrie in de uitstroom.

Als laatste analyseren we observaties van de poolwind ver in de magnetosfeer om het effect van zonlicht te onderzoeken. Vanwege de moeilijkheden met het meten van de poolwind, wordt een alternatieve techniek gebruikt die het verband tussen de snelheid en het zog achter een geladen satelliet uitbuit. Deze methode kan geen onderscheid maken tussen de verschillende soorten ionen, maar we vinden een zeer grote gelijkenis met de H^+ flux dichtheden boven poolkap auroras: gelijkaardig in grootte en gelijkaardig in de afhankelijkheid van zonlicht. Zowel de snelheid als de dichtheid van de ionen vertoont deze afhankelijkheid. Dit toont hoe belangrijk zonlicht is voor de poolwind, maar bevestigt ook de bevinding dat de flux dichtheden van de uitstromen boven poolkap auroras en de poolwind niet significant verschillen. We vinden ook een variatie over de seizoenen, zoals voorspeld in het tweede deel, maar verdere voorspellingen kunnen niet bevestigd worden door de gelimiteerde precisie van de metingen, buiten een preliminair resultaat van een noord-zuid asymmetrie.

Contents

Chapter 1

Introduction

Whether there is life somewhere else in the universe than on Earth is one of the great mysteries that has kept humankind wondering. In addition to all the practical difficulties of finding extraterrestrial life, we do not really know what we are looking for. What would this life look like, or what does "life" actually even mean [e.g., Cleland and Chyba, 2002]? What we do know is that life as we know it on Earth requires liquid water. And to have liquid water on the surface of a planet, that planet needs to possess an atmosphere. Without an atmosphere, the pressure is too low for a liquid state of water to exist. There are other ways for a planet to have liquid water, like Saturn's moon Enceladus, on which "geysers" of water vapor have been observed, and there is strong evidence that it has a vast ocean below its surface [Thomas et al., 2016]. Europa and Ganymede, both moons of Jupiter, are also believed to have liquid water below their surface due to heating by tidal flexing by Jupiter [Cassen et al., 1979; Spohn and Schubert, 2003]. These moons may therefore also be possible places to harbour extraterrestrial life.

However, until now, the only place in the universe where we know life exists is our own planet Earth, which has an atmosphere. So why does Earth have an atmosphere? Not all planets have an atmosphere. And will it keep its atmosphere forever? The answers to these questions lie at the basis of the answer to why Earth has life and some other planets do not. They lie at the basis of the answer to the question which planets may perhaps have life. Understanding why some planets have an atmosphere and how it evolves will help to advance us towards an answer to the question of extraterrestrial life and where to look for that life.

These questions are exemplified by taking a look at Earth's closest neighbours:

Venus and Mars. These two planets are relatively similar to Earth. Venus has almost the same radius as the Earth, and Mars' radius is half that. Both planets have a solid surface and rocky composition, and are located at comparable distances from the Sun. Yet their atmospheres represent two very different cases. Venus has a very dense atmosphere, with a pressure high enough to support liquid surface water, if only its surface temperature were not so high [Ingersoll, 1969]. The very large fraction of greenhouse gases in the Venusian atmosphere has caused the surface temperature to rise so high that water would still evaporate. It is not sure yet whether Venus ever had liquid water on its surface [Kurosawa, 2015]. Mars, on the other hand, does not have a thick atmosphere. It has a very tenuous atmosphere, that is not capable of providing the necessary pressure to sustain liquid surface water. Nonetheless, there is convincing evidence that in the past Mars did have water flowing on its surface [Baker, 2001]. This suggests that Mars must have had a thicker atmosphere in the past. While Venus, Earth, and Mars formed from similar material, they have very different atmospheres now. Why did these atmospheres evolve in such a different way?

In its most basic form, one can see a planetary atmosphere as a mixture of gases trapped in a gravitational well. Particles with enough energy can escape, those with too little energy cannot. But a star constantly emits energy, heating the atmosphere of the planets and energizing its particles, enabling them to escape.

There are two main forms of energy coming from a star like the Sun. One form is electromagnetic radiation or solar illumination. The other form of energy is the energy carried by the solar wind, a collection of charged particles emitted by the Sun traveling through space at several hundred km s^{-1}. Very simply put, these two forms of energy cause two mechanisms for atmospheric particles to escape. Solar illumination heats the atmosphere and thus increases the energy of the atmospheric particles, part of which will then have enough energy to escape Earth's gravitational well. Meanwhile, the particles in the solar wind impact on the atmosphere, thereby knocking atmospheric particles away (although most of the time the solar wind imparts its energy to the atmosphere in more indirect ways, as we will see later).

Because the particles in the solar wind are charged, they are affected by magnetic fields. As Earth has a magnetic field, most of the particles of the solar wind are diverted away around Earth. The magnetic field acts as a shield protecting Earth's atmosphere from the solar wind. At present, Mars has only remnant crustal magnetic field [Acuna et al., 1998], but it is believed that Mars used to have a global intrinsic magnetic field [Connerney et al., 2001; Spohn et al., 2001]. It is thought that Mars also used to have a denser atmosphere [McKay and Stoker, 1989] and that Mars' magnetic field protected its atmosphere from the impact of the solar wind. But when Mars lost its magnetic field, its atmosphere

was no longer protected, which could explain why its atmosphere disappeared, stripped away by the solar wind [Brain and Jakosky, 1998].

But this simple and appealing scenario runs into problems when we look at Venus. Venus has a very dense atmosphere but does not have a magnetic field either. Despite it being closer to the Sun, where the solar wind and illumination are more intense, the absence of a protecting magnetic field has not prevented Venus from keeping its very dense atmosphere.

There are other ways to lose an atmosphere. A more erratic loss process is by asteroid or comet impacts, which can blow away a large part of the atmosphere. About 4 billion years ago there was a period lasting some 300 million years, called the Late Heavy Bombardment, during which it is hypothesized that asteroid impacts occurred much more frequently [Wetherill, 1975; Gomes et al., 2005]. Asteroid and comet impacts can of course not only remove atmospheric material, but also bring atmospheric and other material to a planet. Meteoroids and interplanetary dust particles entering the atmosphere form a source of incoming material as well [Plane, 2012]. There are also mechanisms that cause a loss of atmospheric mass, not from above, but from below. For example absorption at the surface through chemical processes like oxidation or by biological life forms. The Earth can also be a source of atmospheric gases, for example by volcanic outgassing. We will not go further into these processes.

The effects of the solar wind and solar illumination on the atmosphere of both magnetized and non-magnetized planets are actually much more complex than explained above. This might be a part of the key to this apparent paradox of why Venus still has a large atmosphere, like Earth, despite not having a magnetic field, like Mars. So let us take a closer look at how all of this works. In what follows, we will introduce the concepts of the interaction of the Sun with the atmosphere and ionosphere of planets like Earth, Venus, and Mars. Considerably more attention will be given to two specific topics, the polar wind and small-scale polar cap arcs, since they form the main subjects of the research reported on in this thesis.

1 Energy from the Sun

The Sun is the most important source of energy for Venus, Earth, and Mars. This energy is emitted by the Sun in two main forms.

1.1 Solar illumination

The Sun's present day radiation spectrum can be roughly approximated by that of a black body at a temperature of approximately 5800 K [Meyer-Vernet, 2007]. This spectrum peaks in the visible light, as can be seen in figure 1.1, which makes up about 40% of the total irradiance [Liou, 2002]. Almost 50% of the total irradiance consists of electromagnetic radiation with longer wavelengths than visible light, namely infrared (IR), microwaves, and radio waves. About 10% has shorter wavelengths, called ultraviolet (UV), and also a very small part with even more extreme wavelengths (x-rays and gamma rays). At the shorter wavelengths the black body radiation approximation becomes less and less good, so that the spectrum is completely different below 100 nm.

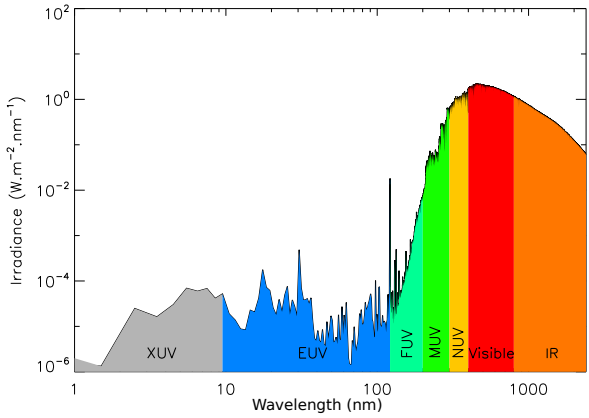

Figure 1.1: The irradiance spectrum of the Sun with both axes in a logarithmic scale to make the small, but important contribution of the EUV visible. Courtesy of Gaël Cessateur.

An important effect of solar illumination is that it heats the atmosphere of planets. But that is not the only effect of the solar illumination. The radiation with wavelengths below ∼100 nm, often called extreme UV radiation (EUV), makes up only 0.001% of the total irradiance [Meyer-Vernet, 2007], but it still has an important impact on the atmosphere. It has considerably more energy per photon, and thus has the capability of setting an electron free from a neutral atom or molecule in the atmosphere, unlike the radiation at longer wavelengths. This process creates a pair of a negatively charged electron and a positively charged ion, and is called **ionization**.

The intensity of the EUV irradiance fluctuates a lot. It is generally parameterized

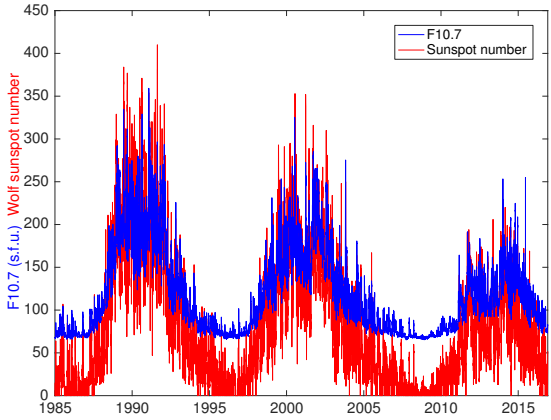

Figure 1.2: The solar cycle clearly visible in the sunspot number and the F10.7 measurement.

by the F10.7 measurement. This is the flux density of electromagnetic radiation with a wavelength of 10.7 cm. This is only one wavelength in the radio wave part of the spectrum, but the flux densities of the EUV radiation correlate well with it, and this wavelength can be reliably measured on a daily basis, regardless of weather conditions.

F10.7 measurements in figure 1.2 show that the EUV irradiance varies on a daily scale, but overall also exhibits a fluctuation over an 11-year period, called the solar cycle [Meyer-Vernet, 2007] (every 11 years the polarity of the Sun's magnetic field reverses, so the full period is actually 22 years). Many solar phenomena follow this solar cycle. For example, just like F10.7, the number of sunspots visible on the surface of the Sun follows the 11-year solar cycle, a fact that was already recognized (more or less) as early as 1844 [Schwabe, 1844]. Solar flares, very bright explosions of electromagnetic radiation at the surface of the Sun, are more frequent during the maximum of the solar cycle than during the minimum [Crosby et al., 1993].

1.2 Solar Wind

The other form of energy is the flux of particles expelled by the Sun, called the **solar wind**. Because of the very high temperature of the corona of the Sun, plasma is constantly flowing away from the Sun. Its existence was originally postulated to explain the observed acceleration of ions in a comet's

tail [Biermann, 1951, 1952]. The solar wind consists of two types: the fast solar wind and the slow solar wind. In the vicinity of Earth, the slow solar wind has an average speed around 400 km s^{-1}, the fast solar wind around 750 km s^{-1} [Meyer-Vernet, 2007]. This plasma mostly consists of electrons and protons (also called ionized hydrogen: H^+), but also includes a fraction of ∼5% of fully ionized helium (He^{2+}), and very small proportions of (fully ionized) heavier elements, although the precise composition can vary a lot and is different between the fast and slow solar wind [Feldman et al., 2005].

The solar wind also carries a magnetic field, called the **interplanetary magnetic field** (IMF). It has the imprint of the magnetic field of the Sun but is also caused by currents inside the solar wind. The magnetic field lines of the solar wind remain connected for a long time to the magnetic field of the Sun during the radial expansion of the solar wind. And because the Sun rotates, these magnetic field lines are draped in the shape of a spiral, called the **Parker spiral** [Parker, 1958]. At the distance of Earth, this spiral makes an angle of approximately 45° with the radial direction from the Sun. The solar wind is also affected by the solar cycle. Coronal mass ejections, or CMEs, are large structured outbursts of plasma and magnetic field at the surface of the Sun and are, just like solar flares, more frequent during solar maximum [Webb and Howard, 1994].

The main form of energy in the solar wind is the kinetic energy of its particles, which is proportional to $\rho_{SW} v_{SW}^2$ (with ρ_{SW} the solar wind mass density and v_{SW} its velocity). There is also energy in thermal motion of the solar wind particles (proportional to $n_{SW}(T_{SW,e} + T_{SW,i})$, with n_{SW} the number density and $T_{SW,e}$ and $T_{SW,i}$ the electron and ion temperatures in the solar wind) and in the electromagnetic fields of the solar wind (which is proportional to B_{SW}^2, with B_{SW} the magnetic field of the solar wind), but these are negligible compared to the kinetic energy. The magnetic field in the solar wind plays a vital role nonetheless, as we will see later on.

2 Interaction with a planet

The solar illumination and the solar wind interact with planetary systems in an entirely different way. As opposed to the solar wind, solar illumination is not affected by the planetary magnetic field and can thus directly interact with the atmosphere. Its main effect is that it heats the atmosphere, but another very important consequence of the electromagnetic waves hitting the atmosphere is that it ionizes a part of the atmosphere.

2.1 Solar illumination: Ionosphere

High energy UV entering an atmosphere can knock away electrons from the neutral particles composing the atmosphere. As a consequence, a part of that atmosphere will consist of positively charged ions and negatively charged electrons. This ionized part of the atmosphere is called the **ionosphere**.

In the late 19th century the existence of currents in the atmosphere (and thus charges to carry it) were already hypothesized to explain the observed variations of the Earth's magnetic field. It was at the turn of the century, when Marconi was successful in wirelessly transmitting radio signals across the Atlantic ocean, that the existence of charges in the atmosphere was clearly proven. His success could only be explained by the reflection of these radio waves on electric charges in the upper atmosphere [Martyn, 1947].

The way electromagnetic radiation from the Sun interacts with the atmosphere critically depends on the constituents of the atmosphere and how efficient they are at absorbing it. The ions and electrons also constantly recombine, forming again neutrals, and thus the balance between ionization and recombination determines the ionized fraction. At lower altitudes in the atmosphere the density is high enough so that particles of opposite charge will recombine almost instantaneously. Additionally, much of the ionizing radiation is already absorbed higher up. At higher altitudes in the atmosphere, the density is not high enough to efficiently cancel out all charges created, resulting in a plasma.

This complex system of interactions creates at Earth an ionosphere that consists of three main layers [Schunk and Nagy, 2000], called the D-, E-, and F-region, as you can see in figure 1.3. These separate regions were discovered by reflection of radio waves [Appleton, 1927], and defined in term of the maximum frequency that could be reflected on it. The E- and F-region also both coincide with a peak in electron density (and thus ionization).

The **F-region** is the highest of these regions. It is dominated by O^+ ions. The bottom of the F-region is at approximately 150 km altitude. The F-region itself can be divided into two sub-layers: the **F1-region**, which is the lowest and reaches up to approximately 250 km altitude, and the **F2-region**, which contains the electron density peak of the F-region. In the F1-region the most important processes for the ionosphere are the ionization of atomic oxygen and the chemical reactions of the ions with the neutrals. In the F2-region other processes, like transport, start to become important.

Below the F-region is the **E-region**, which was actually the first layer that was experimentally discovered [Appleton, 1927]. The E-region extends from roughly 100 km to 150 km altitude and is dominated by molecular ions NO^+,

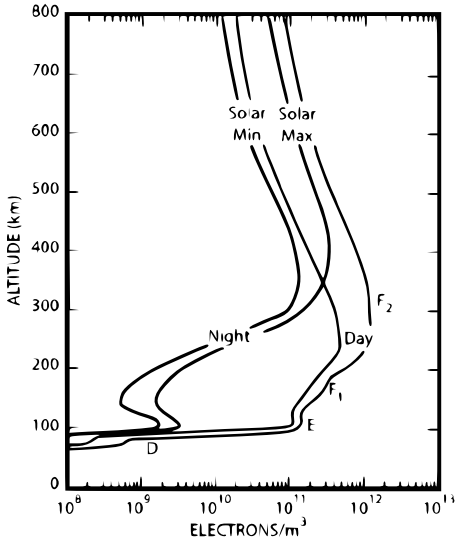

Figure 1.3: The altitude profile of ionospheric electron density. From Richmond [1987].

O_2^+, and N_2^+. Because more ion species (and neutral species) are at play here, the photochemistry becomes more complex in the E-region [Schunk and Nagy, 2000]. Below 100 km and down to 60 km is the **D-region** [Nicolet and Aikin, 1960]. The chemistry becomes even more complex in this region, since it consists of several molecular ions, both positive and negative, and water cluster ions. Most of the radiation capable of ionizing atmospheric particles is absorbed above 60 km altitude, and thus the ionization rate at lower altitudes is too low to maintain any significant ionization.

At the topside of the ionosphere, above the ionization peak of the F-region, ionospheric density decreases roughly exponentially. At higher altitudes lighter ions like H^+ and He^+ start to dominate over the O^+. This is called the **protonosphere** [Johnson, 1960]. The altitude where this happens can vary a lot between day and night and between different latitudes, but typically occurs somewhere between ∼600 km and a few 1000 km. The density of the neutral atmosphere is much larger than the ionospheric density up to several 1000 km altitude, but the ionospheric density decreases slower with altitude than the neutral density, so that the ion over neutral ratio increases gradually (but still remains far below one up to much higher altitudes).

Since solar illumination is the main cause of ionization, there is almost no ionization during the night. The described regions are present at the dayside of

the atmosphere, but the ionosphere shrinks strongly during the night, as can be seen clearly from figure 1.3. The F1- and the D-region disappear almost completely during night time. At higher altitudes the recombination is less efficient and so the F2-region remains, despite being reduced. The ionization rate in the E-region also drops markedly, but it is somewhat maintained by other processes.

2.2 Solar wind

Since the solar wind consists of charged particles with a mass, it interacts in a fundamentally different way with planets. This interaction is also very different between planets possessing an internal magnetic field and planets without a magnetic field.

2.2.1 Magnetized planets: Magnetosphere

The internally generated magnetic field of a planet shields its atmosphere from the onslaught of the solar wind to some extent. The result is a region in space that is dominated by the planetary magnetic field, rather than the magnetic field in the solar wind. This is called the **magnetosphere** [Baumjohan and Treumann, 1996]. A simplified figure of Earth's magnetosphere is shown in figure 1.4.

The boundary of the magnetosphere is called the **magnetopause** [Cahill and Amazeen, 1963; Cowley, 1995]. This is a relatively sharp border across which the magnetic field changes its magnitude and direction from being mostly determined by the terrestrial magnetic field to the magnetic field in the solar wind. The sharp transition in magnetic field across this border is caused by currents inside the magnetopause. The magnetopause acts as a barrier preventing plasma from the solar wind from entering the magnetosphere. This barrier is not perfect, however, and plasma from the solar wind still manages to penetrate the magnetosphere through a variety of mechanisms.

As Earth's magnetosphere forms an obstacle for the solar wind, which at this distance from the Sun is supersonic and super-Alfvénic, a **bow shock** is formed upstream of the magnetosphere [Ness et al., 1964; Kucharek et al., 2008]. When the solar wind passes through the bow shock it gets compressed, slowed down and thermalized. After the bow shock, the solar wind is diverted around the magnetosphere. The region outside the magnetosphere, between the magnetopause and the bow shock, is called the **magnetosheath**.

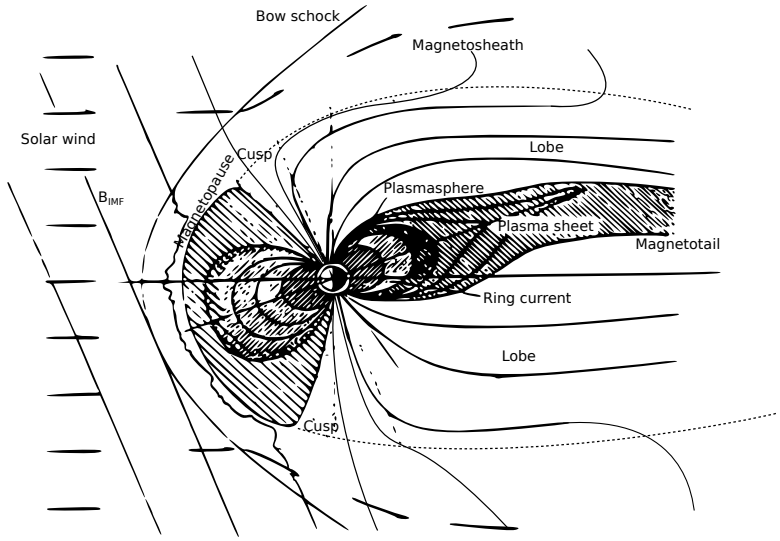

Figure 1.4: A schematic view of the magnetosphere. Adapted from Parks [1991].

Earth's magnetic field, far enough from the surface, can be approximated by a dipole. This magnetic field is distorted by the pressure of the solar wind and the interaction with the interplanetary magnetic field. On the side facing the Sun, the magnetosphere is compressed. On the other side, the magnetic field lines are stretched out far from Earth, forming what is called the **magnetotail** [Ness, 1965; Dessler and Juday, 1965; Axford et al., 1965].

At the top and bottom of figure 1.4 the magnetic field lines of the magnetosphere are connected to those of the IMF. Therefore these field lines are called **open magnetic field lines**[1], as opposed to the magnetic field lines in other parts of

[1]In this text we will use the terms "open" and "closed" and "open magnetic field line" and "closed magnetic field line", as is common terminology in the field of magnetospheric physics. Since the divergence of a magnetic field is always zero, the magnetic flux through any closed surface will always be zero. This means that no magnetic field line can really be "open", and must always return eventually. With an "open field line" we mean any field line of Earth's magnetic field that is on one end connected to the Earth and on the other to the interplanetary magnetic field (and is finally connected to another open field line at the opposite side of Earth again, possibly after going through the Sun or somewhere else far in space). Analogously, a closed field line is a line that on both sides is connected to Earth directly, without being connected to the IMF. A magnetic field line only connected to the IMF is just called an IMF line.

the magnetosphere that are not connected to the IMF. The latter are called **closed magnetic field lines**.

The region from where the open magnetic field lines are bent towards the dayside to where they are bent away from the Sun is called the **cusp** [Hansen et al., 1976]. These open field lines provide a way into the magnetosphere for the solar wind and even down into the atmosphere, and the cusp is thus an important weakness in the shield of the magnetosphere.

The regions of open field lines in the outer part of the magnetotail stretched away from the Sun are called the **magnetospheric lobes** (or lobes in short) [Dessler and Juday, 1965; Axford et al., 1965]. The magnetic field lines of the lobes are also connected to the IMF and thus solar wind plasma may enter, but due to the antisunward motion of the solar wind this is not so obvious. Typically only solar wind electrons enter, called the polar rain [Fairfield and Scudder, 1985]. The lobes have generally low plasma densities dominated by plasma from ionospheric origin [Engwall et al., 2009a; André et al., 2015].

The region of closed magnetic field lines in the magnetotail is the **plasma sheet**[Axford et al., 1965]. It extends down to the region where the magnetic field is again close to the dipolar configuration. The plasma in the plasma sheet becomes gradually denser going from the lobes towards the equatorial plane. The plasma sheet is not only denser than the lobes, its plasma is also hotter and more energetic [Gary, 1991; Delcourt et al., 1994; Arzner and Scholer, 2001]. Its origin can be the ionosphere as well as the solar wind. It is not completely clear yet which is the main contributor, but its certainly also depends on the geomagnetic conditions and solar illumination [e.g., Maggiolo and Kistler, 2014].

More inward[2] in the magnetosphere, also called the **inner magnetosphere**, the closed magnetic field lines have a shape closer to that of the dipole field. The plasma of the ionosphere may flow upwards, but is bound to the magnetic field lines and thus cannot escape. As a result, a torus-shaped volume filled with trapped cold plasma from ionospheric origin is formed. This is called the **plasmasphere** [see Darrouzet et al., 2009, for an overview]. It is often seen as an extension of the ionosphere into the magnetosphere.

2.2.2 Non-magnetized planets: Induced magnetosphere

The lack of an intrinsic magnetic field of a planet does not mean the solar wind has unimpeded access to its atmosphere. The charged particles of its ionosphere interact with the magnetic field in the solar wind, and, similar as in Earth's magnetopause, a current is set up that creates a boundary layer. In analogy, this

[2] as seen in the equatorial plane

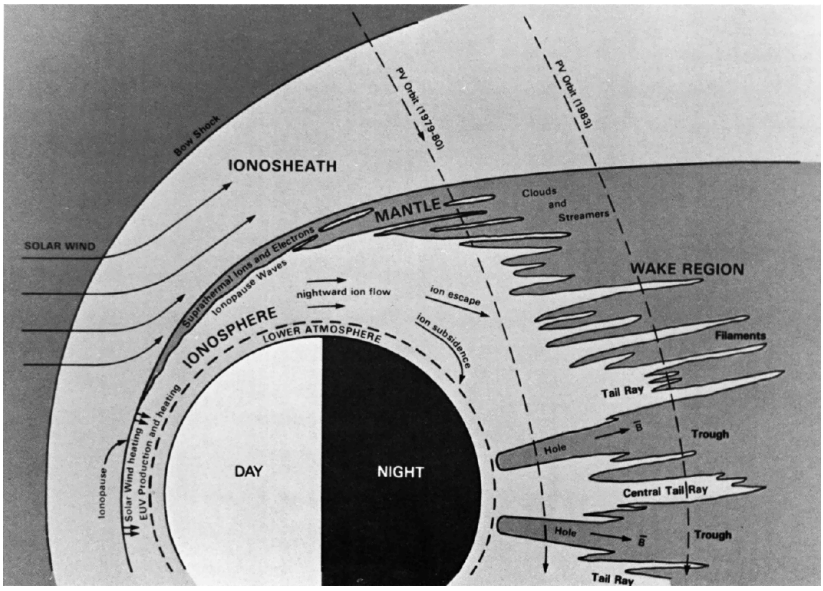

Figure 1.5: A schematic view of the induced magnetosphere of Venus. From Brace et al. [1987].

boundary layer is called the **ionopause** [Brace et al., 1987]. But this boundary layer is much closer to planet's surface, at the top of the ionosphere, leaving a part of the neutral atmosphere exposed to the solar wind.

At the ionopause the solar wind is diverted around the obstacle after being shocked by an upstream bow shock. The IMF is blocked and gets draped around the planet, leading to a long magnetic tail behind planet. This situation is shown in figure 1.5 for Venus. This type of magnetic structure created by the interaction of the IMF and the ionosphere is called an **induced magnetosphere**. Mars and Venus have a similar induced magnetosphere, except that the crustal magnetic fields at Mars cause some exotic features like multiple small cusps [Acuña et al., 2001] and even auroras [Bertaux et al., 2005].

3 Magnetospheric physics

The magnetosphere blocks the solar wind from the Earth, but it also interacts with the solar wind. This interaction provides a way for the solar wind to penetrate into the magnetosphere, and for energy to be transferred from the

solar wind into the magnetosphere, and even into the ionosphere. In order to understand the processes involved, we must first know how charged particles behave in such magnetic fields. We will take a look at this in section 3.1, before we continue to look at the connection and processes between the magnetosphere and the solar wind and ionosphere.

3.1 Charged particles in magnetic fields

A magnetic field **B** interacts with a charged particle with charge q via the **Lorentz force F**:

$$\mathbf{F} = q\left(\mathbf{E} + \mathbf{v} \times \mathbf{B}\right), \tag{1.1}$$

where **v** is the particle's velocity and **E** is the electric field that might be present. The resulting motion may be complex, but it can be broken down into several components so that the particle's path becomes more clear.

3.1.1 Helical motion

Equation 1.1 shows that the magnetic field only affects the motion perpendicular to the magnetic field. And it only changes the direction of this velocity, not its magnitude. Therefore, in a uniform magnetic field, a charged particle will gyrate around a magnetic field line, but travel freely along the magnetic field direction, creating a helix shaped path around a magnetic field line. This will also hold approximately in a less uniform magnetic field, provided it does not vary significantly over distances on the order of the gyration radius, nor varies strongly along the parallel direction (compared to the parallel velocity). Since the gyration does not cause any overall movement, particles will tend to move only parallel to the magnetic field lines.

3.1.2 Drift motion

An electric field along the magnetic field will accelerate the charged particle normally. A constant electric field perpendicular to the magnetic field, however, will cause the center of the gyration to drift perpendicularly to the magnetic field with a velocity $\mathbf{v}_E$ equal to

$$\mathbf{v}_E = \frac{\mathbf{E} \times \mathbf{B}}{B^2}. \tag{1.2}$$

This is often called the **E × B drift**.

This description of the motion as the parallel motion plus the perpendicular drift is called the **guiding center motion**.

Similar drifts can be determined when the electric field does vary over time but slowly compared to the gyration frequency (called **polarization drift**) or in the presence of other forces with a perpendicular component. In a non-uniform magnetic field there are drifts due to the gradient (**gradient drift**) or curvature (**curvature drift**) of the magnetic field (without the presence of any additional force). Whereas the direction of the $\mathbf{E} \times \mathbf{B}$ drift is independent of the particle's charge, the gradient drift and curvature drift are not, and as such can cause a current. We will not go further into this, however.

3.1.3 Magnetic moment

In the guiding center motion, we neglect the gyration of the particle. Yet this motion is associated with kinetic energy. Therefore we define the **magnetic moment** as

$$\mu = \frac{mv_\perp^2}{2B}, \tag{1.3}$$

where m is the mass of the particle and $v_\perp$ the magnitude of the velocity perpendicular to the magnetic field. The magnetic moment of a charged particle moving into a stronger or weaker magnetic field remains constant in the absence of any additional force. This is true as long as the magnetic field does not change significantly over the time of one gyration. Therefore the magnetic moment is also called an adiabatic invariant of the motion.

As a consequence, the perpendicular velocity of a charged particle moving in a converging magnetic field[3] in the direction of increasing magnetic field strength will increase to balance the increase of magnetic field strength. The parallel velocity decreases accordingly to conserve the particles to total kinetic energy. The opposite occurs for a particle moving into a weaker magnetic field. In the guiding center motion context, this results in an apparent force that repulses charged particles from regions of increasing magnetic field strength, called the **mirror force**. Note that the mirror force does no work, as it should be since it is a magnetic force, because all the parallel velocity lost is turned into perpendicular velocity and vice versa.

Particles on closed field lines may be trapped this way, bouncing up and down between the points where their parallel velocity has become zero, called

[3]Please note that the terms "converging" and "diverging magnetic field" are used in this text implying the colloquial meaning of these words. They certainly do not mean "having a non-zero divergence". According to the Maxwell equations the divergence of a magnetic field is always equal to zero: $\nabla \cdot \mathbf{B} = 0$. Nothing contradicting this is meant with these terms.

mirror points. The higher the ratio of a particle's parallel velocity over its perpendicular velocity, the lower its mirror point will be. When a particle's mirror point is in the ionosphere, it may collide there, and thus not mirror. The area in the phase space (i.e. the space defined by $(v_{\parallel}, v_{\perp})$) populated by these particles, is called the **loss cone**.

There are other adiabatic invariants of the motion related to the gradient drift and the curvature drift, called the longitudinal invariant and the drift invariant, but we will not discuss them further.

3.2 Ionospheric projection

Every point in the magnetosphere is magnetically connected to the ionosphere. Because of this, the ionosphere affects the magnetosphere and vice versa. Regions of closed magnetic field lines connect on both sides directly to the ionosphere, one in the northern hemisphere and one in the southern hemisphere. These two projections along the magnetic field line into the ionosphere are called **conjugate points**.

A large part of the magnetosphere is connected to a relatively small part of the ionosphere in the high-latitude ionosphere. The open magnetic field lines of the lobes connect to a region near the magnetic poles (see figure 1.6), called the **magnetic polar cap** (or polar cap in short when no confusion is possible). The plasma sheet connects to a small band, typically 10° wide in latitude, around the magnetic polar cap, called the **auroral oval**. As its name suggests, it is the area where the aurora borealis (in the northern hemisphere) and the aurora australis (in the southern hemisphere) occurs. All the magnetic field lines of the magnetopause and the cusp project to one small spot at the dayside border of the magnetic polar cap and the auroral oval, also called the **cusp**.

The location of the auroral oval depends on the level of geomagnetic activity. The typically the poleward boundary is at 70° MLAT, but during long periods of geomagnetically quiet times, the magnetic polar cap becomes small, and the poleward boundary of the auroral oval can go poleward of 80° magnetic latitude (MLAT) [Milan et al., 2009]. During more active times the magnetic polar cap can expand, and the poleward boundary of the auroral oval can go down to 60° MLAT or lower.

The magnetic field lines of the magnetosphere inward of those regions mentioned above are connected to the ionosphere at lower magnetic latitudes.

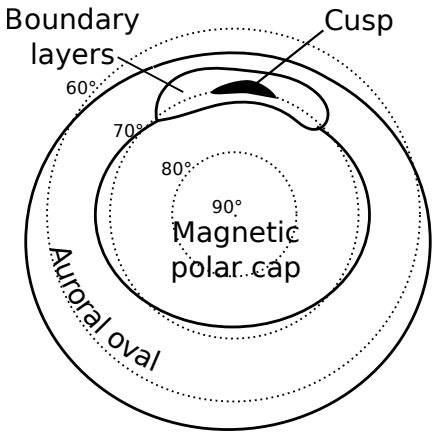

Figure 1.6: A schematic view of the high-latitude ionosphere.

3.3 Convection

In a quasi-neutral, collision-less plasma and in the absence of any additional forces, if the conductivity is infinite (or very large), the only electric field that may exist, is one that can be eliminated by a Lorentz transformation, or

$$\mathbf{E} = -\mathbf{v} \times \mathbf{B}, \tag{1.4}$$

where $\mathbf{v}$ is the velocity of the plasma. As a result, in the frame of reference moving with this plasma, the electric field is zero. This is called the **frozen-in** condition, because in such a plasma the magnetic field changes in such a way as if it were to move along with the plasma, i.e., as if it were frozen into the plasma. In this context we can speak of moving magnetic field lines. This movement of plasma together with the magnetic field is called **convection**.

In a reference frame in which the plasma is moving there will, consequently, be an electric field given by equation 1.4, which is called the **convection electric field $\mathbf{E_c}$**. This is related to the electric drift given, as given in equation 1.2. Indeed, both expressions are equivalent (with $\mathbf{E}$ and $\mathbf{B}$ perpendicular). Note that there are other types of bulk motion which can result from other drifts, but we will reserve the term convection for the bulk motion of the plasma due to electric drift.

3.4 Reconnection and the Dungey cycle

The solar wind plasma and its magnetic field can often be approximated by the frozen-in condition. From the reference frame of the Earth there is thus a convection electric field. The magnetopause shields the magnetosphere from the solar wind, so that the convection electric field is also kept out. This shield is not perfect, however. When the orientation of the IMF differs strongly from the direction of the magnetospheric magnetic field like in figure 1.7 (a), i.e., when there is a strong magnetic shear, the IMF field lines and the magnetospheric field lines may merge and form two "new" magnetic field lines, as shown in panels (b) and (c) of figure 1.7. This process is called **magnetic reconnection**.

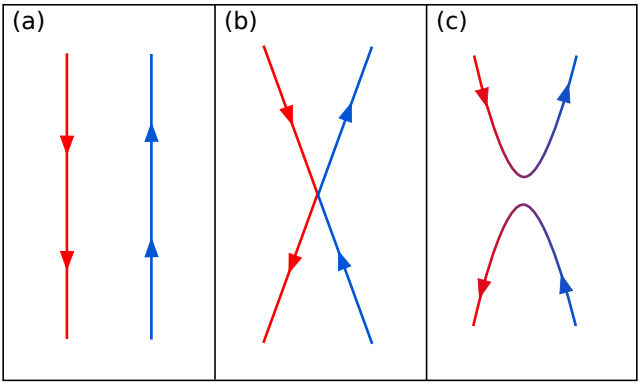

Figure 1.7: A very simplified, schematic representation of the reconnection process.

Applying this to the dayside magnetosphere, called **dayside reconnection**, this process has the result of turning one closed magnetospheric field line and one IMF field line into two open magnetic field lines (i.e., both connected to the IMF and the terrestrial magnetic field). The field lines of the IMF move together with the solar wind, and since the open field lines are connected to the IMF, they will drift accordingly due to the convection electric field (when frozen-in conditions apply). As a result the newly opened magnetic field line will slowly be pulled from the dayside, across the cusp, towards the nightside, as sketched in figure 1.8, and transported backwards into the lobes, while the solar wind keeps moving farther away and stretching out the magnetic field.

When more and more magnetic field lines are being peeled off from the dayside and convected towards the nightside, large magnetic tension is created in the magnetotail between magnetic field lines with opposite direction. At this point, magnetic reconnection can occur again. The same process as in figure 1.7 can

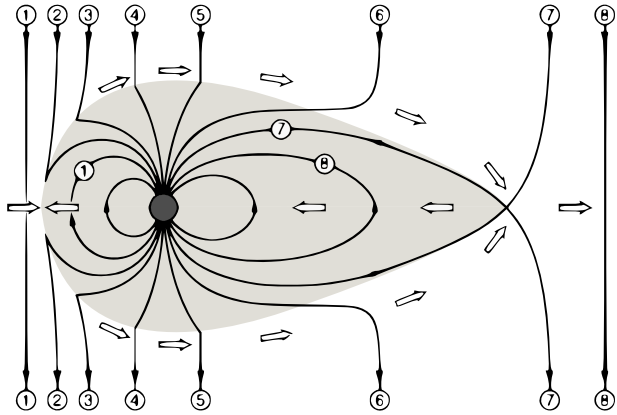

Figure 1.8: The Dungey cycle. From Baumjohan and Treumann [1996].

be applied, but tilted by 90°. Oppositely to reconnection on the dayside, this turns two open field lines into one closed field line and one IMF field line. This is called **nightside reconnection**. When this occurs, the magnetic tension stored in the stretched field lines is released, and the closed field line snaps back to Earth. Afterwards this field line is transported back to dayside along the flanks. This whole process is called the **Dungey cycle**, named after Dungey [1961] who was the first to apply magnetic reconnection to the magnetosphere and propose this cycle.

Since the magnetic field of the Earth is directed northwards (i.e. from south to north) at the dayside magnetopause, dayside reconnection occurs most efficiently when the IMF field is directed southwards, or has a southward component. During periods of northward IMF, this type of dayside reconnection cannot occur, and the IMF field lines in the magnetosheath are blocked by the magnetosphere, and draped around the magnetopause, as in panel (a) of figure 1.9, building up magnetic tension at the dayside magnetopause. However, on closer inspection of this configuration, one can see that the situation is again primed for reconnection to occur. In this case it is a bit more complex. When on one side the field lines reconnect, as shown in panel (b) of figure 1.9, this turns an open field line, which is pulled to the nightside, and an IMF field line, draped across the dayside magnetopause, into an open field line draped across the dayside magnetopause to the other side and an IMF field line no longer blocked by the magnetopause. When the same process occurs on the other side, the end product is a closed field line and an IMF line shown in panel b of figure 1.9. This process is called **high-latitude reconnection** [Kessel et al., 1996].

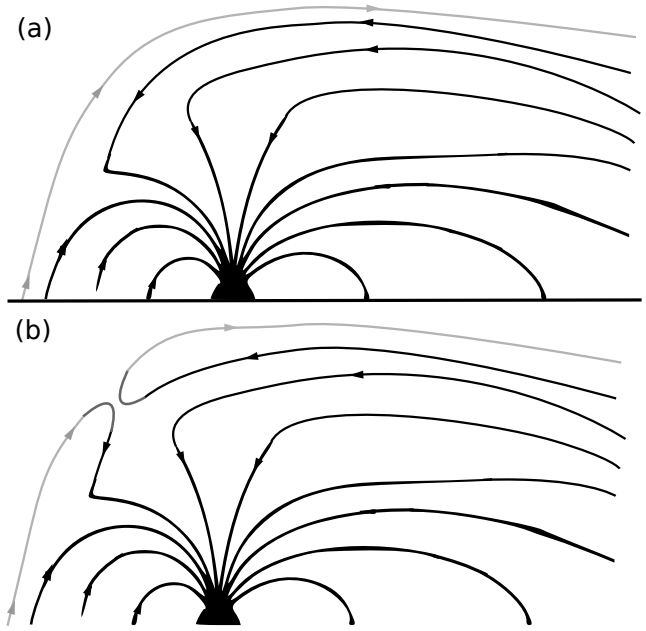

Figure 1.9: High-latitude reconnection in the northern lobe.

Dayside reconnection (occurring during southward IMF) opens magnetic field lines on the dayside and drags them towards the nightside, and thus it is said to "open" magnetic flux. High-latitude reconnection (occurring during northward IMF) closes magnetic field lines and pulls them back to the dayside, and so is said to close magnetic flux. Please note that this description of the Dungey cycle is a simplified view of these magnetospheric processes and that magnetic field lines are no real physical phenomenon. This description of moving and merging magnetic field lines is merely a useful and intuitive visualization of the real physical processes.

3.5 Ionospheric convection

The convection electric field in the solar wind penetrates all the way down along the magnetic field lines into the ionosphere. Due to collisions in the ionosphere the conductivity is finite, and thus the frozen-in condition is not fully satisfied. Nonetheless will the convection electric field cause the plasma in the ionosphere to drift along with the plasma higher up [Förster et al., 2007].

During southward IMF, this results in a two-cell convection pattern in the

ionosphere, as shown in figure 1.10. The dayside reconnection region maps down to the cusp, and the antisunward convection from the dayside into the magnetotail causes a similar antisunward convection in the ionosphere from the cusp across the polar cap towards the nightside auroral oval, which is connected to the recently closed magnetic field lines of the plasma sheet. From the nightside of the auroral oval, the convection flows back towards the dayside.

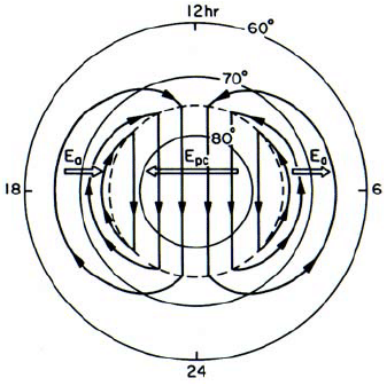

Figure 1.10: Idealized two cell convection in the ionosphere. From Kelley [2009].

Just like with the simple picture of the convection at high altitudes, this description of the ionospheric convection is very simplified. In reality the convection patterns may be much more complex. During periods of northward IMF, the convection stagnates, since no magnetic flux is being opened, or may turn sunward in the polar cap when high-latitude reconnection occurs, and the convection patterns become even more complex with more than two convection cells.

Because of the collisions of the drifting ions with the neutral particles in the atmosphere, the ionosphere loses a part of its kinetic energy. These collisions heat both the atmosphere and the ionosphere, which is called **frictional heating**, and even causes fast neutral winds [Killeen et al., 1995; Förster et al., 2008]. In this way, the ionosphere acts as a drag on the magnetospheric convection, drawing energy from magnetosphere and the solar wind.

3.6 Current systems

The magnetic field in the magnetosphere is not merely a superposition of the interplanetary magnetic field and Earth's magnetic field. The plasma in the magnetosphere acts in such a way that large-scale current systems are set up which deform Earth's dipolar magnetic field. Figure 1.11 shows a schematic overview of the current systems in the magnetosphere.

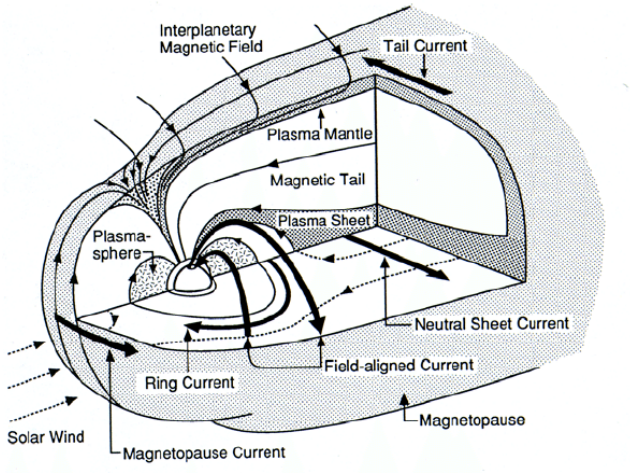

Figure 1.11: Large-scale current systems in the magnetosphere. From Potemra [1984].

One such current system is the **magnetopause current**, which is responsible for the sharp transition between the magnetospheric magnetic field and the IMF. How sharp this transition is depends on many factors. The thickness of the transitional layer of the magnetopause can vary from a few 100 km up to a few 1000 km [Russell and Elphic, 1978; Phan and Paschmann, 1996; Haaland et al., 2014]. It is affected by the plasma parameters at either side as well as the strength and orientation of the magnetic fields. Due to the orientation of the Parker spiral and the orbital motion of Earth, the plasma parameters in the magnetosheath are different between the dawn side and the dusk side flank of the magnetosphere [Walsh et al., 2012]. The plasma parameters on the inside of the magnetosphere may exhibit similar asymmetries [De Keyser et al., 2017]. Also the orientation of the boundary layer itself with respect to the flow of the solar wind is asymmetric, and because of the convection electric field in the solar wind this is an important asymmetry. The orientation of the current inside the magnetopause with respect to this electric field will typically be opposite between dawn and dusk [De Keyser et al., 2017]. All these differences can cause

an asymmetry in the thickness of the magnetopause between dawn and dusk. An interesting discussion of these dawn-dusk asymmetries in the magnetopause thickness can be found in the papers by Haaland et al. [2014], De Keyser et al. [2017], and Haaland et al. [2017].

The elongated shape of the magnetotail is created by a current sheet at the center of the plasma sheet, called the **neutral current sheet**, and the currents in the magnetopause of the tail, called the **tail current**. The current of the neutral current sheet flows from the dawn side of the tail to the dusk side, and connects to the tail current, forming a sort of Θ-shape, when looking in a dawn-dusk cross-section.

In the inner magnetosphere, the **ring current** is current carried by the particles of the radiation belts, which are energetic particles on magnetic field lines between ∼2 and ∼6 R_E bouncing up and down between mirror points. The gradient and curvature drift make the electrons and ions drift in opposite directions, setting up a current.

A part of these-large scale currents are diverted into the ionosphere. They flow along the magnetic field to and from the magnetosphere, and are called **Birkeland currents**. The ionosphere plays an important role for these currents. In the collision-less magnetosphere, it very difficult for currents not caused by drifts to flow perpendicularly to the magnetic field. In the ionosphere, however, collisions with other particles can increase the perpendicular conductivity allowing these currents to close in the ionosphere. Figure 1.12 shows the high-latitude ionosphere and the regions of current into and out of the ionosphere. They close horizontally in the ionosphere between adjacent regions, but also across the polar cap.

The **Region 1** Birkeland currents are the more poleward regions and connect to the magnetospheric boundaries. **Region 2** Birkeland currents are the more equatorward regions and connect with the ring current Cowley [2000].

Additionally, at certain times there are field-aligned currents that flow from the neutral current sheet in the magnetotail and close in a segment on the night side of the auroral oval. This is called the **substorm current wedge**, because it is associated with substorm activity.

Magnetospheric currents closing in the ionosphere are affected by the conductivity of the ionosphere, which is determined by parameters like the ionospheric density and temperature. Therefore the state of the ionosphere can affect the magnetospheric currents. The magnetospheric currents also affect the ionosphere. The collisions that enable the perpendicular conductivity also heats the neutral and charged particles of the atmosphere [Cole, 1962]. This is called **Joule heating**, by which the ionosphere acts as a resistance on the current

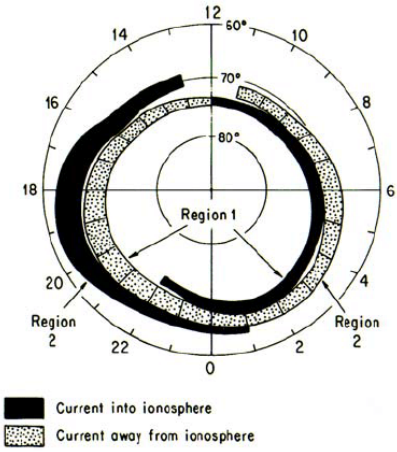

Figure 1.12: Regions of field-aligned currents in the ionosphere. From Iijima and Potemra [1976].

system. This is why the literature often speaks of **Magnetosphere-Ionsphere coupling** (M-I coupling).

3.7 Corotation

At the invariant latitudes of the plasmasphere, the plasma of the ionosphere, where the density is high enough, is dragged along by the neutral atmosphere rotating with the Earth. As mentioned before, the frozen-in conditions do not fully apply in the ionosphere. Nonetheless, the motion of the ionospheric plasma perpendicular to the magnetic field due to the rotation of the Earth will cause an electric field in the $-\mathbf{v} \times \mathbf{B}$ direction, similarly to the convection electric field in the solar wind, called the **corotation electric field**. According to equation 1.2 this electric field makes the plasma drift perpendicularly to the magnetic field (and the corotation electric field), which will cause the plasma at higher altitudes to also corotate with Earth.

The strength of the corotation electric field goes down with increasing distance, and at a certain point the convection electric field due to the interaction of the solar wind and the magnetosphere becomes more important. There the direction of the nett electric field and corresponding drift changes. Convection allows for the field lines to be emptied of the trapped plasma. During magnetically active times this leads to the density of the plasmasphere dropping relatively sharply [Gringauz, 1963; Carpenter, 1966]. This is called the **plasmapause**.

4 Atmospheric escape

With this background we can start to take a look at the processes that can cause atmospheric loss. For neutral particles, the escape process can be relatively simple. Once its altitude is above the region where collisions are important, called the **exobase**, the neutral particle in the gravitational field of its planet will just follow a ballistic trajectory. If its upward velocity is large enough, it will escape. For a charged particle, however, this is very different. Direct collisions between particles may be very rare in space outside the atmosphere, but it is full of magnetic and electric fields which affect the charged particles and may help them or prevent them from escaping.

We first introduce the escape process for neutral particles in section 4.1. Then we introduce the ion escape processes. Since the space environment of magnetized and non-magnetized planets is quite different, the escape processes differ too, although there are many similarities too. So first we introduce the escape processes from non-magnetized planets in section 4.2 and then those from magnetized planets in 4.3.

4.1 Thermal escape

One of the simplest processes of atmospheric escape is when the atmosphere is heated and part of its neutral population has enough energy to escape. The minimum upward velocity v_{esc} needed to escape, called the **escape velocity**, provides just enough kinetic energy to overcome the gravitational potential:

$$\frac{mv_{esc}^2}{2} = \frac{GMm}{r}, \tag{1.5}$$

where m is the particle's mass, G is the gravitational constant, M is the planet's mass, and r is the distance to the planet's centre. Note that the escape velocity is independent of the particle's mass m, since it appears on both sides of equation 1.5 and thus cancels.

The velocities of the particles at the exobase are approximately distributed as a Boltzmann distribution [Schunk and Nagy, 2000], like in figure 1.13. The shape of this distribution depends on the temperature of the atmosphere. The fraction of the distribution that has an upward velocity higher than the escape velocity will manage to escape. This type of escape is called **Jeans escape** after Jeans [1925], who originally postulated it as a mass loss process of stars. It implies an atmosphere which is evaporating. A particle population in equilibrium with a non-negligible temperature always has a part of its distribution above escape velocity, even without extra energy input. However, this part may become

negligibly small. Since the Boltzmann distribution depends on the temperature (and thus energy), lighter particles have a wider distribution and thus a larger fraction above the escape velocity.

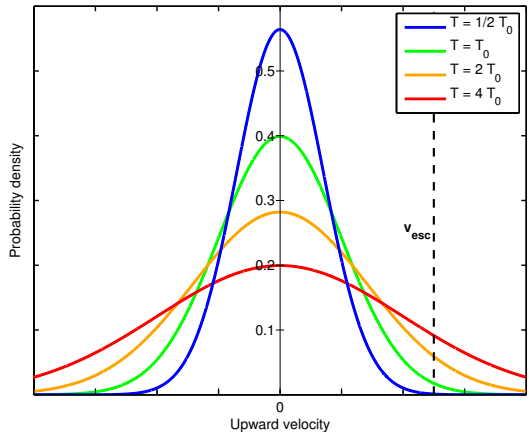

Figure 1.13: Boltzmann distributions of the velocity in one direction.

For Jeans escape, typically the fraction of the population with velocities larger than v_{esc} will be very small, much smaller than shown (for illustrational purposes) in figure 1.13. When a larger part of the population escapes, this can become quite violent and turbulent, and the large portion of upflowing lighter particles can drag along heavier particles, causing them to escape in similar numbers [Hunten, 1982; Volkov et al., 2011]. This is called **hydrodynamic escape**, or sometimes also ***blowoff***. Usually this is how a primitive atmosphere evolves to its more long-term state. Since both Jeans escape and hydrodynamic escape are just escape due to the particles' thermal energy, these processes are called **thermal escape** processes.

Thermal escape for hydrogen atoms from Earth's present day atmosphere can be estimated by calculating the Jeans flux. Assuming an exobase at 500 km altitude, a hydrogen density of 8.5×10^{10} m^{-3} [Anderson and Hord, 1977], and a temperature of 900 K (temperatures in the thermosphere and at the exobase can easily range from 600 K to 1200 K [Roble et al., 1987]) we find a flux of $\sim 2 \times 10^{26}$ atoms s^{-1}, or roughly 0.3 kg s^{-1}, over the whole surface of the Earth. Due to the shape of a Boltzmann distribution, the Jeans flux is quite sensitive to the exobase temperature. For example, the same flux for 600 K is $\sim 5 \times 10^{24}$ s^{-1}, while for 1200 K it is $\sim 1 \times 10^{27}$ s^{-1}.

To put this into context, the Earth's atmosphere has a total mass of about

5×10^{18} kg [Trenberth and Smith, 2005]. So if this (mass) escape rate of 0.3 kg s^{-1} were to remain constant, it would take more than 500 billion years for the whole atmosphere to escape. This is ignoring the fact that Earth's atmosphere consists for more than 99% out of atoms or molecules with a larger mass than hydrogen, which would therefore be much less likely to escape via this process. So this present day rate is not very important for the long term evolution of Earth's atmosphere, but this rate does not have to remain constant. Moreover, for other planets such rates might be very different, and be thus may be very important indeed.

At Venus the Jeans escape of hydrogen atoms is estimated at about 2.5×10^{19} atoms s^{-1} [Lammer et al., 2006]. This is much lower than at Earth, and is partially due to the fact that there is less hydrogen present in the Venusian atmosphere. At Mars the escaping Jeans flux is more important, since its weaker gravity requires less velocity to escape, but it also does not have so much hydrogen atoms at Earth. It is modeled to be of the order of 1.5×10^{26} atoms s^{-1} [Lammer et al., 2003].

There are many other ways that atmospheric particles can escape, these processes are called **non-thermal escape**. Many of them involve some kind of direct or indirect interaction with the solar wind. Even if these other processes also only increase a particle population's temperature, they are still classified as non-thermal escape.

4.2 From a non-magnetized planet

The induced magnetosphere caused by the currents in the ionopause provide some protection from the solar wind, so that it cannot reach the denser part of the atmosphere directly. The ionopause also forms a barrier that is difficult for the ionospheric ions to cross, and thus also prevents ions from escaping. Nonetheless, the solar wind can still cause loss of atmospheric particles in a variety of ways. Moreover, once an ion manages to reach beyond the ionopause, it is basically lost as it is then dragged along by the solar wind convection. Solar illumination also plays important role here. We give some estimations of the loss rates caused by these processes. However, note that these estimates mainly come from models.

4.2.1 Photochemical escape

One important non-thermal escape mechanism is due to solar illumination and atmospheric chemistry and is called **photochemical escape**. There is

a whole array of chemical reactions in which the resultant particles can have an increased energy, higher than the thermal population. Energetic radiation can, for example, split up a molecule into two atoms, or ionize it, or both. Similar processes can be caused by impacts with electrons (often energetic photo-electrons), as well as exothermic chemical reactions [Nagy et al., 1981; Hunten, 1982; Lammer, 2013a]. Certain reactions are endothermic, but any excess energy of the impactor can be imparted as kinetic energy or an excited state of a resultant, often leading to energetic neutrals.

Dissociative recombination of O_2^+ seems to be particularly relevant for oxygen escape on Mars, in which O_2^+ and an electron come together and end up forming two neutral O atoms. This reaction releases a lot of energy creating energetic oxygen atoms. Models of escape at Mars due to this process suggest O fluxes of 5.0×10^{24} s^{-1} [Lammer et al., 2003]. At Venus gravity is too strong for this process to be important, but other types of photochemical reactions may lead to H fluxes of 3.8×10^{25} s^{-1}[Lammer et al., 2006].

4.2.2 Sputtering

One of the most obvious ways how solar wind can erode the atmosphere of an unmagnetized planet is by directly colliding in the atmosphere and imparting kinetic energy to atmospheric particles. This is called **sputtering**. The magnetic barrier created by the induced magnetosphere is often high above the dense part of the atmosphere, however, so that the solar wind only reaches the low density part of the atmosphere. As a consequence, direct collisions may not be as frequent and sputtering not as important as expected at first sight. It is estimated to cause 5×10^{24} s^{-1} O^+ ions to flow out from Venus [Luhmann and Kozyra, 1991] and only $\sim5\times10^{23}$ s^{-1} from Mars [see Chassefière and Leblanc, 2004, and references therein].

4.2.3 Ion pickup

Another way how the solar wind can directly cause erosion at a non-magnetized planet is when neutral particles from the atmosphere, become ionized above the ionopause, which they can cross easily. This can be caused by EUV radiation or charge exchange with a solar wind proton. In the latter process, the neutral atmospheric particle loses an electron to a solar wind proton [Hunten, 1982]. When ionized above the ionopause, the atmospheric particle will be "picked up" by the convection electric field of the solar wind and be dragged away. This process is called **ion pickup**. Models predict that this process may be quite

efficient with outflows of $\sim 10^{25}$ ions s^{-1} for both Venus and Mars [Luhmann and Kozyra, 1991].

These pickup ions may impact again onto the planetary atmosphere because of their typically very a large gyroradius [Luhmann and Kozyra, 1991]. In this way they can impart their newly gained energy to the atmosphere and play the role of the solar wind ions in the sputtering process, the importance of which may be increased this way.

4.2.4 Detached ionospheric clouds

A similar mechanism to ion pickup is the detachment of ionospheric clouds. The solar wind streaming so close next to the ionospheric plasma of an unmagnetized planet can cause disturbances and instabilities at the interface between both plasmas like Kelvin-Helmholtz instabilities. These can lead to large **clouds of cold ionospheric plasma detaching** from the rest of the ionosphere and leaving the induced magnetosphere. Outside of the magnetosphere this cloud of plasma is then dragged off by the solar wind, just like in ion pick up. Therefore it is sometimes also called mass-loaded ion pickup. Loss due to detached ionospheric clouds may be just as important as ion pickup, but this is not sure since it depends on the stability of the streaming interface [Terada et al., 2002; Möstl et al., 2011].

4.3 From a magnetized planet

The intrinsic magnetosphere presents a much larger barrier for the solar wind than an induced magnetosphere. Earth's magnetic field itself can trap charged particles. Through its interaction with the magnetosphere, though, some of the solar wind's energy still manages to energize the ionosphere. For the outflow from a (terrestrial) magnetized planet, we focus on Earth. We organize the discussion according to the regions from where the outflow originates, since the magnetic field, due to its own spatial structure, causes the outflow to be structured as well. Moreover, there are many observations concerning Earth's ion outflows, and these give good estimates per region.

4.3.1 Cusp outflow

One major hole in the magnetosphere is the cusp. The magnetic field lines are directly connected to the interplanetary magnetic field and provide a direct way for the solar wind particles into the atmosphere [Heikkila and Winningham,

1971; Nilsson et al., 1996; Escoubet et al., 2008]. And because the magnetic field converges in the cups, it funnels solar wind particles from a large area in space into a much smaller region in the atmosphere. Some of these particles are also accelerated by the reconnection process. A part of the solar wind particles is reflected by the mirror force but many reach all the way down into the ionosphere. There they collide and consequently heat the ionosphere and cause extra ionization, leading to upflow [Seo et al., 1997; Strangeway et al., 2005].

However, in the cusp there is also a more indirect energy input. Due to its magnetic connection with the solar wind and the reconnection region, there is a lot of plasma wave activity in the cusp [André et al., 1990; Strangeway et al., 2005; Nilsson et al., 2012]. Depending on their frequency, these waves can be particularly efficient in further energizing upflowing ions. The energization in the direction perpendicular to the magnetic field does not directly help the ions to flow upward, but the mirror force in the cusp efficiently redirects this perpendicular velocity into parallel velocity. As a result, the cusp is a region of strong ionospheric outflows.

Despite the small source region, the large energy input may still lead to important fluxes. It turns out that this energy input is more efficient in causing O^+ ions to escape than H^+ ions. The average H^+ flux has been estimated to be of the order of 5×10^{24} s^{-1} [Pollock et al., 1990; Yau and André, 1997], whereas the O^+ flux is estimated as around 1 or 2×10^{25} s^{-1} [Pollock et al., 1990; Yau and André, 1997; Nilsson et al., 2012]. The perpendicular heating seems to be particularly efficient for O^+ ions since its spectral density is close to the gyrofrequency of the O^+ ions [Waara et al., 2011].

The fluxes in the cusp vary strongly depending on the geomagnetic conditions. O^+ fluxes of up to even 3×10^{26} s^{-1} have been observed during periods of high geomagnetic activity [Strangeway et al., 2005]. Not only the strength, but also their path into the magnetosphere depends on geomagnetic conditions. Many of the fast ions can escape directly along the magnetic field lines to interplanetary space [Slapak et al., 2015], but due to convection, the slower part of the population may flow over the polar cap [Green and Waite, 1985] and into the magnetospheric lobes or even ultimately into the plasma sheet. The ions with the lowest energy may not even escape the gravitational pull and fall down into the polar ionosphere [Lockwood et al., 1985].

4.3.2 Auroral outflows

The auroral oval is the region where the aurora borealis and australis occurs. This is caused by energetic charged particles precipitating into the atmosphere.

When they collide with atmospheric particles, they can excite them. The visible light of the auroras is the light sent out by the excited particles when they de-excite or recombine.

There are two main types of aurora [Colpitts, 2015]. One type is caused by pitch angle diffusion, a process in which the velocity of hot plasma sheet particles is modified in the direction parallel to the magnetic field, so that they fall into the loss cone and thus precipitate in the auroral atmosphere. Wave-particles interactions are thought to be the main cause for this [Kennel and Petschek, 1966], however, it is not yet well-understood and it is still an active research field [e.g., Meredith et al., 2009; Thorne et al., 2010; Nishimura et al., 2013; Horne et al., 2003]. The precipitation consists of both electrons and ions, but the electrons are the vast majority. They are responsible for the **diffuse aurora** with a very faint and unstructured glow that may often not even be visible. This type of aurora is not the spectacular phenomenon that most people connect to aurora, but since it occurs typically everywhere in the auroral oval and usually all the time, it is a very important form of energy input into the ionosphere, causing heating and ionization.

The very bright and spectacular curtains of green light that are typically connected to auroras are **discrete aurora**, the other type of aurora, and are caused by downward accelerated particles. They occur prevalently during geomagnetically active times, typically during periods of southward IMF, when there is a lot of dayside reconnection and convection. The two main mechanisms of acceleration are quasi-static field-aligned electric fields and field-aligned acceleration by Alfvén waves [Colpitts, 2015].

The quasi-static field-aligned electric fields are part of a narrow U-shaped potential, like in figure 1.14, with electric fields perpendicular to the magnetic field at the sides of the structure. This is of course a simplification, often these potential structures are much more complex. The perpendicular electric fields can cause drifts of plasma perpendicular to both the electric and the magnetic field. Through this potential structure also flows a field-aligned current, part of a current system which is generated somewhere in the magnetosphere and closes in the ionosphere. The downward accelerated electrons carry current upward. Outside the potential structure upward flowing electrons carry a downward current. The ionosphere is a large resistor for this current system. The field-aligned electric field actually also acts as a resistance by accelerating electrons without increasing the current.

The precipitating particles do not only excite atmospheric particles, they also heat and ionize many particles, increasing the ionospheric density (and thus also the conductivity). Additionally, the convection in the auroral oval heats the ionosphere via frictional heating [Schunk and Nagy, 1978] and the current

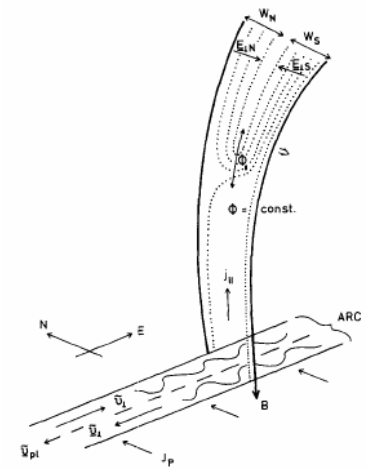

Figure 1.14: Schematic representation of the U-shaped potential structure associated with a discrete arc. From Haerendel et al. [1996].

systems are a source of Joule heating [Cole, 1962; Cai et al., 2013]. This can cause a lot of ionospheric upflow and associated charge depletion (due to thermal expansion), which is sometimes referred to as auroral bulk upflow.

The particle precipitation in the diffuse auroras is much less intense than in discrete auroras, but the low energy electron precipitation, sometimes called soft electron precipitation, can be more efficient in causing upflow. It penetrates less deep and thus ionizes at an altitude where the density is lower and its contribution is thus less easily canceled out by recombination [Seo et al., 1997; Moore and Khazanov, 2010].

The large majority of this upflow does not have velocities high enough to escape. At higher altitudes the field-aligned electric fields or plasma waves can further accelerate the ions [Wahlund et al., 1992; Maggiolo, 2015]. The large amount of energy available in the auroral zone means that it may be an important region for ion outflow, and especially for heavier ions like O^+. These ions flow on closed magnetic field lines which lead to the plasma sheet.

4.3.3 Polar wind

Inside the auroral oval is the magnetic polar cap. This is a region of open magnetic field lines connected to the solar wind via the magnetospheric lobes. Unlike the cusp and the auroral oval, the polar caps are a region of relatively

little energy influx. The main source of energy is solar illumination, just like for Jeans escape. But the dynamics of charged particles are more complex than those of neutral particles, making the outflow very different.

In an ionosphere in hydrostatic equilibrium, gravity will drive diffusion and cause the electrons with much smaller mass to be, on average, on higher altitudes than the ions, separating the positive and negative charges. However, a charge separation creates an electric field that acts to counter-balance this separation. The resulting ambipolar electric field acts to pull electrons down and ions up and is known as the Pannekoek-Rosseland electric field [Pannekoek, 1922; Rosseland, 1924]. At high latitudes, where the magnetic field points more or less upwards, the Pannekoek-Rosseland electric field is parallel to the magnetic field.

However, since the polar ionosphere is on open magnetic field lines, its plasma can always escape, and no hydrostatic equilibrium can be reached [Dessler and Michel, 1966; Nishida, 1966]. The electrons, being much lighter, are less gravitationally bound and can escape much more easily than the ions. But again, electrons escaping without the ions would cause a large charge separation, so an ambipolar electric field acts to drag the ions along. In this way, excess kinetic energy of the escaping electrons is transferred to the ions, accelerating them upward [Dessler and Cloutier, 1969; Lemaire and Scherer, 1969, 1970]. In analogy with the solar wind, this type of outflow was termed the **polar wind** [Axford, 1968].

The polar wind was predicted on a theoretical basis, and direct observations [Hoffman, 1970; Hoffman et al., 1974; Hoffman and Dodson, 1980] and indirect evidence [Brinton et al., 1971] confirmed its existence not much later with measurements from the Explorer 31, the Explorer 32, ISIS 2. These early missions measuring the polar wind directly employed spacecraft that flew over the polar cap at low altitudes (i.e. 3000 km altitude or lower). At higher altitudes the polar wind becomes very difficult to measure. EUV light irradiating a spacecraft flying through space causes electrons to be emitted from its surface. At high altitudes the ambient plasma density can become so low that there is not a large enough flux of electrons to the spacecraft to compensate for this. Thus the spacecraft will acquire a positive surface charge. This creates a potential which makes it impossible for ions with a too low energy to overcome this potential to reach the detectors on board the spacecraft. The outflowing particles of the polar wind have typically very low energies of only a few eV.

Nonetheless, later the DE mission managed to observe polar wind ions at altitudes between 8000-20000 km [Gurgiolo and Burch, 1982; Nagai et al., 1984], and could confirm their supersonic character, although a significant part of the population was missed due to the spacecraft potential. The POLAR mission had an instrument on board actively controlling the spacecraft potential, so that

they could measure most of the polar wind ion distribution down to energies of 1-2 eV at altitudes of ∼50000 km [Su et al., 1998a]. Such experiments are very energy consuming, however, since a current must constantly be maintained to counteract spacecraft charging. They can thus only be used for a limited amount of time and are not suited for large statistical studies of the polar wind. More similar studies were done [and we refer to Yau et al., 2007, for an overview].

In the lobes the spacecraft potential becomes so high that the polar wind becomes invisible to particle detectors. Even spacecraft potential control instruments cannot keep the potential low enough, and thus a large part of the population may be missed. There is an alternative way to measure the polar wind in an indirect way, exploiting the spacecraft potential itself [Eriksson et al., 2006; Engwall et al., 2006], which will be explained in chapter 5. This has resulted in a set of observations of the polar wind in the lobes at altitudes as far as 20 R_E [Engwall et al., 2009a,b; André et al., 2015; Haaland et al., 2016].

Most of these observations, at both low and high altitudes, have all led to more or less similar H^+ ion fluxes at the order of $\sim 10^{25}$ to 10^{26} ions s^{-1} (when integrating the measured flux densities over two polar caps) [Nagai et al., 1984; Huddleston et al., 2005; Cully et al., 2003; Engwall et al., 2009a,b; André et al., 2015]

For O^+ ions the situation is more complex. According to the classical polar wind models O^+ ions are too heavy to be accelerated by the ambipolar electric field [Lemaire and Scherer, 1972]. Yet oxygen ions have been observed in most polar wind measurements [e.g., Gurgiolo and Burch, 1982; Waite et al., 1985; Yau et al., 1991; Abe et al., 1993; Su et al., 1998a]. Many additional acceleration mechanisms have therefore been proposed to explain this presence [see Yau et al., 2007, for an overview]. An important proposed solution is the presence of suprathermal photo-electrons [e.g., Khazanov et al., 1997; Su et al., 1998b; Glocer et al., 2012], since the strength of the ambipolar electric field is critically dependent on the temperature of the electrons. Others have argued that these O^+ ions may originate in the cusp, where there is considerably more energy input, and have been convected over the polar cap, mixing with the polar wind [Nagai et al., 1984; Lockwood et al., 1985; Nilsson et al., 2010].

Yau et al. [1988] and Cully et al. [2003] found O^+ fluxes over a wide range from 10^{23} to 10^{26} s^{-1}, but these most likely also included ions originating in the cusp. Abe et al. [1993] observed fluxes of 10^{24} s^{-1}, and argued that these ions are indeed from the local polar cap. Similarly Su et al. [1998a] found O^+ fluxes of the order of 10^{24} s^{-1} at altitudes of 8 R_E, but could not conclude anything about the origin of the ions.

Since solar illumination is the main source of energy for the polar wind, the intensity of the solar illumination has an effect on the outflowing fluxes. Several studies found increases in H^+ fluxes from low to high F10.7 with a factor of 2 [André et al., 2015], 3 [Engwall et al., 2009b; Chandler et al., 1991], or even 4 [Cully et al., 2003]. Yau et al. [1988] on the other hand found a (statistically marginal) decrease with a factor 2. These differences may be due to differences in the observed energy ranges, the experimental method, or even the origin of the ions. For O^+ even larger increases were found but also even larger differences [Yau et al., 1988; Cully et al., 2003]

Just as important as the intensity of the solar illumination is the actual presence of solar illumination, as the magnetic polar cap rotates on a daily and seasonal basis in and out of the sunlight. The best way to parametrize this is the solar zenith angle (SZA) of a position in the ionosphere. This is the angle between the direction towards the Sun and the direction perpendicular to the surface. So a SZA of 0° means the Sun is straight up in the sky; a SZA of 90° (or larger) means the Sun is at (below) the horizon. The border between the sunlit and the dark side is called the terminator. At higher altitudes, because of the transparency of the atmosphere, the terminator will have an angle higher than 90° and thus positions with a SZA larger than 90° may still receive sunlight, depending on their altitude (and depending on how much radiation is absorbed by the atmosphere below).

Not many observational studies have characterized the polar wind in terms of SZA. Su et al. [1998a] observed a strong drop in H^+ and O^+ densities over the SZA range from 90° to 105° at 5000 km altitude. A higher upward velocity was found for all ions above the dayside polar cap than the nightside by Abe et al. [1993], and Abe et al. [2004] observed the velocity decreasing from small to large SZA. Polar wind models including photo-electrons have shown results with similar polar wind density dependence on the solar zenith angle [Su et al., 1998b; Glocer et al., 2012]. In the next chapters the effect of solar illumination on the polar wind outflow is one of the main subjects.

Finally, it should also be mentioned that even in the polar cap there is some particle precipitation. Cold electrons originating in the solar wind flow down into the polar ionosphere [Newell et al., 2009]. This is called the **polar rain**, and it is a hallmark of open magnetic field lines. They have field-aligned velocities and typically energies of a few 100 eV and relatively low densities. There is not much known about their effect on the ion outflow. However, considering their their low energy input the effect is not expected to be strong.

Although the theory of the polar wind was developed to describe outflow at Earth, it is not exclusive to magnetized planets. In fact, the polar wind theory was originally developed in conjunction with the solar wind [see, e.g. Lemaire

and Scherer, 1973]. Later it was also hypothesized that a similar ambipolar electric field as in the polar wind may exist at the nightside of Venus based on outflowing ion velocities [Hartle and Grebowsky, 1990, 1993, 1995]. Also at Mars an ambipolar electric field may cause ion outflow [Dubinin et al., 2011]. Since "polar" may be an inappropriate term for non-magnetized planets, some authors call it **planetary wind** or **electric wind**. Evidence for the existence of such outflows has been mainly indirect, but they may be important [Dubinin et al., 2011].

4.3.4 Polar cap arc outflows

Aurora Borealis and Australis is a phenomenon that occurs mostly in the auroral ovals, but sometimes, when the activity in the auroral oval dies down, such optical arcs can also be seen at higher latitudes over the polar caps. The first recorded observations of such arcs at high latitudes were by Douglas Mawson and his crew during during their dramatic Australasian Antarctic Expedition lasting from 1911 until 1914 [Mawson, 1925]. They typically occur during times when the interplanetary magnetic field is northward for a long period [Berkey et al., 1976] and when there is little or no activity in the auroral oval [Davis, 1963]. Another property common to most of these arcs at polar latitudes is that they are aligned approximately in the Sun-Earth direction [Zhu et al., 1997]. This is why they are often called sun-aligned arcs. However, it was found that some arcs deviate from this direction quite significantly and that the arcs are rather aligned in the direction of the cusp [Zhang et al., 2016]. The term sun-aligned may thus not be very appropriate. These arcs are often also referred to by a variety of other terms, like transpolar arcs, polar cap aurora, or polar cap arcs. In this text we will use the term **polar cap arcs**.

Many classification systems have been suggested to group polar cap arcs according to their characteristics and explain their origin [see, for example, Zhu et al., 1997; Kullen et al., 2002; Newell et al., 2009]. This has been a long debate and many of the differences in classifications may be due to different observational methods. However, it seems there are two main families of polar cap arcs[4]: theta aurora and small-scale polar cap arcs.

Theta aurora, sometimes also called transpolar arcs, are large arcs that stretch from one side of the auroral oval to the other side and are often many hundred kilometers wide [Zhu et al., 1997]. Together with the auroral oval they form a shape like the Θ symbol, as can be seen in figure 1.15, which explains their name. The mechanism suggested by Milan et al. [2005] seems to explain the

[4]from private communications with R. Maggiolo who led an international team of the International Space Science Insitute (ISSI) on polar cap arcs.

formation of this type of arc quite well [Fear and Milan, 2012b,a; Fear et al., 2014]. They are located on closed magnetic field lines connected to an extension of the plasma sheet into the magnetospheric lobes. This is also clearly visible in the plasma populating these field lines. Since this type of polar cap arc is basically an expansion of the auroral oval into the polar cap (and connected to an expansion of the plasma sheet into the lobes) all types of the auroras in the auroral oval can be present.

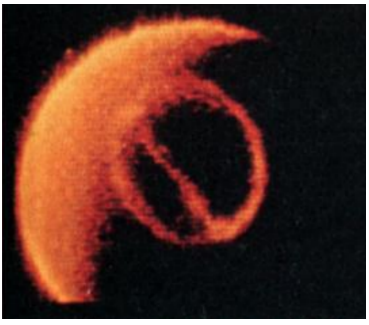

Figure 1.15: An observation of a Θ-aurora. From Frank et al. [1982].

The **small-scale polar cap arcs** are small-scale in the sense that their width is typically of the order of a few 10 km [Maggiolo et al., 2011], as opposed to the much wider theta aurora. They are only caused by precipitating electrons. An example of such a small-scale polar cap arc, can be seen in figure 1.16. A quasi-static field-aligned electric field accelerates electrons downwards. This electric field configuration is very similar to the U-shaped potential structures involved in the discrete auroral arcs in the auroral oval, but the potential drops are on average an order of magnitude smaller than those of discrete auroral arcs [Maggiolo et al., 2011] and so the precipitating electrons have lower energies. Therefore the light emission of small-scale polar cap arcs is also less intense, and can often even be too low to be visible.

At higher altitudes, above the acceleration region, the signature of these small-scale polar cap arcs is clearly visible as strongly field-aligned upward flowing ions [Maggiolo et al., 2006, 2011, 2012]. These are ions of ionospheric origin that have been accelerated upward by the same electric field that accelerates electrons downward. In figure 1.17 such an observation by a satellite of the Cluster mission is shown. Because the energy gained in the field-aligned electric fields is much higher than the thermal energy of the ions, the total velocity of the particles is very closely aligned to the magnetic field, as can be seen in the pitch-angle (the angle between the velocity and the magnetic field) distribution in the top panel of figure 1.17. In the energy distribution in the middle panel,

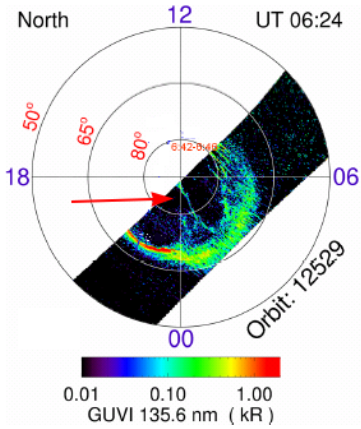

Figure 1.16: A GUVI image at wavelength 135.6 nm of the polar cap, evidencing a small scale polar cap arc. From Maggiolo et al. [2012].

the narrow energy band of the ions also evidences this and forms an inverted-V shape similar the well-known inverted-V's in the electron data below the acceleration region of discrete auroral arcs. In the bottom panel, the strong electric field perpendicular to the magnetic field is the sign of the sides of the U-shaped potential.

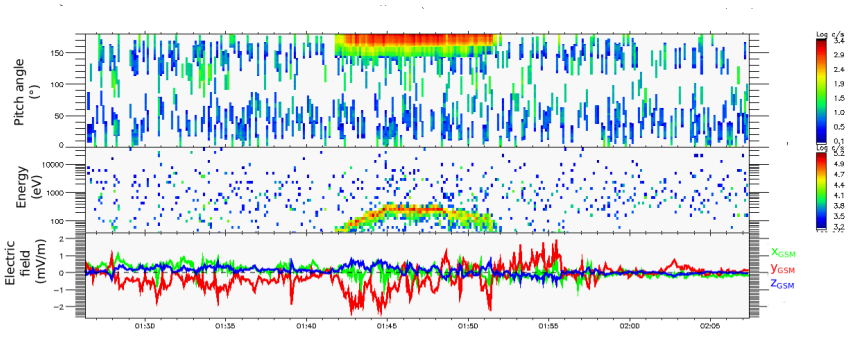

Figure 1.17: A clear example of ion outflow above a small-scale polar cap arc as observed by the CIS-CODIF (ion distribution) and EFW (electric field) instruments on board the Cluster satellite C1.

The structure of these polar cap arcs is not always as simple as in 1.17 but can sometimes have a more S-like shape and the field-aligned upflowing ions (and downflowing electrons) are in ∼40% of the events accompanied by a background

of hot isotropic plasma [Maggiolo et al., 2011]. Multiple arcs can exist in the polar cap at the same time.

It is not clear whether these arcs lie on open or closed magnetic field lines. In arcs with only upward accelerated ions and downward flowing electrons, like in figure 1.17, the electrons are very reminiscent of polar rain and this suggests an open field line topology. However, in events with a hot isotropic background population the background population has the signature of plasma sheet-like plasma [Maggiolo et al., 2011], implying closed field lines. Just like the field line topology, the mechanism responsible for these small scale polar cap arcs is not yet understood.

Similarly to discrete arcs in the auroral oval, the field-aligned electric fields of small-scale polar cap arcs is very efficient in accelerating both H^+ and O^+ ions. Small-scale polar cap arcs are small in geographical extent, though, and thus have a small source area. Maggiolo et al. [2011] estimated the total outflow due to the small scale polar cap arcs as on average of the order of $\sim 10^{24}$ s^{-1} (with an upper boundary of $\sim 10^{26}$ s^{-1}). This is smaller than, for example, the polar wind fluxes, and polar cap arcs are a sporadic event, thus they may not be such an important source of outflow. However, as mentioned earlier, it may be difficult for O^+ ions to escape via the polar wind. But the field-aligned acceleration above the polar cap arcs is more than enough for them to escape, and thus the outflow above small-scale polar cap arcs may be more important for O^+ than the polar wind. In chapter 3 we will go deeper into this and investigate the effect of solar illumination on the outflow above such polar cap arcs.

4.3.5 Plasmaspheric escape

At lower invariant latitudes, plasma can also escape from the ionosphere. Despite the fact that the particles of the plasmasphere are trapped on closed field lines, the plasma might still get lost. When geomagnetic activity increases, the convection electric field becomes stronger on the nightside of the plasmasphere, and the nightside plasmapause recedes inward, causing a sunward surge forming a plume at the dayside plasmasphere [Goldstein and Sandel, 2013]. This is called a plasmaspheric plume. As the geomagnetic activity continues, the plume does not rotate, but steadily becomes thinner. When activity stops, the plume starts rotating and gradually becomes less dense. Note that other mechanism have been proposed for the formation of plasmaspheric plumes [see e.g., Lemaire, 2000], but overall a plasmaspheric plume is a large cloud of plasma detaching from the plasmasphere.

Another mechanism of plasma escape from the plasmasphere has been proposed and follows from the inbalance between the gravitational, centrifugal, and pressure gradient forces [Lemaire and Schunk, 1992]. The resulting radially outward drift leads to a constant low-energetic outflow called the **plasmaspheric wind**. There is indirect evidence for the plasmaspheric wind based on the discrepancy between calculated and observed refilling times of the outer flux tubes in the plasmasphere [Lemaire and Schunk, 1992; Yoshikawa et al., 2003]. The longer observed times suggest that there needs to be an additional sink for the plasma. Also observations of weaker density gradients at the plasmapause during long geomagnetically quiet periods have been interpreted as possible evidence for plasmaspheric winds [Tu et al., 2007]. Direct observations of the plasmaspheric wind are very difficult due to the very low velocities involved. One study reported such observations and, based on only 6 events, gave an estimate of the radially outflowing ion flux of 5×10^{26} s^{-1} [Dandouras, 2013].

4.3.6 Other mechanisms

There are other energization processes that are present in all of the regions, but may not be enough to cause escape alone. **Centrifugal acceleration**, for example, will increase the field-aligned velocity of particles flowing on curved magnetic field lines if there is convection [Cladis, 1986; Nilsson et al., 2008, 2010]. This can be particularly important for outflow in the cusp. It can cause significant acceleration but occurs at higher altitudes where most of the gravitational potential is already overcome.

The mirror force, which was already explained earlier, is also an important mechanism. It is not an energization mechanism, since it does not add any energy, but it converts perpendicular (to the magnetic field) velocity into parallel velocity (for an upward moving particle). In this way velocity perpendicular to Earth's surface, which would be useless to a neutral particle, may still help a charged particle escape, depending on the orientation of the magnetic field. Certainly at high latitudes this is important. Frictional heating and Joule heating also increase the ionospheric (and atmospheric) temperature and thus increase outflow.

5 Escape from the magnetosphere

Neutral particles that manage to escape Earth's gravitational pull are lost for ever. This is not true for ions and electrons. Charged particles may acquire

enough upward velocity to overcome gravity, but they can still be caught in the magnetosphere. The particles flowing out from the auroral oval are on closed magnetic field lines and will flow into the plasma sheet. Even polar wind ions, which are on open field lines are not home free, since convection may move those magnetic field lines towards the center of the tail where they can reconnect. Polar wind ions are typically relatively slow, so their fate depends on the ratio between their parallel velocity and the convection velocity. If they don't manage to reach interplanetary space before the magnetic field line they are on reconnects, they end up in the plasma sheet. The same is true for slow cusp ions. Haaland et al. [2012] estimated that on average only 10% of the polar wind ions detected in the lobes will reach interplanetary space. For O^+ ions that may possibly be present in the polar wind it is even worse [Ebihara et al., 2006].

In this context, cusp outflow and polar cap arc outflow may become more important for ion loss, and especially for O^+ ions. In most cases, the outflow above polar cap arcs is sufficiently accelerated to make everything escape from the magnetosphere [Maggiolo et al., 2011]. Cusp outflow has a velocity distribution with a wider spread, but a large part even of the O^+ ions has high enough velocities to directly reach interplanetary space [Slapak et al., 2015] or reach far into the magnetospheric tail.

It is not completely clear what happens with the particles in the plasma sheet. Some may precipitate in the ionosphere, some may be convected towards Earth and injected into the ring current population. However, reconnection also occurs closer to Earth, typically around 20-30 R_E distance [Nagai et al., 1997; Imber et al., 2011], but sometimes even as close as 10 R_E [Miyashita et al., 2005b; Du et al., 2011]. This is called the near-Earth neutral line, as opposed to the distant neutral line which is typically around $\sim$100 R_E [Daly, 1986; Birn et al., 1992; Grigorenko et al., 2009] (which was used by Haaland et al. [2012] as the boundary in their estimation). When this happens, the plasma in the plasma sheet farther than the reconnection point may be transported away from the Earth in the form of a plasmoid towards and possibly beyond the typical position of the distant neutral line [Hones, 1979; Slavin et al., 1989, 1999; Miyashita et al., 2005a], to be lost to interplanetary space after all.

The ring current population will also decay. Part of it will precipitate into the ionosphere due to pitch angle diffusion and thus returns to the atmosphere. Another part is lost to space again by charge exchange, in which an energetic ring current particle receives an electron from a neutral particle, creating an energetic neutral particle no longer bound by the magnetic field [Hunten, 1982; Daglis et al., 1999]. Yet another part may be lost across the magnetopause due to large gyroradii. The plasmaspheric plumes are still in the magnetosphere, but their plasma can be lost via dayside reconnection [Chandler et al., 1999].

6 Does a magnetic field really protect?

It is clear that even in the presence of a magnetic field, there are still many ways for ionospheric particles to escape. The total escaping ion flux from Venus, without a magnetic field, has been estimated from measurements as being of the order of 10^{24}-10^{25} s^{-1} [Barabash et al., 2007b; Fedorov et al., 2011]. For Mars, with only its crustal magnetic field, similar fluxes were found, although, with an even wider spread in the observations going from 10^{23}-10^{25} s^{-1} [Verigin et al., 1991; Lundin et al., 1990; Barabash et al., 2007a; Lundin et al., 2009; Nilsson et al., 2011; Lundin et al., 2013; Fränz et al., 2015; Brain et al., 2015]. At Earth, combining all ion outflows gives a total flux of the order of 10^{26} to even 10^{27} s^{-1}. It should be noted, however, that the low energy ion populations pose the same observational difficulties at Venus and Mars as they do at Earth. The fewer number of satellites to do measurements make the challenge to constrain these losses even larger. It has been suggested that the low energy ions may constitute a large part of the outflowing population [Lundin et al., 2008; André and Cully, 2012; Fränz et al., 2015]. So a large fraction is probably missed by the measurements. It also not clear how much of the outflow from the Earthly ionosphere manages to also escape the magnetosphere.

Nonetheless, the conclusion is that, to our current knowledge, the ion escape from Venus and Mars is smaller than the escape from Earth, or at best of the same order, despite Earth's protecting magnetic field. Therefore people are starting to question the notion that an intrinsic magnetic field protects an atmosphere from erosion by the solar wind [e.g., Strangeway et al., 2010]. The magnetosphere indeed shields off most particles coming from the Sun from directly impacting in the atmosphere, but this shield is not perfect. Many solar wind particles still manage to enter Earth's atmosphere. Moreover, by extending much farther into space than (the dense part of) the atmosphere, the magnetosphere provides a much larger target for the solar wind. And the energy impacted onto the magnetosphere is in part transmitted through the magnetic field into the upper layers of the atmosphere. One could perhaps compare it to holding an opened umbrella against a strong, stormy wind. It might prevent the wind from directly hitting your body, but trying to hold on to the umbrella and keeping it straight may cause more discomfort than facing the wind head on. However, not all of this energy is transmitted down and its efficiency in causing atmospheric escape may depend on many parameters, like the strength of the magnetic field, its orientation, the orientation of the planet's rotational axis, the planet's mass, the planet's proximity to the Sun, the atmospheric composition, ...

When we want to understand the long term evolution of planetary atmospheres, changes over time in many of these factors also have to be taken in account, as

well as changes in the energy coming from the Sun. For example, solar dynamics and evolution tells us that the Sun's luminosity was up to 30% less during its history [Bahcall et al., 2001]. On the other hand, young stars have a much more active corona, and observations show that this leads to much higher intensities of high energy radiation like X-ray and EUV radiation [Lammer, 2013b]. It is not clear whether this more active corona resulted in a stronger or a weaker solar wind, although, some evidence suggests that the solar wind may have been more intense in the past [Wood, 2006; Lammer, 2013b].

One would of course also have to include the sources of atmospheric material, from Earth and from space. For example, present day estimates of the accretion rate due to interplanetary dust particles at Earth typically fall in a range from 0.05 to 3 kg s^{-1} [Plane, 2012]. This means they are comparable to the ion outflows, although they consist for a large part out of metals.

Understanding the broad array of processes that can cause atmospheric escape will help us do the accountant's job of calculating the outflowing fluxes and check if the atmospheric and magnetospheric budgets are balanced and if more or less is escaping in the presence of an internal magnetic field. Who knows, a magnetosphere may in some cases turn out to be like an anti-theft system that costs more money than would ever be stolen by thieves.

As mentioned in this introduction, solar illumination is one of the two major forms of energy coming from the Sun. In what follows we will try to contribute a piece to this puzzle by investigating the effect of solar illumination on the ion outflows from the polar ionosphere. In chapter 3 we will investigate the outflow above polar cap arcs and parametrize the effect effect of solar illumination by looking at its solar zenith angle dependence. Chapter 4 details a study in which we extrapolate the results from polar cap arc outflows to the whole polar cap, as suggested in chapter 3, and see what the results are for the polar wind fluxes from the whole polar cap. In chapter 5 we analyze ion data high up in the magnetospheric lobes to verify the solar zenith angle result from chapter 3 and the predicted results from chapter 4, to the extent possible. Finally, in chapter 6 we will discuss the results from those three chapters together in the broader context of this thesis and give an overall conclusion.

Chapters 3, 4, and 5, which constitute the main results of this thesis, are all written in the form of separate academic papers. They are self-consistent and can thus be read separately. Therefore, some introductory material is shortly repeated. At the time of writing, both chapters 3 and 4 have been published in peer-reviewed journals. Chapter 5 is planned to be submitted for publication in the near future.

Chapter 2

Instrumentation and magnetic field models

In this chapter we explain the basic concepts of the detectors with which the measurements used in this thesis were made. We also introduce the magnetic field models that are used to provide the context of the observations.

1 Cluster instrumentation

In chapters 3 and 5 we will be working with observations from the Cluster satellites. ESA's Cluster mission consists of a set of 4 satellites flying in a coordinated configuration. The satellites of the Cluster mission were to be sent into space in 1996, but only 47 seconds after liftoff the Ariane-5 rocket carrying them exploded, and all the satellites were lost [Taylor et al., 2010]. ESA ordered the rebuilding of the satellites and in 2000 they were finally brought into a polar orbit of $\sim$4$\times$16 R_E by two Soyuz rockets. The orbital period is approximately 56 hours. The satellites spin with a period of 4 seconds.

The mission studies the structures of Earth's plasma environment and is therefore fitted with a large suite of plasma instruments [Escoubet et al., 1997]. The five instruments that will be used in this work are the following: the Hot Ion Analyser (HIA) and the ion COmposition and DIstribution Function (CODIF) analyser, which are both part of the Cluster Ion Spectrometry (CIS) experiment; the Electron Drift Instrument (EDI); the Electric Field and Wave (EFW) experiment; and the FluxGate Magnetometer (FGM).

1.1 The Cluster Ion Spectrometry instrument

The CIS instrument is the experiment on board Cluster that measures the ion distribution functions. It consists of two experiments: CODIF, which has the capability to differentiate between ions with different mass, and HIA, which cannot distinguish different ion species but has a higher sensitivity and angular resolution. Since the Cluster satellites traverse many different regions, the CIS instruments have to be able to measure plasma with properties over wide ranges. Therefore both HIA and CODIF can be operated in several modes with different sensitivities.

1.1.1 The Hot Ion Analyser

The Hot Ion Analyser concept consists of what is called a quadrispherical electrostatic analyser. A cross-section of it can be seen in figure 2.1, which shows that it consists of two concentric half spheres. The outer sphere has a circular opening on top, above which there is a circular top cap. At the bottom there is a microchannel plate (MCP) electron multiplier which detects the impacting ions. Between the inner and outer spheres a potential difference is applied which deflects the ions on a path between the two spheres to the MCP. With this setup only particles with a small incoming angle (between $-\delta$ and $+\delta$ on figure 2.1) can enter the instrument and only those with an energy over charge ratio within a narrow range will reach the MCP.

To detect particles with an energy over charge ratio in a different range, the potential difference is changed. An exponential sweep over 31 logarithmically spaced levels is done to measure the full energy over charge ratio range from $\sim$5 to 32$\times$ 10^6 eV/e, with e being the elementary charge.

The instrument is circularly symmetric around the central axis, so that the detection works regardless of the incoming direction of the particle in the plane perpendicular to the symmetry axis. To measure the angle of the component of the velocity in this plane, the MCP is divided in different sectors, as shown in figure 2.2. One half is divided into 16 equal sectors, thus providing an angular resolution of $\sim$11.2°. The other half, which is meant for high resolution measurements of the solar wind, is divided into 8 sectors of $\sim$5.6°, 8 sectors of $\sim$11.2°, and two outer sectors of $\sim$22.5° without detectors. This way an instantaneous energy distribution in 2 spatial dimensions can be acquired.

The angle of the component of the velocity in the plane perpendicular to the spin axis of the spacecraft is found by measuring while the spacecraft spins. In highest resolution mode, once per $\sim$0.062 second (i.e., a 64th of a spin period)

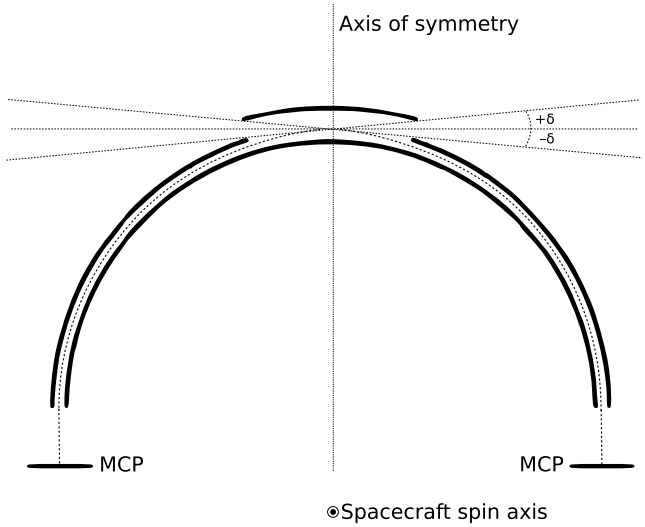

Figure 2.1: Schematic cross-section of the HIA instrument. Adapted from Rème et al. [1997].

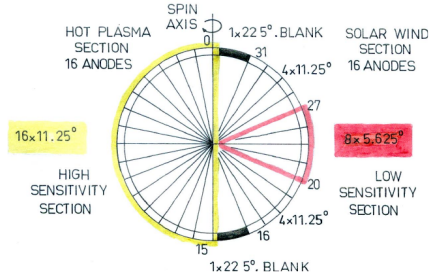

Figure 2.2: Principle of HIA sectoring. From Rème et al. [2001].

a 2D distribution is made, so that over one full spin period a 3D distribution is acquired with an angular resolution of $\sim$5.6° for the second angle.

1.1.2 The ion COmposition and DIstribution Function analyser

The concept of the ion COmposition and DIstribution Function analyser is the same as that of HIA, except that after exiting the electrostatic analyser between the two half spheres and before the MCP, there is also Time Of Flight-section (TOF) to determine the mass over charge ratio. This way the distribution for the major magnetospheric ion species (i.e., H^+, He^+, He^{++}, and O^+) can be found.

In order to do this, the ions are additionally accelerated (post-acceleration) by a potential drop after the electrostatic analyser before hitting a very thin carbon foil. The ions pass through the carbon foil and produce secondary electrons which are detected by the MCP. The time of this detection serves as the start time. The time when the ion hits the MCP and is detected is used as the stop time. From the time difference the velocity of the ion is known. Knowing the energy over charge ratio (i.e., the sum of the original energy and the energy gained in the post-acceleration) and the velocity, the mass over charge ratio can be calculated. Corrections for the energy lost in the passing of the carbon foil have to be taken into account; this can be determined during pre-flight calibration.

Contrary to HIA, the MCP of CODIF is divided into 16 equal angular sectors, and the 2D-distribution is, in high resolution mode, measured 32 times per spacecraft spin, so that the full 3D distribution has an angular resolution of $\sim 22.5° \times 11.2°$.

1.2 The Electric Field and Wave experiment

The Electric Field and Wave experiment is an instrument that, as its name suggests, can measure the electric field. It has also other functions, but these will not be discussed here. EFW employs a relatively simple concept. Each spacecraft has two perpendicular pairs of probes mounted on booms extending, in opposite directions in the spin plane, away from the spacecraft. The probe to probe distance is approximately 100 m.

In order to keep the potential of the probes close to the local plasma potential a bias current is sent to the probes. The potential difference between a probe and the spacecraft, or a probe and its opposite probe is measured. The average electric field on this scale can then be found by dividing the potential difference

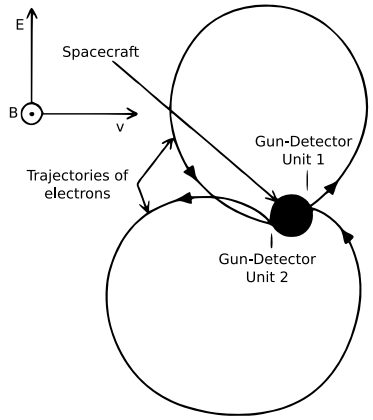

Figure 2.3: Simulated trajectories of emitted electrons that return to the spacecraft (radius of orbit and size of spacecraft not to scale). From Balogh [2005].

from probe to probe by their spatial separation. This way the two components of the electric field in the spin plane can be measured. EFW has a dynamic range 0.3 to 700 mVm^{-1} with a variable time resolution down to 10^{-4} s. Note that the component of the electric field perpendicular to the spin plane cannot be obtained. Under the assumption that the electric parallel to the magnetic field is negligible, the three-dimensional vector can be found.

1.3 The Electron Drift Instrument

The Electron Drift Instrument is another instrument that measures the electric field by emitting a beam of energetic electrons which is recaptured, and then estimating the drift of the gyration center of the electrons [Paschmann et al., 1997].

EDI consists of two gun-detector elements on opposite sides of the spacecraft. Given a certain magnetic and electric field strength, there is only one direction per electron gun in which the beam can be emitted so that it returns to the detector at the other side of the spacecraft, as shown see figure 2.3. From the directions of emission for which the beam returns, the perpendicular displacement can be found via triangulation. The electron guns are redirected by a servo loop to find the correct direction in which the electron beam returns.

The energy of the emitted electrons is on the order of keV and their gyroradius is on the order of a few km. Therefore this technique has the advantage that

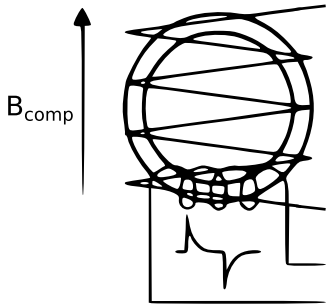

Figure 2.4: The concept of a fluxgate magnetometer. Adapted from Balogh [2005].

it is not affected by small or local variations in the plasma as opposed to the double probe technique. The other side of the coin is that the electron drift estimation requires a strong enough magnetic field for the electron beam to not disperse too much, cannot measure rapid variations of the magnetic field and even becomes very difficult when it varies too rapidly, and can become impossible in the presence of large fluxes of ambient electrons with the same energy as the beam.

1.4 The FluxGate Magnetometer

The Cluster magnetic field investigation consists of triaxial fluxgate magnetometers (FGM) [Balogh et al., 1997]. The fluxgate magnetometers consist of a ring core made of ferromagnetic material that is wound by a coil carrying an alternating current [Balogh, 2005], as shown in figure 2.4. Around this another coil is placed. The alternating current magnetizes the ring core and drives it through its hysteresis loop. Due to the symmetry of the hysteresis loop in the absence of a background magnetic field, no current is induced in the outer coil. However, in the presence of a magnetic field the hysteresis loop is offset which drives a current in the outer coil. This current is measured and the magnitude of the signal is proportional to the magnitude of the component of the background magnetic field in the direction along the outer coil.

By combining three fluxgate magnetometers, the three components of the magnetic field can be measured. Each spacecraft has two of these triaxial fluxgate magnetometers, one placed at the end of a 5.2 m long boom, the other at 1.5 m from the end of the boom. The instrument can sample up to 67 vectors per second at a resolution up to $8{\times}10^{-12}$ T.

1.5 Cold, low-density plasma measurements

As explained in the introduction low-density, low-energy ions can be very difficult to detect due to spacecraft charging. There are alternative ways to measure their density and velocity, however. In the following two sections we explain two methods, one to obtain the density and one to obtain the velocity, which overcome this problem by exploiting the spacecraft potential.

1.5.1 Ion density

The spacecraft potential depends, among others, on the density of the surrounding plasma. The (positive) spacecraft charge is caused by EUV radiation knocking away more electrons from the surface of the spacecraft than the surrounding plasma can resupply to compensate. The resulting spacecraft potential depends on many factors like irradiance and spacecraft properties (shape, surface material, etc.), but with careful calibration a relation between the spacecraft potential and the plasma density can be deduced [Pedersen et al., 2001, 2008; Lybekk et al., 2012]. The spacecraft potential can be measured by the EFW instrument.

The density n can be written as an exponential function (or superposition thereof) of the spacecraft potential V_{sc}. For the dataset used in chapter 5, a relation from Lybekk et al. [2012] is used, additionally multiplied with a normalization function $\phi_n(t)$ to account for variations in the irradiance:

$$n(t, V_{sc}) = \phi_n(t)\ A\ e^{\frac{-V_{sc}}{B}}. \tag{2.1}$$

$\phi_n(t)$ is given by the value of $F_{10.7}$ at time t divided by the average $F_{10.7}$ of the year of t. The parameters A and B are given for specific ranges of V_{sc} and years, and they can be found in Lybekk et al. [2012].

This technique makes it possible to obtain the electron density, which should equal the total ion density if we assume quasi-neutrality. Note, however, that it cannot distinguish between ion species.

1.5.2 Ion bulk velocity

When the speed of a spacecraft relative to the plasma it's traveling through is supersonic, it will create a wake behind it. The electrons will re-enter this wake more easily than ions due to their higher thermal velocity, creating an electrically charged wake. A charged spacecraft can significantly enhance this wake, because it pushes the ions away [Eriksson et al., 2006], as shown in figure

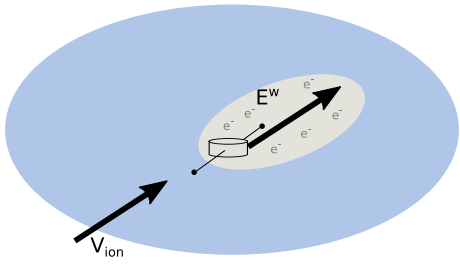

Figure 2.5: Schematic representation of the wake formation.

2.5. This enhanced wake occurs when the kinetic energy associated with bulk flow of the ions is smaller than the energy needed to overcome the spacecraft potential, but larger than the ions' thermal energy, i.e., when

$$kT_i < \frac{m_i {v_i}^2}{2} < eV_{sc}, \tag{2.2}$$

where T_i, m_i, and v_i are the ion temperature, mass, and bulk flow, respectively, and V_{sc} is the spacecraft potential.

This charge separation sets up an electric field that can be measured, although this requires multiple electric field experiments. The problem is that usually there is not only the electric field due to the wake but also an ambient convection electric field. The Cluster satellites are well equipped for this, with the EFW and EDI instruments. EFW measures the electric field on the scale of the probe booms, which is affected by the wake, and thus measures the superposition of the wake electric field and the ambient convection electric field. EDI, on the other hand, is unaffected by the small scale effect of the wake and thus measures only the convection electric field. The electric field created by the wake can thus be found by the difference between both measurements: $\mathbf{E}^{\mathrm{w}} = \mathbf{E}^{EFW} - \mathbf{E}^{EDI}$. Assuming the ions are unmagnetized on the scale of the wake, the electric field $\mathbf{E}^{\mathrm{w}}$ is in the direction of the plasma flow $\mathbf{v}$ and may be written as

$$\mathbf{E}^{\mathrm{w}} = g\mathbf{v} = g\mathbf{v}_\perp + gv_\parallel \frac{\mathbf{B}}{B}, \tag{2.3}$$

where g is some scalar function which may depend on the plasma properties or the plasma flow speed v, but is independent of the flow direction [Engwall et al., 2006, 2009a]. If the frozen-in condition applies, the perpendicular component of the flow velocity should be the convection velocity and can thus be found from the electric field measured by EDI: $\mathbf{v}_\perp = \mathbf{E}^{EDI} \times \mathbf{B}/B^2$.

EFW can only measure the electric field in the spin plane of the spacecraft, but as long as the component of $\mathbf{E}^{\mathrm{w}}$ in the spin plane is not too small, this can be

resolved. Decomposing $\mathbf{E}^{\mathrm{w}}$ into components E_x^{w} and E_y^{w} in the spin plane, an expression for $v_{\parallel}$ is found by dividing equation (2.3) for one component by that for the other and rearranging:

$$v_{\parallel} = \frac{E_x^{\mathrm{w}} v_{\perp,y} - E_y^{\mathrm{w}} v_{\perp,x}}{E_y^{\mathrm{w}} B_x - E_x^{\mathrm{w}} B_y} B. \tag{2.4}$$

This method can only be used when the cold ion population is the only one present. If there is also a hot ion population present, these hot ions will cancel out the wake.

2 Magnetic field models

Earth's magnetic field can very roughly be approximated by a magnetic dipole, but is actually much more complex. An accurate representation can be given using an expansion in spherical harmonics, of which the dipole term is the first order. The International Geophysical Reference Field (IGRF) is such a model that attempts to describe Earth's internal magnetic field as accurately as possible [Thébault et al., 2015].

The magnetic field in the magnetosphere is not only caused by Earth's internal magnetic field, but also has contributions from the large-scale current systems in the ionosphere and magnetosphere. One set of models that is often used in the field of space physics are the Tsyganenko models [Tsyganenko and Usmanov, 1982; Tsyganenko, 1987]. These semi-empirical models use analytical expressions to calculate the contributions from the main magnetospheric current systems and use a large database of satellite data to get a best fit and constrain the model parameters. The external contributions included in these models are the magnetopause current, the ring current, the tail currents, and the large scale field-aligned currents.

The models we use in this thesis are the Tsyganenko 89 model (T89) [Tsyganenko, 1989] and the Tsyganenko 96 model (T96) [Tsyganenko, 1996]. The T89 model takes the Kp index (a 3-hourly index to represent geomagnetic activity) as input and was one of the first models to include the 2-dimensional effects of the dipole tilt on the magnetotail. The T96 model takes solar wind pressure, and the GSM y- and z-component of the IMF and the Dst index (Disturbance Storm Time index, an hourly index index to represent geomagnetic storm activity) in order to more accurately model the interaction between the solar wind and the magnetopause and its effect on the Birkeland current systems.

These magnetic field models can be used, for example, to find the ionospheric projection of the position of a satellite in the magnetosphere, as we do in

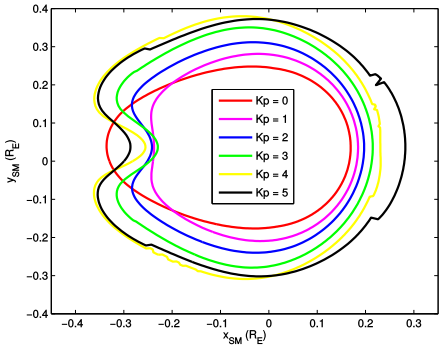

Figure 2.6: Magnetic polar cap found using the T89 model for several Kp inputs

chapters 3 and 5, or to find the shape and position of the magnetic polar cap, as we do in chapter 4. The latter can be done by tracing magnetic field lines upward from the ionosphere to see if they return to the ionosphere or not, in order to find the border between the open and closed magnetic field lines. An example of this is shown in figure 2.6. It shows how the surface area of the polar cap increases with increasing Kp. However, it also shows that there is an issue with the nightside shape of the polar cap area from the T89 model for Kp higher than 0. It is not clear what this "bulge" represents, although it is most likely an artifact from the model rather than a real physical phenomenon.

Chapter 3

Outflow above polar cap arcs

The low-energy ion outflow above the polar cap can be very difficult to measure due to spacecraft charging. There is another type of ion outflow from the polar ionosphere, however, in which the ions are much more accelerated. This outflow can therefore be directly measured by ion experiments on board satellites. In this chapter we analyze the effect of solar illumination on this type of outflow. We present the work as it was published in **Geophysical Research Letters** in March 2015.

***Maes, L.**, Maggiolo, R., De Keyser, J., Dandouras, I., Fear, R. C., Fontaine, D. and Haaland, S. (2015), Solar illumination control of ionospheric outflow above polar cap arcs. Geophys. Res. Lett., 42: 1304–1311. doi: 10.1002/2014GL062972.*

Solar illumination control of ionospheric outflow above polar cap arcs

L. Maes[1], R. Maggiolo[1], J. De Keyser[1], I. Dandouras[2,3], R. C. Fear[4], and D. Fontaine[5], and S. Haaland[6,7]

[1]Belgian Institute for Space Aeronomy, Brussels, Belgium, [2]University of Toulouse, UPS-OMP, UMR 5277, IRAP (Institut de Recherche en Astrophysique et Planétologie), Toulouse, France, [3]CNRS, IRAP, 9 Av. Colonel Roche, BP 44346, 31028 Toulouse cedex 4, France, [4]Department of Physics and Astronomy, University of Leicester, Leicester, UK, [5]Laboratoire de Physique des Plasmas, Velizy, France, [6]Max-Planck Institute for Solar Systems Research, Katlenburg-Lindau, Germany, [7]Department of Physics and Technology, University of Bergen, Bergen, Norway

Abstract. We measure the flux density, composition and energy of outflowing ions above the polar cap, accelerated by quasi-static electric fields parallel to the magnetic field and associated with polar cap arcs, using Cluster. Mapping the spacecraft position to its ionospheric footpoint, we analyze the dependence of these parameters on the solar zenith angle (SZA). We find a clear transition at SZA between $\sim$94° and $\sim$107°, with the O^+ flux higher above the sunlit ionosphere. This dependence on the illumination of the local ionosphere indicates significant O^+ upflow occurs locally above the polar ionosphere. The same is found for H^+, but to a lesser extent. This effect can result in a seasonal variation of the total ion upflow from the polar ionosphere. Futhermore, we show that low magnitude field-aligned potential drops are preferentially observed above the sunlit ionosphere, suggesting a feedback effect of ionospheric conductivity.

1 Introduction

The polar ionosphere is a major source of outflowing ions [Moore et al., 1999; Yau and André, 1997]. Because these ions flow on open field lines, they can escape into interplanetary space and contribute to atmospheric erosion [Haaland et al., 2012; André and Cully, 2012]. If trapped in the magnetosphere they can affect magnetospheric dynamics due to the significant amount of heavy ions (mostly O^+) in the ionospheric plasma [Lotko, 2007; Kronberg et al., 2014]. Therefore it is important to have a correct assessment of the flux and composition of outflowing ions above the polar caps.

One main outflow mechanism is the polar wind [see Yau et al., 2007, and references therein]. Due to the open geometry of the magnetic field, no hydrostatic equilibrium can be established so that ionospheric plasma can escape [Dessler and Michel, 1966]. The lighter electrons tend to escape more easily than the ions, which causes a charge separation that sets up an ambipolar electric field that decelerates the electrons and accelerates the ions to guarantee neutral outflow [Axford, 1968; Banks and Holzer, 1968]. This electric field maintains a constant flow of plasma with energies of a few eV from the ionosphere into the magnetospheric lobes [Engwall et al., 2009a]. In the classical polar wind theory, O^+ ions are deemed too heavy to escape. Yet observations have shown a significant amount of O^+ in the polar wind [Nagai et al., 1984; Waite et al., 1985; Abe et al., 1993; Su et al., 1998a]. Therefore additional acceleration mechanisms have been proposed [see Tam et al., 2007, for an overview].

A second high-latitude escape mechanism is cusp outflow. Soft electron precipitation and wave activity [e.g. Zheng et al., 2005; Moore and Khazanov, 2010; Nilsson et al., 2012] heat the ionosphere below the cusp and energize the escaping ions [Lockwood et al., 1985]. This way O^+ ions can be energized enough to overcome the gravitational potential. Despite the cusp's small spatial extent, cusp outflow is a significant source of magnetospheric ions, with total number fluxes estimated at 10^{25} s^{-1} [Nilsson et al., 2012], and with energies typically higher than those of polar wind ions. It has been suggested that the O^+ ions observed in the polar wind actually originate in the cusp and have drifted over the polar cap [e.g. Green and Waite, 1985; Nilsson et al., 2012], eliminating the necessity for the additional acceleration mechanisms mentioned earlier.

A third ion escape route is through acceleration by quasi-static electric fields parallel to the magnetic field and associated with polar cap arcs. While similar to discrete arcs in the auroral oval, polar cap arcs occur poleward of the auroral oval. They typically appear during quiet times [Davis, 1963] and periods of prolonged northward interplanetary magnetic field (IMF) [Berkey et al., 1976]. In this paper we focus on small-scale polar cap arcs, as opposed to the larger scale theta auroras [see Zhu et al., 1997, for an overview of classification schemes].

At high altitudes above polar cap arcs, in-situ measurements detect upward accelerated ion beams characterized by strongly field-aligned velocities [Maggiolo et al., 2006, 2012]. There is a significant amount of O^+ ions present in the upflow, although the H^+ ions mostly dominate [Maggiolo et al., 2011]. In contrast to cusp outflow, where the ratio of O^+ over H^+ energies is well above unity (typically $\sim$4 - $\sim$16 when detected by Cluster above the polar ionosphere [Maggiolo et al., 2006; Nilsson et al., 2012]), the energy of both species in polar cap ion beams is roughly the same as a consequence of the electrostatic acceleration of the ions by a strong field-aligned electric field. This parallel

electric field is part of a U-shaped potential profile associated with a bipolar perpendicular electric field structure at high altitude [De Keyser and Echim, 2010]. Integrating the high-altitude perpendicular electric field correlates well with the maximum ion energy [Maggiolo et al., 2006, 2011]. This parallel electric field at the same time accelerates electrons downward, which causes the luminescence of the polar cap arc [Maggiolo et al., 2012].

Similar potential structures have been observed in discrete auroral arcs and have been studied extensively [e.g. Lyons et al., 1979; Akasofu, 1981; Ergun et al., 1998; Marklund et al., 2011]. The field-aligned potential drops above polar cap arcs, 400 V on average [Maggiolo et al., 2011], are smaller than those associated with discrete arcs in the auroral oval, which typically are a few kV [Partamies et al., 2008].

The objective of this study is three-fold. The first goal is to measure the composition of the outflowing ion beams above polar cap arcs. Secondly, we register the energy of the upward accelerated ions as a proxy for the magnitude of the field-aligned potential drop. Finally, we try to assess the importance of solar illumination of the underlying ionosphere on the ion upflow. The paper is organized as follows. After a description of the data, the method and the event selection, the results of a statistical analysis are presented. We conclude with a discussion of these results in terms of the role of solar illumination, and we infer their implications for the total ionospheric upflow and outflow.

2 Data and Method

Early in the mission, the ESA Cluster satellites were particularly well suited to study polar cap ion beams, as the constellation of 4 spacecraft was in a 4 $R_E \times 19.6$ R_E quasi-polar orbit [Escoubet et al., 1997]. Plasma composition measurement is the goal of the COmposition and DIstribution Function analyser (CODIF), part of the Cluster Ion Spectrometry experiment (CIS), which can differentiate between ions with different masses and energies up to 38 keV [Rème et al., 2001]. The other instrument used here is the Hot Ion Analyser (HIA), also part of CIS. With an energy range from ∼5 eV to 32 keV, HIA has a larger sensitivity than CODIF but cannot distinguish between different ion species [Rème et al., 2001]. We therefore extract the O^+ and H^+ densities in the ion beams from the CODIF data, while we obtain the energy of the ions from HIA.

The sample of ion beams used here is a selection from the database of ∼200 events discussed by Maggiolo et al. [2011]. In about 40% of these events a hot isotropic background population is present in addition to the upflowing ions. This 40% is not included in our set because in such cases it is not always

possible to clearly separate both populations. Also, in order to avoid possible intercalibration issues, we only use measurements from CODIF on Cluster 1, until September 2004, when that instrument stopped working. Events were also eliminated if there were not enough data to obtain a decent median density (i.e. less than 4 datapoints). The resulting sample contains 67 events, relatively well distributed over local time and latitude.

The events were characterized by considering the central 60% of the time interval during which the beams are seen. Indeed, due to the U-shaped potential the ion energy is lower at the beam edges, where the measurements can suffer from the effects of the spacecraft potential that causes part of the ion population to be missed by the detector. In addition, the perpendicular electric field at the edges may also cause ions to drift which can result in significant horizontal transport away from their origin in the local ionosphere. The energy of maximum of flux is taken from the HIA data in the center of the inverted-V where the upward acceleration is maximum.

Because these are cold ion beams, the measured energy can be used to calculate the field-aligned ion velocity. Multiplying this with the O^+ and H^+ densities, we obtain an estimate for the flux densities. If the beams are exactly field-aligned, the cross-sectional area scales inversely to the magnetic field strength; this property is exploited to normalize the flux densities to a common ionospheric altitude of 200 km. By virtue of flux conservation, this provides a measure of the upward ion flux at the altitude of the bottom of the acceleration region. This altitude is not precisely known yet; for discrete auroral arcs observations find it to be between $\sim$0.5 and $\sim$2 R_E [see Karlsson, 2012, and references therein], with simulations showing that the altitude of the acceleration region depends on the energy: at higher altitudes for lower energies [e.g. Gunell et al., 2013]. For polar cap arcs, with potential drops on average an order of magnitude smaller than for auroral arcs, this will thus likely be around $\sim$1 R_E altitude or higher.

To trace the origin of the upflowing ions, we use the T96 magnetic field model [Tsyganenko, 1996] to map the spacecraft position back along a magnetic field line down to its footpoint in the ionosphere at 200 km altitude. We then calculate the solar zenith angle (SZA) at that footpoint, which is the angle between the normal to the surface and the direction to the sun, since this reflects the solar illumination conditions in the local ionosphere. The tracing of magnetic field lines depends on a magnetic field model, and could thus introduce some error. At the altitude of the Cluster spacecraft, however, the total magnetic field is still dominated by Earth's internal magnetic field, so that our estimations of these errors are smaller than one degree.

3 Results

Figure 3.1a displays the measured O^+ number fluxes, ordered according to the SZA of the corresponding field line footpoint in the ionosphere. The O^+ flux densities range over almost three orders of magnitude, from 4.0×10^9 to 2.8×10^{12} m^{-2} s^{-1}, with a mean of 2.8×10^{11} m^{-2} s^{-1}. The figure shows a transition from higher flux densities to lower ones between $\sim$94° and $\sim$107° SZA; the precise location of the transition is hard to pinpoint. Events below 94° SZA all have O^+ flux densities higher than 4.6×10^{10} m^{-2} s^{-1}, with a mean of 3.3×10^{11} m^{-2} s^{-1}, while those above 107° SZA are all lower than 1.5×10^{11} m^{-2} s^{-1}, with a mean of 4.3×10^{10} m^{-2} s^{-1}.

To check the statistical significance of this transition, the events are divided into two groups: below and above 100° SZA. The distributions of the logarithms of the flux densities are given for both groups in figure 3.1b. Note that the mean of the set above 100° SZA falls outside the 1.96σ-interval of the set below 100° SZA; in fact, it is even smaller than the lowest value in the set below 100° SZA. In the same way, the mean of the $< 100°$ distribution is higher than the highest flux density of the $> 100°$ distribution. The statistical significance of the difference between both sets is quite high. When performing a t-test, we find a probability of 7.5×10^{-5} that both sets were drawn from the same lognormal distribution of number fluxes (a reasonable choice given the nature of the distributions in figure 3.1b). Using a Mann-Whitney-Wilcoxon test, which doesn't require normality, we find this probability to be 5.4×10^{-6}.

In figure 3.2a we plot the H^+ flux densities versus the SZA of the footpoints. With values between 8.6×10^{11} and 1.1×10^{13} m^{-2} s^{-1}, and with a mean of 3.1×10^{12} m^{-2} s^{-1}, the flux density is on average an order of magnitude higher than the O^+ flux density, and ranges over a bit more than one order of magnitude. Here too we find a transition between $\sim$94° and $\sim$107°, with slightly lower values at higher SZA. However, the difference is smaller, with mean values of 3.2×10^{12} m^{-2} s^{-1} below and 1.7×10^{12} m^{-2} s^{-1} above the transition, so that the change is less clear than for O^+. This is also seen in the histogram of the logarithm of the H^+ number flux in figure 3.2b. The distributions found for SZA below and above 100° differ less. The mean of the set with SZA $> 100°$ is well within the 1.96σ-interval of the set with SZA $< 100°$. The probability that both sets come from the same distribution is higher, 8.3×10^{-3} from the t-test and 5.3×10^{-3} from the Mann-Whitney-Wilcoxon test, but the division in two distinct sets still has a high statistical significance.

The energy of maximum ion flux is shown in figure 3.3a, ordered according to SZA. The minimum beam energy is 96 eV, the maximum 1669 eV, and the mean energy is 422 eV. Interestingly, we again see a change in the distribution

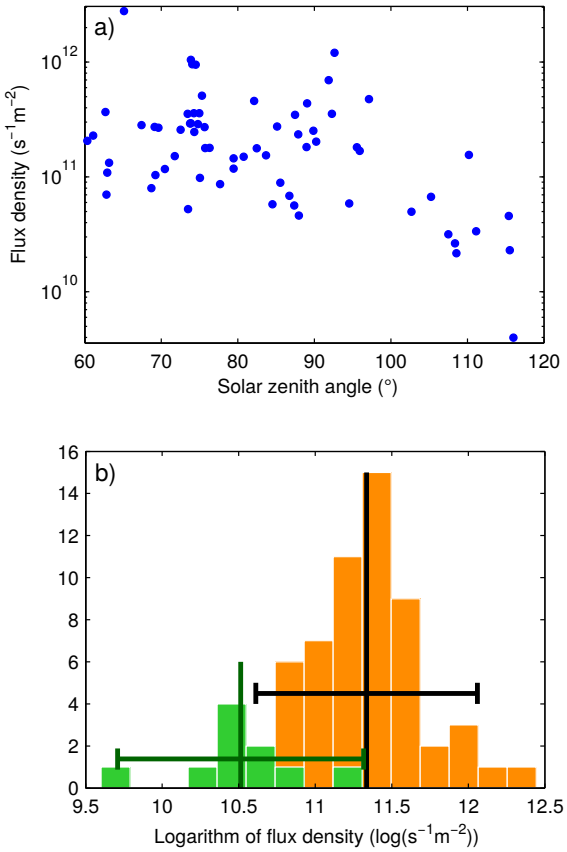

Figure 3.1: **a)** The O^+ flux densities versus the SZA of the ionospheric footpoint. **b)** The histograms of the logarithm of the O^+ flux densities. In orange (green) for the events with SZA lower (higher) than 100°. The vertical black (green) line gives the mean of the orange (green) distribution, the horizontal lines show the 1.96σ-interval.

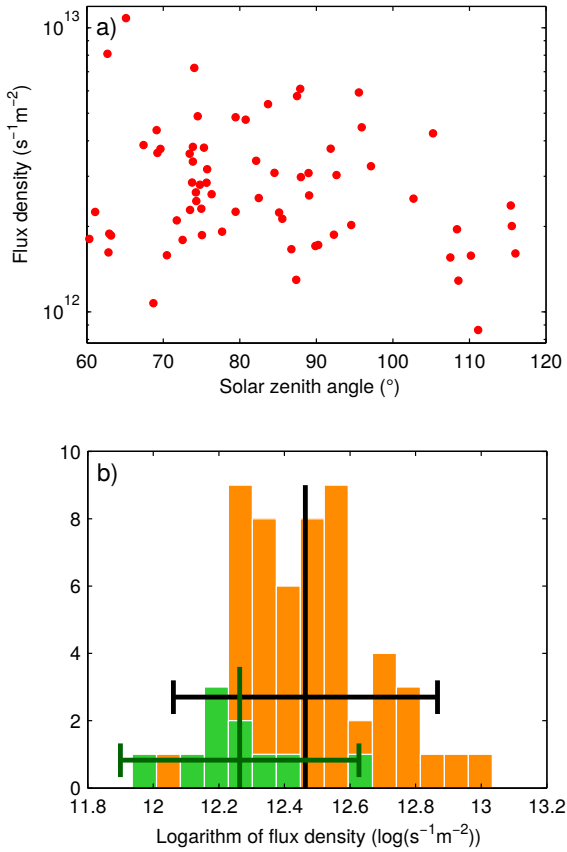

Figure 3.2: **a)** The H^+ flux densities versus the SZA of the ionospheric footpoint. **b)** The histograms of the logarithm of the H^+ flux densities. In orange (green) for the events with SZA lower (higher) than 100°. The vertical black (green) line gives the mean of the orange (green) distribution, the horizontal lines show the 1.96σ-interval.

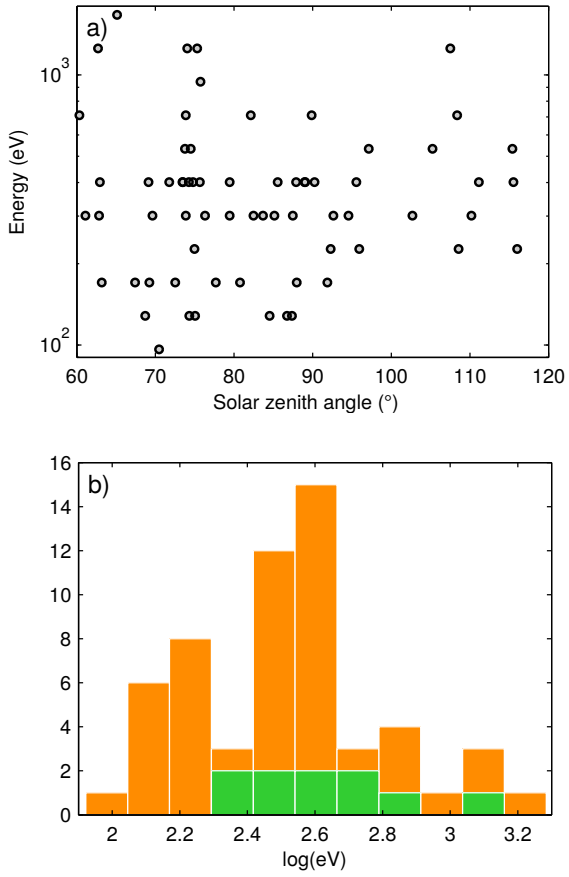

Figure 3.3: a) The energy of maximum of flux in the ion beams versus the SZA of the ionospheric footpoint. **b)** The histograms of the logarithm of the energy. In orange (green) for the events with SZA lower (higher) than 100°.

of energies around ∼100°. Here also, it is not clear where exactly the transition occurs. The difference between the mean energies, 410 eV below and 489 eV above 100°, is not large, but at the higher angles no event with an energy lower than 227 eV is observed, whereas for the lower angles 26% of the observed events have energies below this value. In other words, the first quartile (i.e. the lowest 25%) of the events at SZA below 100° is 170 eV, which is lower than the lowest energy of the events above 100°. On the other hand, the third quartile at the lower SZA is 410 eV, and there are 4 events (out of 10) at the higher SZA with energies higher than this.

4 Discussion

We have found a statistically significant difference in the fluxes of outflowing O^+ and H^+ above polar cap arcs, as well as in their energies, below and above a transition in solar zenith angle that separates a sunlit and a dark ionosphere. Therefore the data clearly suggest a modulation of the upflow from the ionosphere above polar cap arcs by solar illumination.

The transition is found between ∼94° and ∼107°. The SZA of the terminator at an ionospheric altitude h is given by $h = R \cdot (1/\cos(\mathrm{SZA} - 90°) - 1)$, where R is the Earth's radius augmented by the altitude where the atmosphere becomes opaque to UV-light at the relevant wavelengths, i.e. the altitude of the ozone layer of ∼30 km (assuming that the atmosphere is optically thin above and completely opaque below that altitude). This nonlinear relation between h and SZA implies that the terminator at an altitude of ∼45 km has a SZA = 94°, at ∼130 km it is 100°, and at ∼310 km it is 107°. The observed modulation therefore suggests that the O^+ source is situated at the ionospheric field line footpoint directly below the observed beams. It also places this source somewhere between this ∼130 km and ∼310 km, which is fully compatible with the fact that O^+ ionization in the ionosphere is most efficient in the F layer above 150 km altitude. It is also known that the F layer is depleted during nighttime, i.e. that there is a strong solar illumination effect on the ionization in the F layer.

The solar illumination effect leads to a modification of the composition in the ion beams. The O^+/H^+ number flux ratio in the ion beams above a sunlit polar cap, 0.095, is much larger than above a dark polar cap, where it is only 0.026. In terms of mass flux, due to their larger mass, oxygen ions are dominant on the sunlit side, with the ratio being 1.5, but dropping to 0.41 on the dark side. An obvious explanation for this difference in ion outflow could be the observed day/night difference in the O^+ ion content in the F layer: There simply are more ions available to flow up during daytime. Composition and density changes in the F layer will result in changes at higher altitudes. The presence of photoelectrons could also affect the ion upflow above the polar cap, as suggested by several papers [e.g. Axford, 1968; Tam et al., 1995, 1998; Glocer et al., 2012]. An increased scale height in the F region ionosphere will facilitate the O^+ ions reaching the bottom of the acceleration region, and thus is also an important factor in the control of the ion upflow.

The time it takes for the ionosphere to react to the absence of solar illumination after having been sunlit (i.e. relaxation time), or to the presence of solar illumination after having been in the dark, could affect the results, blurring the difference between the sunlit and the dark side of figures 3.1a and 3.2a.

However, when we assume the terminator to be at a SZA of e.g. 100°, we find that all events except one have footpoints in the ionosphere on positions that have been in or out the sunlight for more than 4 hours; most have even been there for more than a day.

Some authors have suggested that upflowing O^+ ions above the polar cap originate in the cusp and have drifted across the polar cap [e.g. Green and Waite, 1985; Nilsson et al., 2012]. However, the observed dependence of the properties of the polar cap ion beams on the SZA at the field line footpoint rather suggest that the O^+ ions we observe in the ion beams originate in the local polar ionosphere. We also do not find a correlation between the flux densities and the distance from the cusp. Further corroborating the idea of an origin in the local ionosphere, is the fact that our data are collected during, or not long after, periods of northward IMF during which there is little or no anti-sunward convection across the polar cap. It is also unlikely that ions have entered the beams from the sides and crossed the magnetic field lines by means of some form of diffusive transport, because then we would expect a large dispersion in the energies of these ions, while we observe a rather narrow energy distribution.

It should be noted that even during northward IMF, the convection could be a cause of errors of a few degrees in determining the SZA. This would blur the transition, certainly considering that convection is not only anti-sunward during northward IMF. Therefore the fact that we do see the transition means that the effect of convection is less significant than that of solar illumination.

The energy of the accelerated ions is a good proxy for the magnitude of the field-aligned potential drop. Therefore, our findings show that the potential drop associated with polar cap arcs also changes between a sunlit and a dark ionosphere. Several studies have found evidence of a dependence of the field-aligned potential drop associated with auroral arcs on solar illumination [Newell et al., 1996, 2010; Cattell et al., 2006; Liou et al., 2011]. However, they all show the higher energies to be suppressed in the sunlight. Liou et al. [2011] also report a monotonic increase of the potential drop with SZA up to 108°. Note, however, that one should be cautious with the analogy with discrete arcs in the auroral oval; these may behave differently and typically involve larger potential differences [Partamies et al., 2008] than those observed above the polar cap arcs in this paper and occur in regions of intense particle precipitation.

Solar illumination enhances the ionospheric electron and ion density and temperature, thereby increasing the horizontal conductivity. Since the field-aligned electric fields in quasi-static arcs are part of a current system with a generator somewhere in the magnetosphere and closing horizontally in the ionosphere, it is likely that the ionospheric conductivity can affect the whole

current system and thus also the field-aligned potential drop [e.g. Lyons, 1980, 1981; De Keyser and Echim, 2010].

In the case of discrete auroral arcs, the precipitating particles dump a lot of energy into the underlying ionosphere. In polar cap arcs the precipitating energy fluxes are smaller due to the lower parallel potential drops and to the absence of trapped populations on polar magnetic field lines. The relative contribution of solar illumination in heating and ionizing the underlying ionosphere is therefore correspondingly larger. Indeed, we did not find a correlation between the flux density and the magnitude of the potential drop, indicating that the precipitating electrons do not significantly affect the ionosphere below, i.e. that the properties of the ionosphere below a polar cap arc are not significantly different from that in the rest of the polar cap.

One might therefore conjecture that the ion outflow above the polar cap ionosphere, i.e. the polar wind, is very similar to the outflow above a polar cap arc, the only difference being that the ionospheric ions above a polar cap arc are accelerated enough so that they can be reliably detected by a charged spacecraft, while the observation of the cold polar wind itself is inherently difficult due to spacecraft potential issues. Although further study is warranted, we can compare our results to studies of O^+ in the polar wind.

The models of Su et al. [1998a,b] and Glocer et al. [2012] show a strong decrease in O^+ density at solar zenith angles between 95° and 105° above the polar cap when incorporating photoelectrons in the polar wind. From satellite observations, Abe et al. [1993] report a transition in the upward ion velocities in Akebono data, from higher on the dayside to lower on the nightside, at altitudes from 5000 km to 9000 km. Using measurements from the POLAR spacecraft, Su et al. [1998a] find a strong decrease in O^+ densities and downward fluxes going from 90° to 105° at altitudes of 5000 km. They conclude that most O^+ ions originate in the cleft ion fountain, or cusp upflow. As mentioned before, in our data we find evidence that this is not the case for the ions observed in the ion beams, which originate in the local ionosphere and have entered the acceleration region from the bottom. It is possible that this study and Su et al. [1998a] consider different populations. Su et al. [1998a] measure much more O^+ ions (they find O^+ being the dominant species at 5000 km altitude), and see mostly downflowing ions originating in the cusp. It is likely that these downflowing ions would not enter the acceleration region, and that we only observe the small population of O^+ ions flowing up from the local ionosphere.

With the aforementioned caveats in mind, we can extrapolate the average measured fluxes to the whole polar cap area. Approximating the poleward boundary of the auroral oval with a circle at 75° magnetic latitude, and using the mean flux densities over all events, we estimate the total upward H^+ and

O^+ number flux (up to the altitude of the bottom of the acceleration region) to be 2.9×10^{25} s^{-1} and 2.6×10^{24} s^{-1}, respectively. Note that these values are obtained mostly during northward IMF conditions. Because of the sunlit/dark difference, we would expect daily and seasonal variations of the total ion flux above the polar cap, most notably in the O^+ flux. We could use the mean flux density of events at SZA $> 100°$ for upflow from a dark polar cap, and the mean of the other events for a sunlit polar cap. Then, for example, from a fully sunlit polar cap, like during summer solstice, the extrapolated total O^+ upflow would be around 3.0×10^{24} s^{-1}, whereas from a polar cap in darkness, like around midnight during winter solstice, it would only be 4.2×10^{23} s^{-1}. Because the sunlit/dark transition occurs at SZA larger than 90°, the variations in the two hemispheres do not cancel each other. The ion upflow, and thus probably also the outflow, from both polar caps combined should still exhibit a seasonal variation, namely from solstice to equinox.

5 Summary

In summary, we find a strong difference in upward O^+ flux above polar cap arcs depending on whether the magnetic field line footpoint is sunlit or not. This is also found for H^+, but less pronounced. The magnitude of the field-aligned potential drop is also found to behave differently. Solar illumination of the local polar ionosphere (particularly the F layer) is therefore considered the main parameter controlling the upflow. Furthermore, the existence of two distinct regimes for the sunlit and dark polar ionosphere suggests that a diurnal and seasonal variation for the total polar wind outflow may exist.

Acknowledgements. This work was supported by the Interuniversity Attraction Pole Planet TOPERS initiated by the Belgian Science Policy Office and by the ESA-Prodex Project CON-Cluster.
We acknowledge the support from the International Space Science Institute through funding of their International Team on Polar Cap Arcs. The authors are grateful to E. Penou for the development of CL, the Cluster CIS software.
All Cluster data can be found at the Cluster Science Archive (www.cosmos.esa.int/web/csa/). The dates and times of the events used in this study can be found in the supporting information.

Contributions. L.M. and R.M. designed the study. L.M. did the data analysis, interpretation and discussion of the results and wrote the paper. R.M. selected the events. R.M., J.D.K., and S.H. helped with the interpretation and discussion of the results. I.D. helped with validation of data. R.C.F. and D.F. helped with discussion of the events and results. All authors critically revised the manuscript.

Chapter 4

Outflow from the whole polar cap

In the previous chapter we showed that solar illumination has an important effect on the flux density and composition of the ions flowing out above small-scale polar cap arcs. We also argued that this effect is due to a modulation of the local ionosphere and should thus also be present in the polar wind. Therefore, in this chapter, we extrapolate this effect to the whole polar cap and examine what happens to the polar wind flux from the whole polar cap while it rotates in and out of the sunlight on a daily and seasonal basis. We present the work as it was published in **Annales Geophysicae** in November 2016.

***Maes, L.**, Maggiolo, R., and De Keyser, J.: Seasonal variations and north–south asymmetries in polar wind outflow due to solar illumination. Ann. Geophys., 34, 961-974, doi:10.5194/angeo-34-961-2016, 2016.*

Seasonal variations and north–south asymmetries in polar wind outflow due to solar illumination

L. Maes[1], R. Maggiolo[1], and J. De Keyser[1,2]

[1]Royal Belgian Institute for Space Aeronomy, Brussels, Belgium, [2]KU Leuven Center for Mathematical Astrophysics, Celestijnenlaan 200B, 3001 Leuven, Belgium

Abstract. The cold ions (energy less than several tens of electronvolts) flowing out from the polar ionosphere, called the polar wind, are an important source of plasma for the magnetosphere. The main source of energy driving the polar wind is solar illumination, which therefore has a large influence on the outflow. Observations have shown that solar illumination creates roughly two distinct regimes where the outflow from a sunlit ionosphere is higher than that from a dark one. The transition between both regimes is at a solar zenith angle larger than 90°. The rotation of the Earth and its orbit around the Sun causes the magnetic polar cap to move into and out of the sunlight. In this paper we use a simple set-up to study qualitatively the effects of these variations in solar illumination of the polar cap on the ion flux from the whole polar cap. We find that this flux exhibits diurnal and seasonal variations even when combining the flux from both hemispheres. In addition there are asymmetries between the outflows from the Northern Hemisphere and the Southern Hemisphere.

1 Introduction

The high-latitude ionosphere is an important source of plasma for the magnetosphere [Hultqvist, 1999; Yau and André, 1997]. O^+ ions of ionospheric origin have been observed in the magnetospheric lobes [e.g. Sharp et al., 1981; Candidi et al., 1982, 1984; Seki et al., 1998] and in the plasma sheet [e.g. Peterson et al., 1981; Maggiolo and Kistler, 2014]. There are three main regions of outflow at high latitudes: the auroral oval, the cusp, and the polar cap. The auroral oval and the cusp are regions of intense ion outflow in response to strong

energy inputs like Poynting flux, particle precipitation, and the work done by strong field-aligned electric fields accelerating ions upwards [Lockwood et al., 1985; Zheng et al., 2005; Moore and Khazanov, 2010; Nilsson et al., 2012]. In the absence of such energy inputs, the main source of energy for ion outflow in the polar cap is solar illumination.

Because the magnetic field above the polar caps is directly connected to the interplanetary magnetic field (IMF), Dessler and Michel [1966] argued that the ion temperature in the ionosphere is sufficiently high so that no hydrostatic equilibrium can be achieved there. The ions are more gravitationally bound, and will, together with the more easily escaping electrons, set up an ambipolar electric field parallel to the magnetic field lines, which accelerates ions upward [Axford, 1968; Banks and Holzer, 1968]. This outflow is named the polar wind.

Compared to the outflow in the cusp and the auroral regions, the polar wind constitutes a mild but steady flux of ions into the magnetospheric lobes, emanating from a relatively large source area. Moreover, during geomagnetically quiet times, the polar cap is the main cold ion source for the magnetospheric lobes [Li et al., 2012]. These ions have temperatures generally not much higher than the ion temperature in the ionosphere and flow at relatively small velocities [Engwall et al., 2009a]. As a consequence, they are very difficult to measure with satellites flying through the lobes, because these cold ions often have energies too low to overcome the spacecraft potential, which can go up to several tens of electronvolts in these regions. The low energization also means that it is very difficult for O^+ ions to escape Earth's gravitational potential via this mechanism, and so very little O^+ is expected in the polar wind. Nevertheless, O^+ ions have been observed above the polar caps and in the lobes [Nagai et al., 1984; Waite et al., 1985; Abe et al., 1993; Su et al., 1998a]. Many additional mechanisms have been proposed to explain this [see, e.g., Tam et al., 2007, for an overview].

Because they flow on open magnetic field lines, these ions can escape the magnetosphere into interplanetary space. In this way they may contribute to the erosion of the atmosphere. Their fate, however, is not certain. It has been argued that the final destination of these ions depends on the ratio of their velocity parallel to the magnetic field and the convection velocity perpendicular to the magnetic field [Ebihara et al., 2006; Haaland et al., 2012; Li et al., 2013], particularly during periods of southward IMF. Haaland et al. [2012] estimated that 90% of the ions flowing into the lobes are convected into the plasma sheet. There they can be recirculated into the inner magnetosphere and finally return to the atmosphere [Dungey, 1961; Seki et al., 2001] or ultimately be lost to interplanetary space [Slavin et al., 1989, 1999].

This is also true for the ions flowing out from the cusp. Many ions in the cusp

are strongly energized and will leave the magnetosphere directly via the open magnetic field lines [Nilsson et al., 2012; Slapak et al., 2015]. But the ions with the lowest energies may be convected across the polar cap and mix with the polar wind ions [e.g. Green and Waite, 1985; Nilsson et al., 2012], so that it is not always possible to discern polar wind ions from the ions originating in the cusp. This also provides another possible explanation for the O^+ observed above the polar caps and in the lobes. Thus, in addition to outflowing ions from the auroral ovals, the polar wind and cusp outflow constitute an important source of plasma for the plasma sheet, since a part of these ions is convected there.

Whereas the ionosphere might be rivalled or even surpassed by the solar wind as a source of H^+ ions for the plasma sheet, there is a much larger proportion of O^+ in ionospheric outflow than in the solar wind, making it the dominant source of O^+ ions. The role of heavy ions like O^+ is still hotly debated [see, for example, Daglis and Axford, 1996; Lotko, 2007; Kronberg et al., 2014], but they might be important for magnetospheric dynamics. Theoretical and modelling studies suggested an impact of O^+ ions on plasma sheet reconnection [Baker et al., 1982; Shay and Swisdak, 2004; Brambles et al., 2010]. Some studies indicate that O^+ ions can trigger substorms [Cladis and Francis, 1992; Yu and Ridley, 2013], and others that sawtooth events may be induced by ionospheric outflow [Brambles et al., 2011; Ouellette et al., 2013]. Observational studies have not really been able to confirm nor refute this [e.g. Peterson, 2002; Kistler et al., 2006; Liao et al., 2014].

Ionospheric outflow, and especially the polar wind, can also be an important source of cold ions for the plasma sheet. It is generally assumed that the ions in the plasma sheet are quickly and efficiently heated [Gary, 1991; Delcourt et al., 1994; Arzner and Scholer, 2001], but some observations do observe a significant population of cold ions in the plasma sheet [Seki et al., 2003; Ebihara et al., 2008]. If there are indeed cold ions in the plasma sheet, the polar wind would be one of the major suspects for the source, next to plasmaspheric winds and plumes. Toledo-Redondo et al. [2015] recently found, while studying reconnection at the dayside magnetopause, that cold ions introduce a new length scale in the reconnection process and thus may affect it.

Since solar illumination is the dominant energy source for the polar wind, the degree of solar illumination of the polar ionosphere should modulate the outflow. This has been evidenced by many observational studies and models [Abe et al., 1993; Su et al., 1998a,b; Glocer et al., 2012; Maes et al., 2015]. Maes et al. [2015], studying outflow above small-scale polar cap arcs using Cluster [Escoubet et al., 2001] measurements, found that the upflow above the polar cap can be roughly divided into two distinct groups based on the solar zenith angle (SZA) of the footpoint of the field line in the ionosphere. The border between both was found

to be around ∼100°, i.e. the solar zenith angle of the terminator at ionospheric altitude. The outflow was more intense for the group at smaller solar zenith angles than for the group at larger ones. The effect was found to be stronger for O^+ than for H^+. The O^+ flux densities (normalized to 200 km altitude) ranged from 4.0×10^9 to 2.8×10^{12} $m^{-2}s^{-1}$, and were on average almost an order of magnitude smaller at the large solar zenith angle. The H^+ flux densities were between 8.6×10^{11} and 1.1×10^{13} $m^{-2}s^{-1}$ and were on average almost a factor of 2 smaller above a dark ionosphere.

Since the rotational axis of the Earth is tilted by ∼23.4° from the perpendicular on the ecliptic plane, the polar cap moves into and out of the sunlight during Earth's orbit around the Sun. The magnetic polar cap is not centred around the geographic poles but rather offset by several degrees latitude, adding a daily modulation to the magnetic polar cap's movement as it rotates in and out of the sunlight.

Earth's magnetic field is not symmetric between the Southern and Northern Hemisphere. The North Magnetic Pole, defined as the point in the Northern Hemisphere at the surface of the Earth where the magnetic field points exactly downwards, is located at 86.3° N, as measured in 2015 [Thébault et al., 2015]. The South Magnetic Pole, analogously defined, is not located at the opposite point in the Southern Hemisphere but at 64.3° S [Thébault et al., 2015]. These positions are also not constant in time. This difference in offset implies that the northern and southern magnetic polar cap will receive different amounts of sunlight throughout the day and the year.

One would expect that these diurnal and seasonal variations in solar illumination of the polar caps, the fact that the terminator has a SZA larger than 90°, and the asymmetries in the magnetic field all have an effect on the total ion outflow and its composition. The goal of this paper is to qualitatively explore these effects. In the next section, we first explain the model we employ to study these effects. We report the results in section 3, first for the simplest set-up: circular polar caps with a symmetric magnetic field (section 3.1). Then we add the asymmetry of Earth's magnetic field (section 3.2), and finally we use a more realistic polar cap shape (section 3.3). This stepwise approach allows us to identify which cause has which effect. In section 4 we discuss these results and their possible implications.

2 Method

To investigate the effects of the difference in outflow from a sunlit and a dark ionosphere, we keep things very simple. Inspired by the two regimes in upflowing

ion fluxes above a sunlit and a dark ionosphere found by Maes et al. [2015], as discussed in the introduction, we assume that there are only two possible flux density values (ions $m^{-2}s^{-1}$): one above a sunlit ionosphere and one above a dark ionosphere. Thus, we ignore all other factors that may have an influence on the outflow and cause a large natural spread, like variations in irradiance, flows, and density fluctuations in the neutral upper atmosphere, geomagnetic activity, etc. The eccentricity of Earth's orbit is also neglected.

For simplicity, we assume the transition between these two regimes to be sharp and located at a solar zenith angle of 100°. Therefore, mathematically, we define the flux density f (ions $m^{-2}s^{-1}$) as a step function:

$$f = \begin{cases} f_{sun} & \text{if SZA} \leqslant 100^\circ \\ f_{dark} & \text{if SZA} > 100^\circ \end{cases} . \tag{4.1}$$

f_{dark} is that above the dark ionosphere. We take their values from the study in Maes et al. [2015] as the average value for upflow below SZA of 100° and above 100°. f_{sun} is equal to 3.3×10^{11} $m^{-2}s^{-1}$ and f_{dark} is 4.4×10^{10} $m^{-2}s^{-1}$ for O^+; for H^+ these are 3.2×10^{12} $m^{-2}s^{-1}$ and 1.7×10^{12} $m^{-2}s^{-1}$, respectively. The total ion flux from the whole polar cap, F_{tot}, is then simply found as follows:

$$F_{\text{tot}} = f_{\text{sun}} \times A_{\text{sun}} + f_{\text{dark}} \times A_{\text{dark}}, \tag{4.2}$$

where A_{sun} is the area of the polar cap which is sunlit and A_{dark} the area which is dark. Note that the flux densities are kept constant, but what does vary is the area of the polar cap which is sunlit and the area which is dark, on a diurnal basis, as the Earth rotates, and on a seasonal basis as the orientation of Earth's rotational axis changes with respect to the Sun. It is thus the variation in the sunlit fraction of the polar caps that introduces a time dependence into the total flux (as well as the size of the total polar cap in the third case, as explained further on).

Note that these flux densities from Maes et al. [2015] actually come from measurements of ion outflow above polar cap arcs. Since precipitating electrons caused by the polar cap arc system deposit energy in the ionosphere below, this might cause concern that these flux densities are not representative of the polar wind. Maes et al. [2015] argued to the contrary, since they found that the magnitude of the relatively small potential drop of the polar cap arcs (and thus the energy of the precipitating electrons) does not seem to have any discernable effect on the flux densities. The fact that the outflow is predominantly controlled by the ionospheric illumination conditions also indicates that the energy deposited in the ionosphere by precipitation in polar cap arcs plays a minor role. Moreover, integrated over the polar cap area, these H^+ flux densities lead to fluxes similar to those found by other studies of the

polar wind [see e.g. Nagai et al., 1984; Cully et al., 2003; Huddleston et al., 2005; Engwall et al., 2009a; André et al., 2015].

The O^+ fluxes fall at the lower end of the ranges found in literature [see, e.g., Yau et al., 1988; Cully et al., 2003], although it is often argued for these O^+ ions that they originate from more energetic sources like cusp outflow and are convected above the polar cap. In Maes et al. [2015] it is argued that this is most likely not the case for their data. Abe et al. [1993] also argued this for the O^+ ions they observed, and they found fluxes very similar to Maes et al. [2015]. Nonetheless, even if the O^+ flux densities are not precise, the variations of the flux should still be correct, since they are caused by the alteration of the polar ionosphere by solar illumination, which happens regardless of the presence of polar cap arcs. Since the main goal of this paper is to give a qualitative analysis of the variations caused by the solar illumination, rather than to provide an accurate estimate of the ion flux, we proceed with these values.

In order to be able to distinguish between the consequences of the different causes mentioned in the introduction, we start with the simplest case of a circular magnetic polar cap, with perfect north–south symmetry. We assume the polar cap, bound by the auroral oval, to have "latitudinal radius" of 15° and to be centred around the geomagnetic poles. The geomagnetic pole is defined as the point where the dipole axis of the magnetic dipole approximation intersects Earth's surface, and is located at ∼80° geographic latitude [Thébault et al., 2015]. It should be noted that the choice of the values of parameters like the SZA of the terminator and the size of the polar cap also affects the results.

After that we add a little more realism by introducing the north–south asymmetry in the magnetic field. We do this by centring the circular polar caps around the invariant magnetic poles [e.g. Emmert et al., 2010; Förster and Cnossen, 2013] instead of the geomagnetic poles. These are located at 82° N and 74° S.

Finally we introduce a more realistic polar cap shape. To this end, we use the Tsyganenko 89 magnetic field model [Tsyganenko, 1989] and define the magnetic polar cap as the region poleward of the boundary between the open and closed magnetic field lines. This is found by starting at ionospheric altitude and following each magnetic field line to see whether it maps back into the ionosphere. In the T89 model a magnetic field line extending beyond 100 R_E is cut off and considered open. The T89 model requires the Kp value as an input parameterizing the geomagnetic activity; in this study we consider the case Kp = 0. While this may not be the most common geomagnetic condition, this seemed the most appropriate value as the polar cap shape is not correctly reproduced by T89 for higher Kp.

3 Results

3.1 Circular polar cap with north–south symmetry

The O^+ fluxes from the northern and southern polar cap for circular polar caps with a symmetric magnetic field are shown in figure 4.1. The fluxes from both hemispheres, given in panel (a) and (b), are identical but shifted by half a year. It is clear that the flux from an individual hemisphere is highest around the summer solstice (around 21 June in the Northern Hemisphere, around 21 December in the Southern Hemisphere) and lowest around the winter solstice, as one would expect. The maximum number of O^+ ions is flowing out when the polar cap is completely sunlit ($F_{\mathrm{tot}} = f_{\mathrm{sun}} \times A_{\mathrm{tot}}$) and is 3.05×10^{24} s^{-1}, and the minimum when the polar cap is completely dark ($F_{\mathrm{tot}} = f_{\mathrm{dark}} \times A_{\mathrm{tot}}$), with only 3.97×10^{23} s^{-1} flowing out. This is a variation of more than 600%. The maximum of the daily average, which represents only the seasonal variation, is the same as the overall maximum, and the minimum of the daily average is 7.15×10^{23} s^{-1}. This is a variation of more than 300%.

For H^+ the maximum is 2.96×10^{25} s^{-1} and the minimum 1.57×10^{25} s^{-1}. For the daily average the minimum is 1.74×10^{25} s^{-1}. This corresponds to a variation of $\sim 90\%$ and almost $\sim 70\%$ respectively. The difference between the maximum and minimum flux is smaller than for O^+, due to the smaller difference between the flux densities in sunlit and dark conditions for H^+.

There is no daily variation in the flux in the period around the summer solstice. This is because, during this time, the magnetic polar cap is sunlit throughout the whole day (at ionospheric altitude) and thus, according to Eq. (2), the total flux is constant ($F_{\mathrm{tot}} = f_{\mathrm{sun}} \times A_{\mathrm{tot}}$). This can also be understood by simple reasoning: at the summer solstice, the geographic pole has a SZA of $90 - 23 = 67°$. This means that the geomagnetic pole, offset from the geographic pole by $\sim 10°$, will have a SZA of $67 + 10° = 77°$ at its local midnight. With a magnetic polar cap with a "latitudinal radius" of 15°, the highest SZA found in the magnetic polar cap is therefore $77 + 15° = 92°$. This indeed remains sunlit if the terminator is at a SZA of 100°. Analogously, one can find that around the winter solstice the polar cap is not completely dark throughout the whole day, with a terminator at 100°.

The largest daily variation occurs in the period before the spring equinox and after the autumn equinox (note that the daily variation is represented by the vertical distance between the upper and lower red line). At this time, the magnetic polar cap rotates into and out of the sunlight. There is still a daily variation around the winter solstice, but less than before and after, because the polar cap is completely dark during part of the day and never becomes fully

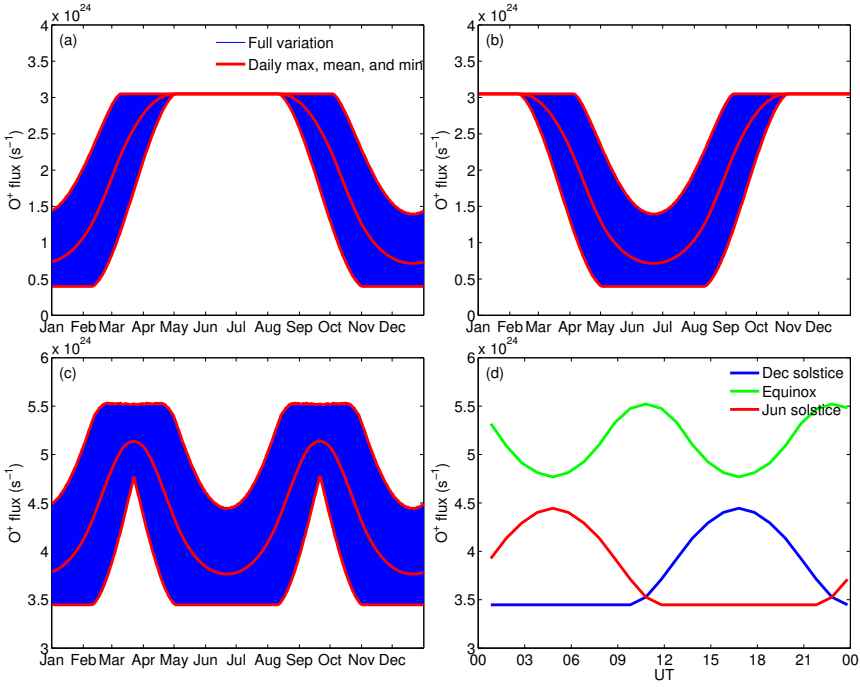

Figure 4.1: O^+ fluxes for a circular polar cap with north–south symmetry. **(a)** Northern Hemisphere. **(b)** Southern Hemisphere. **(c)** Both hemispheres combined. **(d)** UT dependence for both hemispheres combined.

sunlit.

When we combine the flux from both hemispheres, a daily and a seasonal variation persist (see panel (c) of figure 4.1). Because the terminator has a SZA larger than 90°, the proportion of the polar cap receiving sunlight in one hemisphere is not the opposite of that in the other. Therefore, the variations in one hemisphere do not cancel those in the other hemisphere. There is no difference between the two solstices, but there is still a seasonal variation from equinox to solstice. The largest flux from both hemispheres combined, 5.53×10^{24} s^{-1} for O^+ and 5.62×10^{25} s^{-1} for H^+, occurs at the equinox and the lowest, 3.45×10^{24} s^{-1} for O^+ and 4.53×10^{25} s^{-1} for H^+, at the solstice. This is a variation of ∼60 and ∼24% for O^+ and H^+, respectively. For the daily average this variation is ∼ 36 and ∼15%, respectively.

In panel (d) of figure 4.1 we see the UT dependence of the flux from both hemispheres combined, in red for the June solstice, in blue for the December

solstice, and in green for the equinox. In June, there is a peak at 16:48 UT. This is at the local noon of the south geomagnetic pole, which is entering its winter and receiving its daily amount of sunlight in that season. During the solstice, the summer hemisphere does not add to the daily variation, because it is completely sunlit during the whole day. Therefore, all the variation is due to the winter hemisphere, which increases the total combined flux when it receives sunlight (from ∼10:00 until ∼23:00 UT in the north and from ∼22:00 until ∼11:00 UT in the south). Consequently, the flux is constant at 3.45×10^{24} s^{-1} for O^+ and 4.53×10^{25} s^{-1} for H^+ when the polar cap in the winter hemisphere is completely dark. It is maximum when the illuminated proportion of the polar cap in the winter hemisphere is maximum (i.e. local noon): 4.45×10^{24} s^{-1} for O^+ and 5.05×10^{25} s^{-1} for H^+. Thus, the combined O^+ flux varies with about 29% throughout the day at solstice, while for H^+ this variation is of the order of 12%.

At equinox there are two minima, 4.77×10^{24} s^{-1} for O^+ and 5.22×10^{25} s^{-1} for H^+, which coincide with the local noon and midnight at the magnetic poles. The maxima, 5.61×10^{24} s^{-1} for O^+ and 5.64×10^{25} s^{-1} for H^+, happen at the local morning and evening of the poles at ∼10:48 and ∼22:48 UT. Therefore, the maximum outflow at the equinox does not occur during noon at the poles but instead in the morning and evening when the illumination of both polar caps combined is maximized.

3.2 Circular polar cap with north–south asymmetry

We now introduce the asymmetry of the magnetic field by centring the polar caps around the invariant magnetic poles. The resulting number fluxes for O^+ behave as shown in figure 4.2. The southern magnetic polar cap is then located at lower geographic latitudes, and will sway farther into and out of the darkness. The consequence is immediately visible: in the Southern Hemisphere (in panel b) there is a much larger daily variation at the winter solstice and the equinoxes. There are now even two periods (in April and September) where the flux goes from the maximum (when completely sunlit) to the minimum value (when completely dark) in one day. Whether this happens also depends on the actual size of the polar cap and the position of the terminator. Since the north magnetic polar cap is now centred at higher latitudes, there is less variation in the flux from the Northern Hemisphere (panel a).

Another interesting point is that the daily mean flux from the southern polar cap in the local winter is higher than that from the northern polar cap in winter. This is the case during the whole period of approximately 65 days before and after the local winter solstices. The southern daily average flux is higher at the

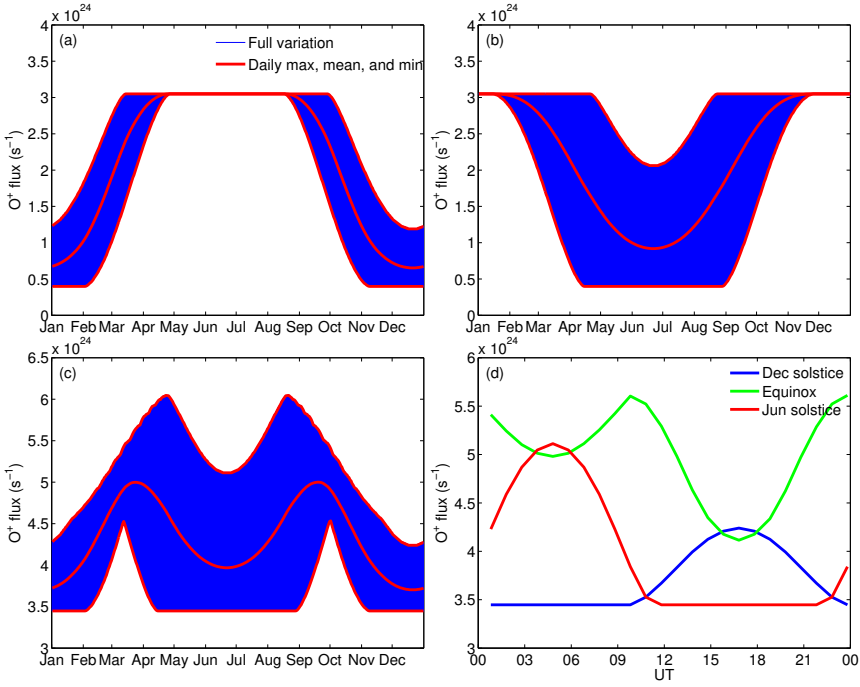

Figure 4.2: O^+ fluxes for a circular polar cap with north–south asymmetry. **(a)** Northern Hemisphere. **(b)** Southern Hemisphere. **(c)** Both hemispheres combined. **(d)** UT dependence for both hemispheres combined.

winter solstice because, due to its larger offset, the southern polar cap will be able to spend more time sunward of the terminator. The difference in the daily average flux at the local winter is at its largest at ∼38% for O^+ and ∼8% for H^+. In the following ∼91.5 days, including the equinox, the daily average flux in the Northern Hemisphere is larger, with the difference peaking at ∼11% for O^+ and ∼6% for H^+. This happens because, during this period, the northern polar cap less often reaches the darkness owing to its smaller offset. In the period of ∼26 days before and after the local summer solstice, the fluxes from both hemispheres are equal. At this time both polar caps are completely sunlit throughout the whole day and the flux is maximized ($F_{\mathrm{tot}} = A_{\mathrm{tot}} \times f_{\mathrm{sun}}$). For the next ∼91.5 days, the Northern Hemisphere has a higher flux again. Thus, the difference between the outflow from both hemispheres due to the asymmetry in the magnetic field itself has a seasonal variation. Both trends oppose each other so that the difference between the average flux over the whole year from the northern and southern polar cap becomes almost, but not exactly, zero.

Panel (c) of figure 4.2 shows the total flux from both hemispheres combined. As in the symmetric case, there is still a seasonal variation. The shape is different, however. The peaks of the daily maximum are not at the equinoxes anymore but closer to the June solstice, namely at 22 April and 21 August. The peaks of the daily mean are still at the equinox. The fluxes are now also not symmetric anymore between both solstices. The Southern Hemisphere's higher daily mean in its winter than that in the north means that the combined flux is higher at the June solstice, 3.97×10^{24} s^{-1} for O^+ and 4.80×10^{25} s^{-1} for H^+, than at the December solstice, 3.70×10^{24} s^{-1} for O^+ and 4.66×10^{25} s^{-1} for H^+. This is a difference of more than 7% and for O^+ and almost 3% for H^+.

In panel (d) of figure 4.2 the UT variation in the outflowing fluxes is shown for this asymmetric case. Contrary to the symmetric hemispheres, the daily peak does not have the same magnitude at the two solstices. This is also visible in panel (c). For O^+ this is 5.11×10^{24} s^{-1} in June and 4.24×10^{24} s^{-1} in December, and for H^+ this is 5.40×10^{25} s^{-1} and 4.94×10^{25} s^{-1}, respectively. At equinox, the two daily minima also do not have the same depth. They are for O^+ 4.98×10^{24} s^{-1} and 4.11×10^{24} s^{-1}, respectively, and 5.32×10^{25} s^{-1} and 4.88×10^{25} s^{-1} for H^+. Note that the two peaks at equinox are not separated by half a day, occurring around ∼10:00 and ∼00:00 UT.

3.3 Realistic polar cap shape: T89

In order to asses the effect of a more realistic polar cap shape, we use the Tsyganenko 89 model for Kp = 0 to obtain the open–closed boundary. The resulting O^+ fluxes are plotted in figure 4.3. One of the main differences with the earlier cases is that overall the flux is lower. This is because the area of the magnetic polar cap found for Kp = 0 with the T89 model is significantly smaller than that of a circular polar cap down to 75° MLAT. This is related to our choice of considering the polar cap for low activity and because of the issues with higher activity mentioned in Sect. 2. For higher activity levels, the polar cap area increases significantly, and together with it the total flux.

Another effect that is immediately clear, which does not appear in the circular case, is that there is still a daily variation during the period around the summer solstice. The magnetic polar cap is still completely sunlit during the whole day at the summer solstice, so this is not what is causing this variation. According to the Tsyganenko model, the magnetic polar cap varies throughout the day in shape and area. The variation is small and relatively irregular. That is what causes the variation in flux during the summer.

When we look at the combined flux from both hemispheres, plotted in panel (c) of figure 4.3, we see that it has a somewhat different shape from the circular

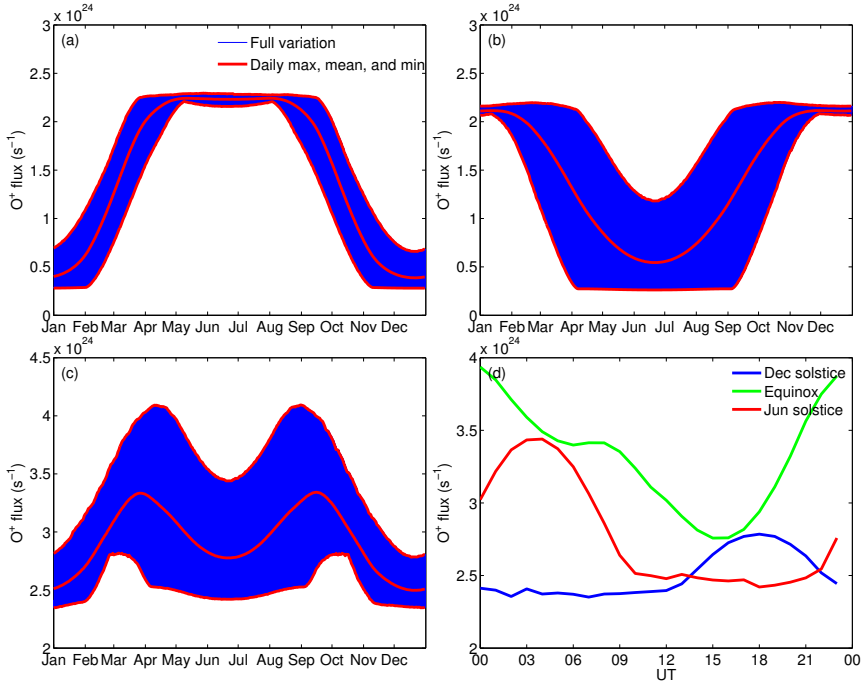

Figure 4.3: O^+ fluxes for a polar cap from the Tsyganenko model. **(a)** Northern Hemisphere. **(b)** Southern Hemisphere. **(c)** Both hemispheres combined. **(d)** UT dependence for both hemispheres combined.

asymmetric case, but overall it looks quite similar. One clear difference is that the daily minimum behaves a bit differently and is not flat around the solstices but dips even further. This is again the effect of the variation in polar cap size.

We also show the fluxes of H^+ in figure 4.4. We do this because in this case, as opposed to the circular cases where H^+ behaves the same way as O^+ except having smaller variations, H^+ exhibits a somewhat different behaviour than O^+. This is because the total area of the polar cap also varies. The effect of the solar illumination is smaller for H^+, since the difference between f_{sun} and f_{dark} is smaller than for O^+, but the effect of the varying polar cap area is the same for both H^+ and O^+.

The H^+ flux from both hemispheres shows a variation of $\sim$31%, with a maximum of 4.09×10^{25} s^{-1} and a minimum of 3.12×10^{25} s^{-1}. For the daily average, going from 3.68×10^{25} s^{-1} down to 3.24×10^{25} s^{-1}, the variation is around $\sim$13%. O^+ is more strongly affected by solar illumination and thus the flux

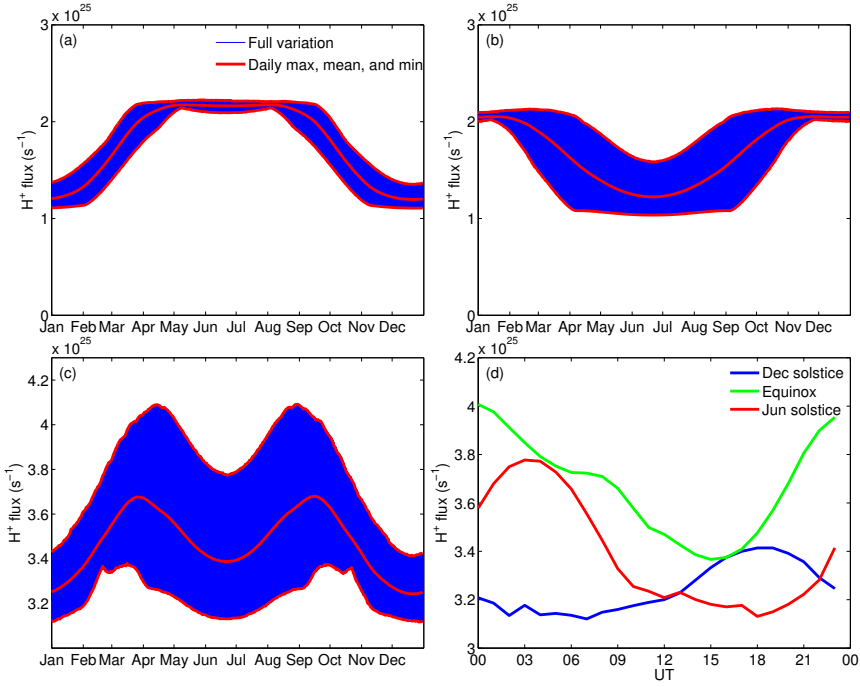

Figure 4.4: H^+ fluxes for a polar cap from the Tsyganenko model. **(a)** Northern Hemisphere. **(b)** Southern Hemisphere. **(c)** Both hemispheres combined. **(d)** UT dependence for both hemispheres combined.

shows larger variations going from 4.09×10^{24} s^{-1} down to 2.35×10^{24} s^{-1}; this is a variation of ∼74%, and ∼ 34% for the daily average, which has a maximum and minimum of 3.34×10^{24} and 2.50×10^{24} s^{-1}. Since the outflows of O^+ and H^+ react differently to solar illumination, the fraction of O^+ in the outflow will also vary. This fraction may vary from ∼7.0 to ∼9.1%, which is a variation of ∼31%, and the daily average from ∼7.1 to ∼8.3%, which is a variation of ∼16%. The total ion flux is dominated by H^+ and will thus show variations similar to the H^+ flux, namely ∼34 and ∼15% for the daily average. However, since the mass of the O^+ ion is about 16 times higher than that of the H^+ ion, the contribution of the O^+ outflow to the total mass flux may be more significant. For the mass flux from both hemispheres combined we find that there are variations of up to ∼55%, and up to ∼25% for the daily average.

We also find a different behaviour in the UT variation in panel (d) of figure 4.3. The two peaks at equinox are in this case very different and again shifted.

The one before at ∼7 UT is with 3.41×10^{24} s^{-1} much lower than the one at midnight, 3.94×10^{24} s^{-1}, and is barely higher than the local minimum only 1 h before, with 3.40×10^{24} s^{-1}. In the H^+ flux in panel (d) of figure 4.4, it is no longer even a local maximum. Like in the previous case, the two minima do not have the same depth, but now they also do not occur at the local noon of the poles, but around ∼6 and ∼15 UT.

The polar caps found from the Tsyganenko model do not have the same area in both hemispheres. On average the polar cap is ∼ 5.8% larger in the north than in the south. Consequently, the average flux over the whole year from the Northern Hemisphere is ∼ 6.7% larger than that from the Southern Hemisphere for O^+ and ∼ 6.2% for H^+. This can be seen in panels (a) and (b) of figure 4.4, if one looks closely. The daily averages are also not equal around the local summer solstices in this case, and around the local winter solstices the H^+ flux from the Southern Hemisphere is almost equal to that from the Northern Hemisphere (∼2% larger at maximum).

4 Discussion

The set-up of this simple model neglects many factors which influence the outflowing flux, like UV intensity, geomagnetic activity, heating of the atmosphere, neutral winds, etc. Their effects should be superimposed on the model results presented here. However, according to observations, the outflowing flux densities should statistically be separable in two groups by the solar zenith angle of their ionospheric origin, with the group with lower SZA having a higher average flux than the other. Therefore, these results should apply to the fluxes averaged over these other conditions.

4.1 Combined flux from both hemispheres

An important result, showing up in all three cases, is that, when combining the total flux coming from both hemispheres, we still see a seasonal and diurnal variation. For the circular and symmetric case, the seasonal variation is caused (only) by the fact that the terminator at ionospheric altitudes has a SZA larger than 90°. This means that the illumination profile of one magnetic polar cap is not the inverse of that of the other, and thus the variations in the flux from both hemispheres do not cancel each other. The fact that the geographic pole and the magnetic pole are not located at the same position implies that this also causes diurnal variations in the summed flux.

For the asymmetric case this also happens, but the asymmetry in the offset of both polar caps is an extra cause of seasonal variation in the summed outflow from both hemispheres. Even with a terminator at 90°, there are still variations over the seasons and days, whereas in the symmetric case the flux would remain constant over the whole year with the terminator at 90°. The variations due to this effect are comparable to those due to the terminator effect, if not a bit larger. In terms of daily averages (and thus the seasonal variation) they are smaller, however, about ∼50%. Note also that these variations due to both causes do not always occur at the same time, so they may combine to a larger variation at some times or counteract each other at other times.

For the calculations with the polar cap shapes from the Tsyganenko model, the north–south asymmetry in the polar cap area and the variation in the area constitute again two extra causes of seasonal variation for the total combined flux.

4.2 Importance to magnetospheric dynamics

The variation in the combined flux is important because a large fraction of the ions in the polar wind flow into the plasma sheet [Haaland et al., 2012; Li et al., 2013]. This combined flux thus also represents to some extent the supply of ions from the polar ionosphere to the plasma sheet. Consequently, this may lead to seasonal and diurnal variations in the plasma sheet density or composition. The high latitude ionosphere is an important source of plasma for the plasma sheet, more specifically of O^+ ions. The polar wind is also an important source of cold ions. As discussed in the introduction, the role of heavy ions like O^+ in magnetospheric dynamics is not yet clear, as is the answer to the question of whether ions can remain cold in the plasma sheet, but both cold ions and O^+ ions (cold or not) may affect reconnection or the stability in the tail.

Geomagnetic activity has been clearly observed to exhibit seasonal behaviour. One well-documented example is the occurrence frequency of geomagnetic storms, which has two peaks per year, at the equinoxes [e.g. Sabine, 1856; Cliver et al., 2000; Echer et al., 2011]. This seasonal behaviour is often attributed to the Russell–McPherron mechanism [Russell and McPherron, 1973]. This states that the inclination of the Sun's equatorial plane and the inclination of Earth's rotational axis from Earth's orbital plane cause a bias toward larger absolute IMF B_z values (in the GSM coordinate system) around the equinoxes and thus a higher geo-effectiveness. However, it has been argued that this mechanism cannot account for the full variation [Cliver et al., 2000]. Other mechanisms have been suggested (see, e.g., Russell and McPherron, 1973; Tsurutani and Gonzalez, 1995; Cliver et al., 2000, for a discussion of some).

The two peaks at the equinoctial months observed in the occurrence of geomagnetic storms coincide with the two peaks found in this study for the combined ion outflow from both polar caps. At this time of the year the total ion flux from both hemispheres peaks, as well as the H^+ flux, the O^+ flux, the O^+ proportion, and the mass flux. If O^+ indeed can alter geomagnetic activity, seasonal variations in ionospheric outflow should perhaps also be considered as a possible explanation. The same can be said if cold ion outflow can indeed remain cold in the plasma sheet.

4.3 Variations compared to other effects

Ion outflow from the polar ionosphere can also vary due to geomagnetic activity and variations in solar EUV (extreme ultraviolet) intensity. For geomagnetic activity, the outflowing H^+ flux density ($m^{-2}s^{-1}$) is found to increase by ∼300% from low to high Kp [Yau et al., 1988; Cully et al., 2003; Engwall et al., 2009a], and the O^+ outflow rate even by ∼2000% [Yau et al., 1988; Cully et al., 2003]. Haaland et al. [2015], studying cold outflowing ions during geomagnetic storms (identified by their excursion in Dst), find a similar number with an increase of up to ∼300% the average non-storm-time outflow rate during the peak phase.

The effect of the intensity of the EUV flux coming from the Sun has also been studied. Yau et al. [1988] actually found a (statistically marginal) decrease of ∼50% for H^+ with DE 1 data. For O^+, an increase of ∼400% was found. Cully et al. [2003] using Akebono data, however, observed an increase for both H^+ and O^+, of ∼300 and ∼2000%, respectively. Furthermore, Engwall et al. [2009a] and André et al. [2015] found an increase of the ion total flux of ∼200 and ∼100%, respectively. It is worth mentioning that Yau et al. [1988] and Cully et al. [2003] were restricted to an energy range of ∼10 eV–17 keV and ∼1–70 eV, respectively, and Engwall et al. [2009a] and André et al. [2015], using an indirect method involving the spacecraft potential, should have theoretically observed all ions. However, the last of these methods can only be used when the thermal energy of the ions is lower than both their bulk kinetic energy and the energy needed to overcome the spacecraft potential. Therefore, this method only observes ions with energies below Cluster's typical spacecraft potential in the lobes (∼40–60 V).

The variations found in this study, due to the presence or absence of solar illumination, are for the H^+ flux from one hemisphere roughly ∼2 times smaller than those found due to geomagnetic activity and solar EUV intensity. For O^+ they are roughly a factor of ∼3 smaller. When combining the flux from both hemispheres, the variations in this study become much smaller, since the illumination of one hemisphere opposes that of the other to some extent.

However, compared to variations due to geomagnetic activity, those found in this study constitute an increase over an extended period of time (they can last up to several months). In other words, it is a steady increase that may lead to mass loading of the plasma sheet. This difference may lead, for example, to an extra of $\sim 2.7 \times 10^{31}$ ions, of which $\sim 4.4 \times 10^{30}$ are O^+ ions, or $\sim 1.5 \times 10^5$ kg escaping from the ionosphere – and possibly ending up in the plasma sheet – during the 3 months around the equinox compared to the outflow during the 3 months around the December solstice. Moreover, in the context of the importance of ionospheric outflow for magnetospheric dynamics, it is difficult to causally link an increase in geomagnetic activity to the increase in ionospheric outflow caused by increased geomagnetic activity. The variations in outflow found in this study may happen before geomagnetically active times. Variations in F10.7 follow the 11-year solar cycle but also occur on smaller timescales. However, these variations do not have a daily or seasonal periodicity.

To put these numbers into context, we can very roughly estimate the total plasma content in the plasma sheet. Using the formula for H^+ and O^+ densities in the midtail plasma sheet of Maggiolo and Kistler [2014], with an average F10.7 of 150 and Kp of 2 (the values used in this study come from a study during low activity), we find an average H^+ density of ~ 0.26 cm^{-3} and O^+ density of $\sim 3.8 \times 10^{-3}$ cm^{-3}. Using a total plasma sheet volume of $\sim 4 \times 10^{24}$ m^3 from Chappell et al. [1987], we find a total of $\sim 1.0 \times 10^{30}$ ions in the plasma sheet, of which $\sim 1.5 \times 10^{28}$ are O^+ ions, and a total mass of $\sim 2.1 \times 10^3$ kg. Therefore, the additional outflow during the trimester around equinox is $\sim$26 times larger than the total content of the plasma sheet in terms of number of ions, and $\sim$73 times in terms of mass. The additional number of O^+ ions is more than $\sim$291 times the O^+ ions in the plasma sheet during quiet times. In other words, since these 3 months are 90 days, on average the content of almost one additional plasma sheet per day flows out from the polar cap around the equinox compared to around the December solstice, in terms of mass, and more than $\sim$3 additional plasma sheets per day in terms of O^+ ion numbers. This all assumes that the O^+ flux densities used are representative of the polar wind.

The variations due to the polar cap being sunlit or dark, represent a modulation of the background outflow, so these variations should also be factored in with the variations due to geomagnetic activity and solar EUV intensity. It has to be noted that the eccentricity of Earth's orbit, which was neglected in these calculations, also causes a seasonal variation. The current eccentricity of Earth's orbit is $\sim$0.0167; therefore, the intensity of the solar illumination is $\sim$6.9% higher at perigee than at apogee. It is, however, difficult to translate this intensity variation into an increase in outflowing ion flux

4.4 North–south asymmetry in outflow

As mentioned in Sect. 3, the outflow from both hemispheres is expected to be different, due to the asymmetry in the magnetic field. As we found from the asymmetric circular case and the more realistic case, there are two causes for the asymmetry: the difference in the offset of the magnetic pole from the rotational axis and the difference in polar cap area.

The asymmetry in the flux resulting from the difference in offset has itself a seasonal variation. At the local winter solstice, the southern hemisphere has a larger average outflow, because the larger offset from the rotational axis means that the polar cap is more likely to still reach the sunlight. However, around the equinoxes the flux from the Northern Hemisphere becomes larger. This means that, counterintuitively, in the period around the equinoxes there is also an asymmetry in the fluxes. Over the whole year these tend to cancel each other out. However, which hemisphere has the largest average flux over the whole year, as well as the magnitude of the difference, depends on the precise values for the size of the auroral oval and the SZA of the terminator. This dependence is not simple; it is not even monotonous. When changing the position of the terminator and the size of the circular polar caps over a range of values, the difference in average flux over the whole year can go up to a few percent for the O^+ flux, and almost 1.5% for H^+. When comparing the daily averages (in terms of days after the local winter solstice) the difference can go up to almost 150% for O^+ and more than 20% for H^+.

When using the polar caps from the Tsyganenko model, we find a larger area for the northern polar cap. This does not have a seasonal variation but rather shifts the flux from the Northern Hemisphere upwards by a few percent over the whole year. This difference in flux is not due to a difference in solar illumination but instead to a difference in the size of the source area. This difference in polar cap area is a result of the asymmetry in Earth's magnetic field, which is not a perfect dipole and not centred around Earth's centre of mass. There is no a priori reason why this difference in area should persist at high altitudes and cause a difference between the cross section area of the northern and southern magnetospheric lobes, since the higher-order terms of the multipolar expansion of the magnetic field fall off rapidly with distance. Thus, if we assume the asymmetry in Earth's magnetic field dies off at higher altitudes, and neglect any possible external source of asymmetries, the smaller total flux in the south would flow into the same area in the lobes as the higher flux in the north. In this case, not only will the total flux (ions s^{-1}) be lower in the south but also the flux density (ions $m^{-2}s^{-1}$).

4.5 Observability

One can argue that the variations and asymmetries discussed in this study should be visible to some extent in an extensive statistical study of in situ observations of the flux densities in the magnetospheric lobes, despite the fact that we only discussed the total flux. If a statistical study uses a dataset that sufficiently samples the whole polar cap, so that the average is representative of the flux density everywhere in the polar cap, then this average flux density is equal to the total flux divided by the polar cap area. Therefore, the average flux density should also exhibit the temporal variations and the asymmetries of the total flux. We should note, however, that this requires a very good sampling of the whole polar cap. Moreover, for temporal variations, this should be true at all time (down to the relevant timescale). This is a very strong requirement, and one which is rarely (or never) achieved in a realistic dataset of satellite measurements. Nonetheless, even if not all variations are visible, some might still show up in a sufficiently large dataset. For example, a study probing the flux densities in the magnetospheric lobes with enough measurements will most likely observe seasonal variations. Such studies might also be able to find an asymmetry in the outflow from both hemispheres.

5 Conclusions

With a simple set-up, this study explored the consequences of solar illumination modulation of ionospheric outflow above the polar cap as the magnetic polar cap rotates in and out of the sunlight on a diurnal and seasonal basis. The main results can be summarized as follows:

- There are daily and seasonal variations in the ion flux from each polar cap.
- These variations persist when summing the flux from both hemispheres, with maxima at the equinoxes. There are three main causes for this:
  - the fact that the terminator at ionospheric altitude has a solar zenith angle around 100°,
  - the larger offset of the southern polar cap from the rotational axis due to the north–south asymmetry of Earth's magnetic field,
  - the north–south asymmetry in the area of the magnetic polar cap.
- These variations also modulate the supply to the plasma sheet, and possibly affect magnetospheric dynamics. The peaks in combined outflow

coincide with the peaks of geomagnetic storm occurrence at the equinoxes, suggesting that the variations may be a cause for seasonal variation in geomagnetic activity.

- The north–south asymmetry in Earth's magnetic field also causes north–south asymmetries in the outflowing ion fluxes from the polar cap.

Acknowledgements. This work was supported by the IAP network "Planet TOPERS" (P7/15) initiated by the Belgian Science Policy Office (BELSPO). Romain Maggiolo was supported by Cluster/PRODEX PEA 40001009739.
We acknowledge the support from the International Space Science Institute through funding of their international team on "Magnetosphere–ionosphere–thermosphere coupling: differences and similarities between the two hemispheres".
The topical editor, Y. Miyoshi, thanks two anonymous referees for help in evaluating this paper.

Contributions. L.M. and R.M. designed the study. L.M. implemented the method, did the interpretation and discussion of the results, and wrote the paper. R.M. and J.D.K. helped with the discussion of the results and critical revision of the manuscript. All authors critically revised the manuscript.

Chapter 5

Polar wind outflow

In chapter 3 we suggested that the flux densities in the outflow above small-scale polar cap arcs are similar to the flux densities of the polar wind and that therefore the solar zenith angle should also affect the polar wind. We used these results in chapter 4 as assumptions to start from. In this chapter we see whether we can confirm these conclusions and assumptions of chapters 3 and 4 by analyzing the influence of solar illumination on the flux densities in the polar wind at high altitudes. We do this by making use of an alternative method that makes these otherwise inaccessible ions detectable. We present this work in the form of a paper as it is planned to be submitted in the near future.

Solar illumination control of the polar wind

L. Maes[1], R. Maggiolo[1], J. De Keyser[1,2], M. André*[3], A. Eriksson*[3], S. Haaland*[4,5], K. Li*[6], and S. Poedts[2]

[1]Royal Belgian Institute for Space Aeronomy, Brussels, Belgium, [2]KU Leuven Center for Mathematical Astrophysics, Celestijnenlaan 200B, 3001 Leuven, Belgium, [3]Swedish Institute of Space Physics, Uppsala, Sweden, [4]Max-Planck Institute for Solar Systems Research, Göttingen, Germany, [5]Department of Physics and Technology, University of Bergen, Bergen, Norway, [6]Institute of Geology and Geophysics, Chinese Academy of Sciences, Beijing, China

Abstract. Polar wind outflow is an important process through which the ionosphere supplies plasma to the magnetosphere. The main source of energy driving the polar wind is solar illumination. As a result, many studies have found a relation between polar wind flux densities and F10.7, but less is known about their relation with the solar zenith angle of the ionospheric origin, certainly at higher altitudes. The low energy of its particles means that it is very difficult to measure the polar wind at high altitudes due to spacecraft charging. We take advantage of an alternative method that allows to estimate the polar wind flux densities far in the lobes, and analyze measurements made by the Cluster spacecraft at altitudes from 4 up to 20 R_E. We observe a strong dependence on the solar zenith angle in the ion flux density and see that both the ion velocity and density exhibit a solar zenith angle dependence as well. We also find a seasonal variation of the flux density.

1 Introduction

The polar ionosphere is a special region because it is connected magnetically to the magnetic field in the solar wind. On the closed magnetic field lines that thread the lower-latitude ionosphere, a near-hydrostatic equilibrium is established in the trapped plasma of the plasmasphere, but on the open magnetic field lines of the polar ionosphere this is not possible, and ions keep flowing out [Dessler and Michel, 1966; Nishida, 1966]. The term polar wind was coined by Axford [1968], in analogy to the solar wind. Being less heavy, the ionospheric electrons can escape more easily than the ions and an ambipolar

electric field parallel to the magnetic field lines is set up to maintain quasi-neutrality, accelerating the ions [Dessler and Cloutier, 1969; Lemaire and Scherer, 1969, 1970].

This ambipolar electric field is weak but nonetheless manages to cause a significant amount of ions to escape. Its flux is estimated at 10^{25} to 10^{26} s^{-1} [Nagai et al., 1984; Huddleston et al., 2005; Cully et al., 2003; Engwall et al., 2009b,a; André et al., 2015]. As a consequence the magnetospheric lobes are filled by this steady flow of low-energy ions [Engwall et al., 2009a; André and Cully, 2012]. Ions flowing on these open magnetic field lines can escape into interplanetary space and thus the polar wind acts as a sink for ionospheric and magnetospheric plasma. Not all ions flowing out through the lobes manage to escape the magnetosphere, however, since convection transports them perpendicularly to the magnetic field lines so that ions with too low parallel velocities compared to the convection velocity will end up in the plasma sheet [e.g., Ebihara et al., 2006; Haaland et al., 2012].

Not only polar wind ions flow in the lobes, ions energized in the cusp may also pass through the lobes. Compared to the rest of the magnetic polar cap, there is a large energy input into the cusp in the form of Poynting flux and particle precipitation [Strangeway et al., 2005; Moore and Khazanov, 2010; Nilsson et al., 2012]. Therefore, despite its small spatial extent, the cusp is home to large ion outflows, which have been estimated to be of the order of 10^{25} s^{-1} [Pollock et al., 1990; Yau and André, 1997; Nilsson et al., 2012]. Ions flowing out from the cusp can be convected over the polar cap into the lobes and mix with the polar wind, so that it can be difficult to differentiate between "classical" polar wind ions and cusp ions.

Solar illumination is the main source of energy driving the polar wind. Consequently, several studies have found that the flux density in the lobes increases when the solar extreme ultra violet (EUV) flux (parametrized by F10.7) increases [Cully et al., 2003; Engwall et al., 2009a; André et al., 2015]. The solar illumination received by the ionosphere does not only vary with the solar EUV flux but also with the elevation of the Sun, which can be parametrized by the solar zenith angle (SZA). This has gotten somewhat less attention in observational polar wind studies, however. Su et al. [1998a] observed a sharp drop of the densities from SZA of 90° to 105°. Abe et al. [1993] and Abe et al. [2004] also found the polar wind velocity to go down as SZA goes up. Models of the polar wind that include hot photo-electrons predict similar behaviour [e.g., Su et al., 1998b; Glocer et al., 2012]. In a study of outflowing ions above small-scale polar cap arcs, Maes et al. [2015] evidenced a strong drop of flux densities around SZA of ∼100°, and argued that these flux densities should be similar to polar wind flux densities.

Most measurements of the polar wind have been done at altitudes not much higher than ∼10000 km, because at higher altitudes the low-energy ions of the polar wind become increasingly difficult to measure. A spacecraft traveling through space is constantly bombarded by EUV radiation that knocks electrons away from its surface. If the density of ambient plasma is not high enough to compensate for this flux of electrons away from the spacecraft, like at high altitudes in the lobes, the spacecraft will acquire a positive charge. In the lobes the spacecraft potential caused by this positive charge can go up to several ten eV. Since polar wind ions typically have energies only of the order of a few eV, they cannot overcome the spacecraft potential and do not reach the detectors. For this reason they are often referred to in literature as "cold ions". The POLAR mission managed to make measurements of the polar wind at altitudes of 8 R_E using a system actively reducing the spacecraft potential down to 1 or 2 V [Moore et al., 1997; Su et al., 1998a]. This type of potential control, however, can only be used for a limited amount of time, and the ions with energy below the reduced spacecraft potential are still missed.

An alternative method was used by [Engwall et al., 2006]. By exploiting the spacecraft potential to find the plasma density [Pedersen et al., 2001] and the charged wake created behind the spacecraft [Eriksson et al., 2006] to estimate the ion bulk velocity, they managed to measure the polar wind flux densities. This method requires a specific set of electric field experiments, as is present on the Cluster spacecraft [Escoubet et al., 1997], and has given rise to several other investigations of the polar wind far in the magnetospheric lobes [see Haaland et al., 2016, for an overview]. This is also the method used by [André et al., 2015] for creating the dataset used in this study, and will be explained in the next section. This method has the advantage that it can measure polar wind fluxes with low energies at high altitudes, theoretically without a lower limit on the energy. It can also be used over extended periods of time and is thus suitable for statistical studies.

The goal of this paper is to assess the effect of the solar zenith angle of the ionospheric origin on the polar wind flux density at high altitudes in a statistical way. We take advantage of the strong points of this alternative method. In what follows we will first introduce the experimental methods and discuss the data characteristics in section 2. In section 3 we report the results, and we will discuss them and their implications in section 4.

2 Data and method

The main quantity we want to study is the flux density. This is the product of the ion density and the ion bulk velocity. In order to be able to compare flux densities from different altitudes we normalize them to an altitude of 200 km, by dividing them by the ratio of the magnetic field strength measured by the spacecraft over magnetic field strength at 200 km altitude. Note that this is a different altitude than many other studies which typically normalize to higher altitudes, and this should be taken into account when comparing the flux densities with those from other studies.

The density and bulk velocity can be found for cold ions with the two alternative methods explained in sections 2.1 and 2.2, respectively. These methods make full use of the electric field experiments on board the Cluster spacecraft.

The Cluster mission consists of four spacecraft launched into a polar orbit in July and August of 2000 [Escoubet et al., 1997]. Among the set of instruments on board of each spacecraft are two electric field experiments that use different principles and it is this specific combination that allows for this method to find the ion bulk velocity. The Electric Field and Wave (EFW) instrument utilizes two probes mounted on 50 m long wire booms [Gustafsson et al., 1997]. This instrument therefore measures the electric field on a scale of the order of the length of the booms. The Electron Drift Instrument (EDI) emits and recaptures a beam of electrons and acquires the electric field from the drift of the gyration center of the electrons in the beam [Paschmann et al., 1997]. Since the energy of the emitted electrons is of the order of keV, their gyroradius in the lobes is of the order of a few kilometers, and thus this method will not be affected by electric field variations at smaller scales.

2.1 Spacecraft Potential: Plasma density

A satellite in space is constantly hit by solar illumination. Higher-energy radiation can cause electrons to be emitted from the spacecraft's surface. If the density of the surrounding plasma is not high enough to provide a sufficient return flow of electrons to compensate for the electrons escaping from its surface, the spacecraft will acquire a positive charge. This prevents ions with too low energy to overcome the resulting spacecraft potential to reach the onboard instruments. The magnitude of the spacecraft potential depends on the solar irradiance, spacecraft properties (like shape, surface material, area, etc.), and the plasma density. With due calibration, the spacecraft potential can therefore be used to determine the plasma density [Pedersen et al., 2001, 2008; Lybekk et al., 2012]. Typically the density n can be written as an exponential function

(or superposition thereof) of the spacecraft potential V_{sc}. For this dataset the relation

$$n(t, V_{sc}) = \phi_n(t)\ A\ e^{\frac{-V_{sc}}{B}} \tag{5.1}$$

is used. This is the relation given by Lybekk et al. [2012] but additionally multiplied with a normalization function $\phi_n(t)$ to account for daily variations in the irradiance. $\phi_n(t)$ is given by the value of $F_{10.7}$ at time t divided by the average $F_{10.7}$ of the year of t. The parameters A and B are given for specific ranges of V_{sc} and years. They can be found in Lybekk et al. [2012].

Since this method determines the electron density, which by assumption of quasi-neutrality is equal to the total ion density, this method cannot distinguish between different ion species.

2.2 Wake electric field: Ion bulk velocity

An object moving through a medium at supersonic speeds creates a wake behind it. In a plasma, electrons can more easily enter this wake than ions because of the electrons' typically higher thermal speed. This charge separation sets up an electric field. When a spacecraft is charged, the wake behind it may be significantly enhanced [Eriksson et al., 2006]. This enhanced wake occurs when the kinetic energy associated with bulk flow of the ions is smaller than the energy needed to overcome the spacecraft potential, but larger than the ions' thermal energy, i.e., when

$$kT_i < \frac{m_i {v_i}^2}{2} < eV_{sc}, \tag{5.2}$$

where T_i, m_i, and v_i are the ion temperature, mass, and bulk flow, respectively, and V_{sc} is the spacecraft potential.

The EDI experiment is unaffected by the small-scale electric field due to the wake behind the spacecraft, and thus the electric field measured by it is the ambient convection electric field. The electric field measured by the EFW experiment, on the other hand, is a superposition of the large-scale convection electric field and the wake electric field. Therefore the wake electric field can be found from their difference: $\mathbf{E}^{\mathrm{w}} = \mathbf{E}^{EFW} - \mathbf{E}^{EDI}$. Assuming the ions are unmagnetized on the scale of the wake, the electric field $\mathbf{E}^{\mathrm{w}}$ is in the direction of the plasma flow $\mathbf{v}$ and may be written as

$$\mathbf{E}^{\mathrm{w}} = g\mathbf{v} = g\mathbf{v}_{\perp} + gv_{\parallel}\frac{\mathbf{B}}{B}, \tag{5.3}$$

where g is some scalar function which may depend on the plasma properties or the plasma flow speed v, but is independent of the flow direction [Engwall et al.,

2006, 2009a]. If the frozen-in condition applies, the perpendicular component of the flow velocity should be the convection velocity and can thus be found from the electric field measured by EDI: $\mathbf{v}_\perp = \mathbf{E}^{EDI} \times \mathbf{B}/B^2$.

EFW can only measure the electric field in the spin plane of the spacecraft, however, this is no problem as long as the projection of $\mathbf{E}^{\mathrm{w}}$ onto the spin plane is not too small. Decomposing $\mathbf{E}^{\mathrm{w}}$ into components E_x^{w} and E_y^{w} in the spin plane, an expression for $v_\parallel$ is found by dividing equation (5.3) for one component by that for the other and rearranging:

$$v_\parallel = \frac{E_x^{\mathrm{w}} v_{\perp,y} - E_y^{\mathrm{w}} v_{\perp,x}}{E_y^{\mathrm{w}} B_x - E_x^{\mathrm{w}} B_y} B. \tag{5.4}$$

Note that it is unnecessary to know the scalar function g. If there is a population of hot plasma co-existing with the cold plasma, this method does not work, since the hot ions can enter the wake and thus cancel it out.

2.3 Data

The dataset used in this study is a subset of the one compiled by André et al. [2015]. The original dataset contains data from both Cluster 1 and Cluster 3. To select the data, several constraints were introduced to guarantee the quality of the data, which can be found in the appendix of André et al. [2015].

In the present study, however, we will only use data from Cluster 1, for reasons mentioned further on. This subset consists of more than 160000 individual measurements in the magnetospheric lobes at altitudes between 4 and 20 R_E over a period spanning from July 2001 until July 2009. Due to the orbit of Cluster only measurements in the lobes could be made during the months from July until November. These measurements come from 282 passes, of which 142 in the northern and 140 in the southern lobe. Within these passes, the majority of the measurements are 4 seconds apart, but there are also larger gaps up to several hours. Most of the passes have less than 1000 measurements, but some have up to more than 5000. The distribution of the number of measurements per pass is shown in figure 5.1. There are no measurements in 2008 and only 2 passes (in the southern lobe) in 2009 (in July).

2.4 Solar zenith angle

To find the solar zenith angle of the ionospheric origin of the ions, we use the Tsyganenko 89 model [Tsyganenko, 1989] to trace the magnetic field line from the spacecraft's position down to the ionosphere, at an altitude of 200

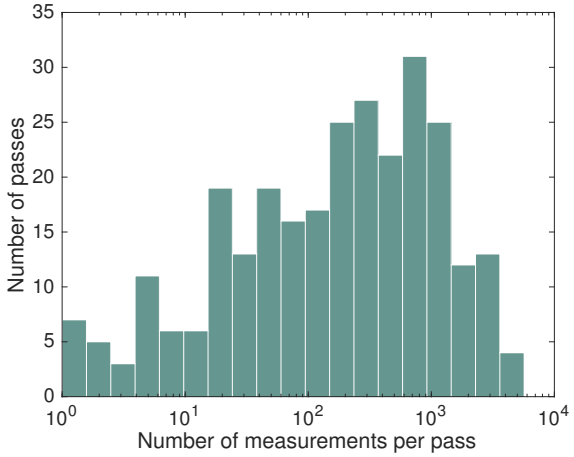

Figure 5.1: Distribution of number of measurements per pass.

km. It is important to note that this is no particle tracing, i.e. all movement perpendicularly to the magnetic field lines has been neglected. Therefore convection may be a cause of significant error on the determined solar zenith angle.

For ions flowing at the velocities as found in the data, the transport time from ionosphere to the position of the spacecraft may be on the order of an hour. We chose not to introduce any correction for this, since the correct determination of the transport time would require knowledge of the exact path, the altitude of acceleration, etc. These are all unknown or very difficult to establish, and thus trying to correct for the transport time would significantly increase the complexity for little to no increase in precision.

We checked the results using several methods for estimating the transport time (including using velocity and distance, constant transport time, etc.) and the overall conclusions do not change. Moreover, the error due to the neglect of the perpendicular motion is most likely much larger.

We also divide the data according to hemisphere. Because of the constant motion of the magnetotail, the northern and southern hemispheric lobes cannot be found by simply looking at the z_{GSM}-coordinate. Therefore, the hemisphere to which the measurements belong is determined by the projection of the magnetic field onto the position vector: north if it is negative, south if it is positive.

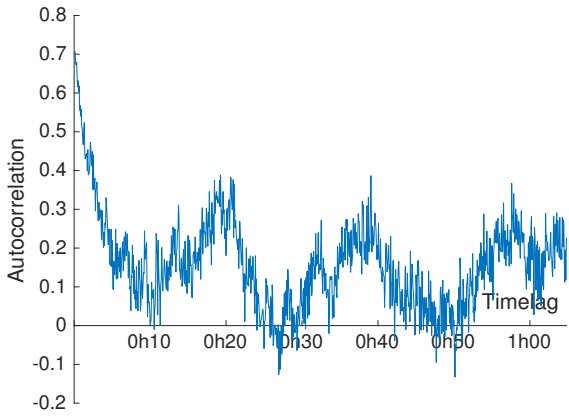

Figure 5.2: Autocorrelation function of the flux density during the pass through the northern lobe on 24 August 2003.

2.5 Statistics

One has to be careful how to deal with such data, from a statistical point of view. Since most of the individual measurements are only 4 seconds apart, they have also been made close to each other in space, and thus cannot be considered independent measurements. Therefore we should not overestimate the statistical significance this large number of measurements suggests. Many statistical constructs and tests, like the standard error (or the interpretation thereof), hypothesis tests, or correlation coefficients, assume independent measurements. The autocorrelation of the flux density for a particular pass shown in figure 5.2 clearly evidences this problem. The autocorrelation does not behave the same for all passes, but what almost all of them have in common is this initial sharp drop of the autocorrelation. For many of them this sharp drop is at some point intercepted by a slower decreasing curve or often even going upward again towards a peak, suggesting some sort of quasi-periodicity in the data. The example shown in figure 5.2 even has multiple peaks at more or less equidistant time lags, which would suggest some periodicity with multiple harmonics.

We interpret the initial drop as the drop in autocorrelation due to measurements being taken progressively farther apart and thus becoming more and more independent. It is unlikely that the other behaviour can be explained this way and thus most likely this has some other cause. There may be a physical explanation, like variation of the density due to compression of the lobes or

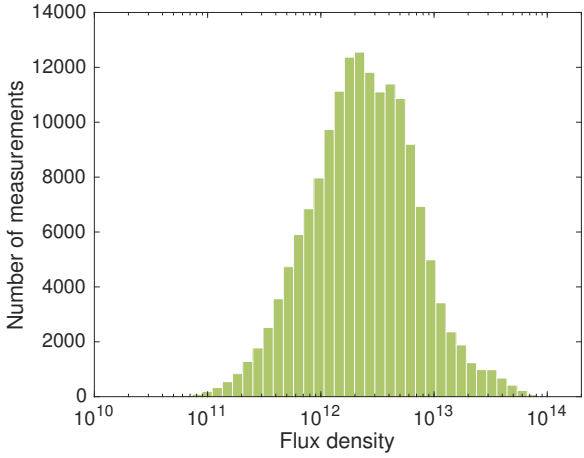

Figure 5.3: Distribution of the flux densities.

movement of the magnetotail caused by variations in solar wind pressure or Kelvin-Helmholtz waves. We did not investigate this, however. It may be an interesting subject for a further study.

In order to acquire more or less independent measurements we define a time t_c as the time for which the autocorrelation first drops below 0.5, so that the coefficient of autodetermination becomes lower than 0.25. The average $\langle t_c \rangle$ for all orbits is 160 seconds, and this is larger than the t_c of 90% of the passes. Therefore, when performing statistical tests, we will average the measurements per 160 s intervals and treat these as individual independent measurements. This issue with independent measurements is also why we chose to work with data from one spacecraft only.

Both the densities and the velocities, as well as the flux densities calculated from them, are distributed according to a distribution closer to a lognormal distribution than a normal distribution, as can be seen in figure 5.3 for the flux density. Therefore, we will plot many of the figures involving these parameters on a logarithmic scale and use logarithmically spaced bins. We will also often use the logarithmic mean, instead of the regular mean, since it is much more representative for these kind of distributions.

Another problem is the unevenly distributed number of measurements per pass as evidenced in figure 5.1. This means that the condition of passes with much more measurements may be oversampled if all single measurements are given equal weight. We will discuss its effect on the results as well.

3 Results

Figures 5.4a and 5.4b show the bivariate distributions of the flux densities (on the y-axis) and solar zenith angle (on the x-axis), for the northern and southern hemisphere, respectively. The color scale shows the number of measurements in each bin. The black line is the average of groups of equal number of data points sorted according to SZA. In figure 5.4c these averages are shown again, but on a linear scale, in blue and red for the northern and southern hemisphere, respectively, and black for both hemispheres combined. A downgoing trend, from low to high SZA, can clearly be seen. The average flux density in both hemispheres in figure 5.4c decreases by a factor of more than 3 from small to large SZA, going from 4.2×10^{12} $s^{-1}m^{-2}$ to 1.2×10^{12} $s^{-1}m^{-2}$.

In order to check the statistical significance of the variation of the flux density over the SZA, we divide the data into two groups according to their SZA, or more specifically, a group with SZA smaller than 100° and a group with SZA larger than 100°. We choose this value, because, due to the transparency of the atmosphere, the terminator at ionospheric altitude will be at SZA larger than 90°, and 100° falls in the ranges found for the transition region in several studies [Su et al., 1998a,b; Glocer et al., 2012; Maes et al., 2015]. The exact value has no meaning, however. In order to have independent values we use the averages per 160 seconds, as explained in section 2.5. The distributions of the flux densities of both groups can be seen in figure 5.5. The statistical significance of the difference between the averages of both distributions is high. When performing a Mann-Whitney-Wilcoxon test, even with the reduced dataset, the probability that both sets come from the same distribution is smaller than 10^{-15}.

Since the flux density is the product of the density and the velocity, it is interesting to see whether it is the density or the velocity that causes the dependency of the flux on the solar zenith angle. Therefore the same type of bivariate histograms as for the flux are shown for the density (normalized to 200 km altitude) in figure 5.6, and for the velocity in figure 5.7. From this we see that both the density and the velocity depend on the solar zenith angle. Together they combine to the flux density, which has an even clearer dependency on the SZA.

The average normalized density for both hemispheres at the smallest SZA, 1.4×10^8 m^{-3}, is more than double that at the largest SZA, 7.0×10^7 m^{-3}. The velocity goes from 29 km s^{-1} at small SZA down 17 km s^{-1} at large SZA. This is a decrease with a factor of 1.7.

Note, however, that acceleration of escaping ions at higher altitudes lowers the densities without changing the amount of outflowing ions, so that densities may not necessarily be a good estimator for the outflow. And due to centrifugal

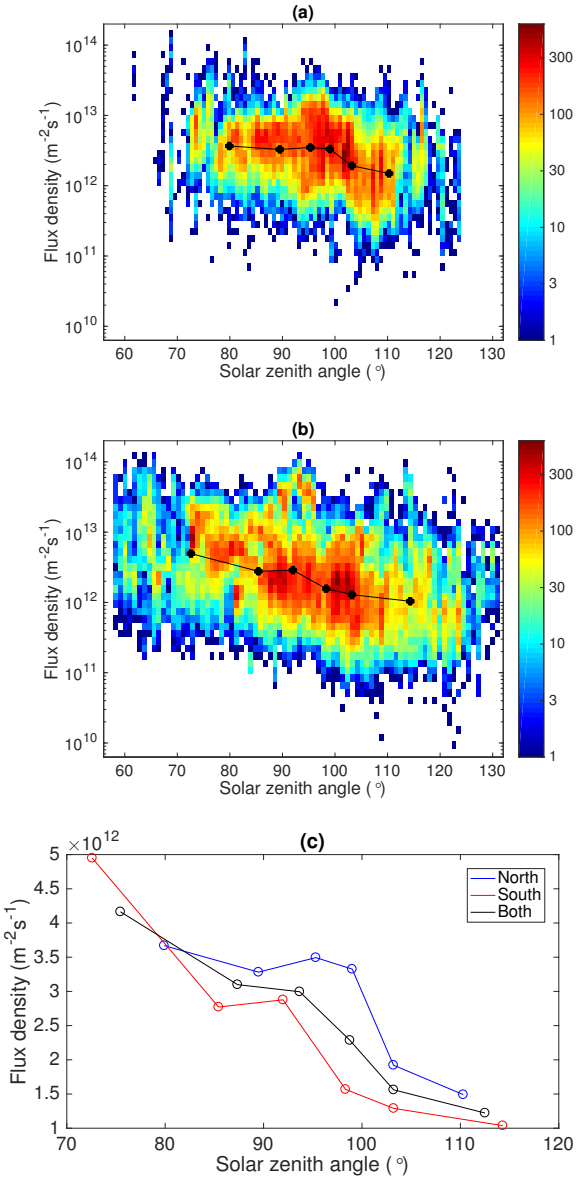

Figure 5.4: Flux density vs SZA. Panels **(a)** and **(b)** show the bivariate distributions of the flux density (on the y-axis) and the SZA (on the x-axis), for the northern and southern hemisphere, respectively. The black dotted line shows the average per equal amount of sorted data. Panel **(c)** shows the averages on a linear scale.

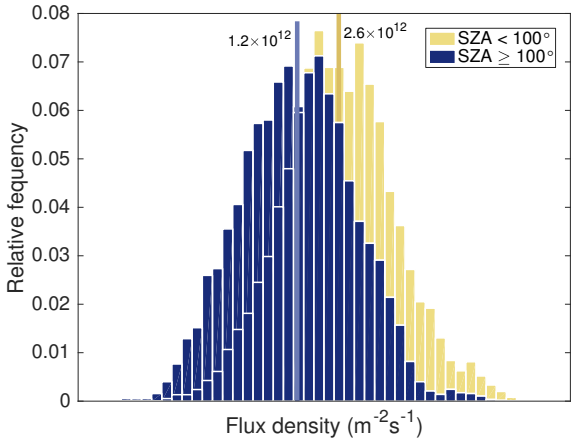

Figure 5.5: Distribution of the flux densities, split up according to SZA.

acceleration the velocity may not be easily comparable at different altitudes. These issues do not play a role for the flux densities, by virtue of flux conservation.

The magnetospheric lobes are magnetically connected to the magnetic polar caps. And since the magnetic polar cap rotates on a seasonal (and diurnal) basis, the SZA of the mapped spacecraft positions has a time dependency. Therefore one might also expect a similar time dependency of the flux densities. Figure 5.8 shows the bivariate histograms of the flux densities and the time of year. This figure collects data covering more than 8 years. As mentioned in section 2, all the data come from the months July till November.

An overall trend going from low to high flux densities can be seen for the southern hemisphere in figures 5.8b and c. This is as one would expect for a hemisphere going from its summer solstice to its winter solstice. For the northern hemisphere a downward trend can be seen to some extent, as expected for a hemisphere going from its summer solstice to its winter solstice, although there is a large peak in September.

For both hemispheres the seasonal trend is much less clear than for the SZA. This is to be expected, since the SZA does not depend solely on the day of year, but also on the position in the polar cap and on the time of the day.

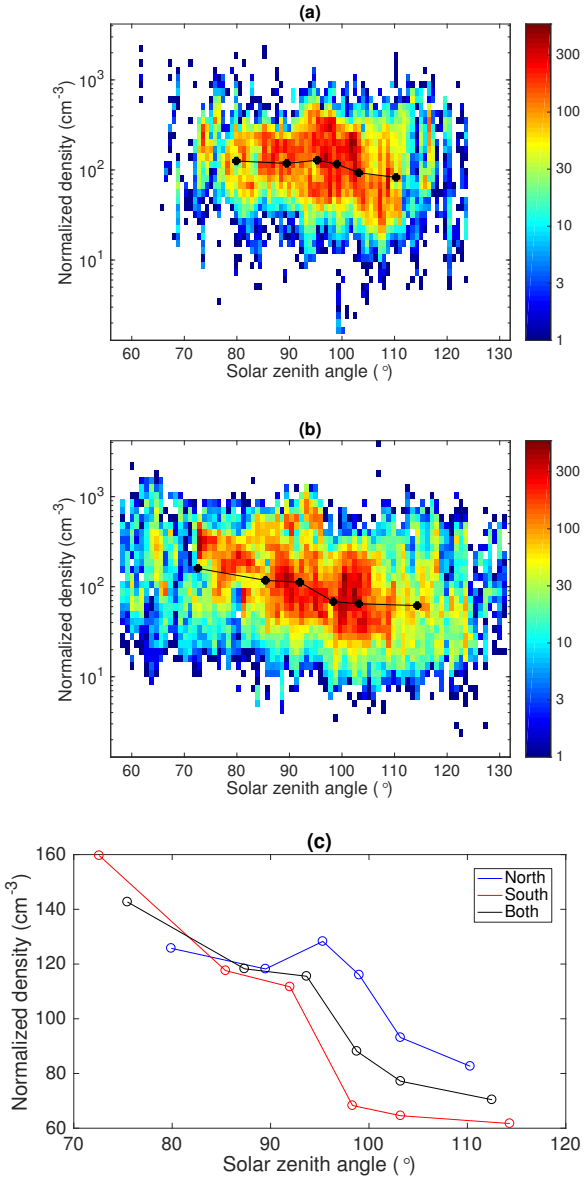

Figure 5.6: Density vs SZA. Panels **(a)** and **(b)** show the bivariate distributions of the (normalized) density (on the y-axis) and the SZA (on the x-axis), for the northern and southern hemisphere, respectively. The black dotted line shows the average per equal amount of sorted data. Panel **(c)** shows the averages on a linear scale.

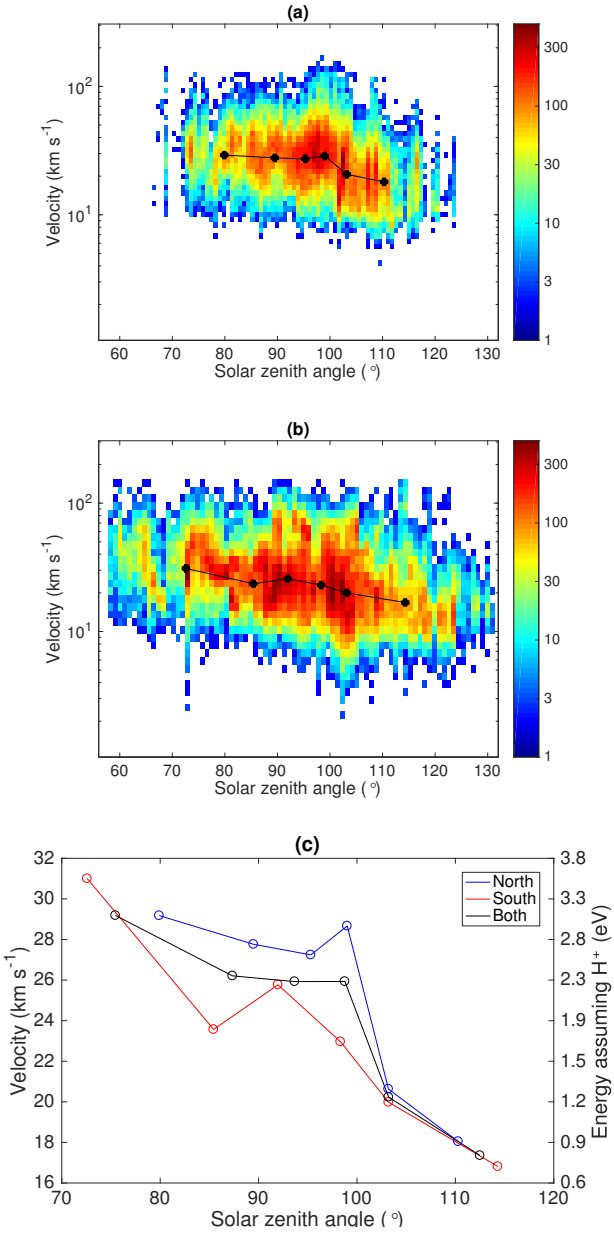

Figure 5.7: Velocity vs SZA. Panels **(a)** and **(b)** show the bivariate distributions of the velocity (on the y-axis) and the SZA (on the x-axis), for the northern and southern hemisphere, respectively. The black dotted line shows the average per equal amount of sorted data. Panel **(c)** shows the averages on a linear scale.

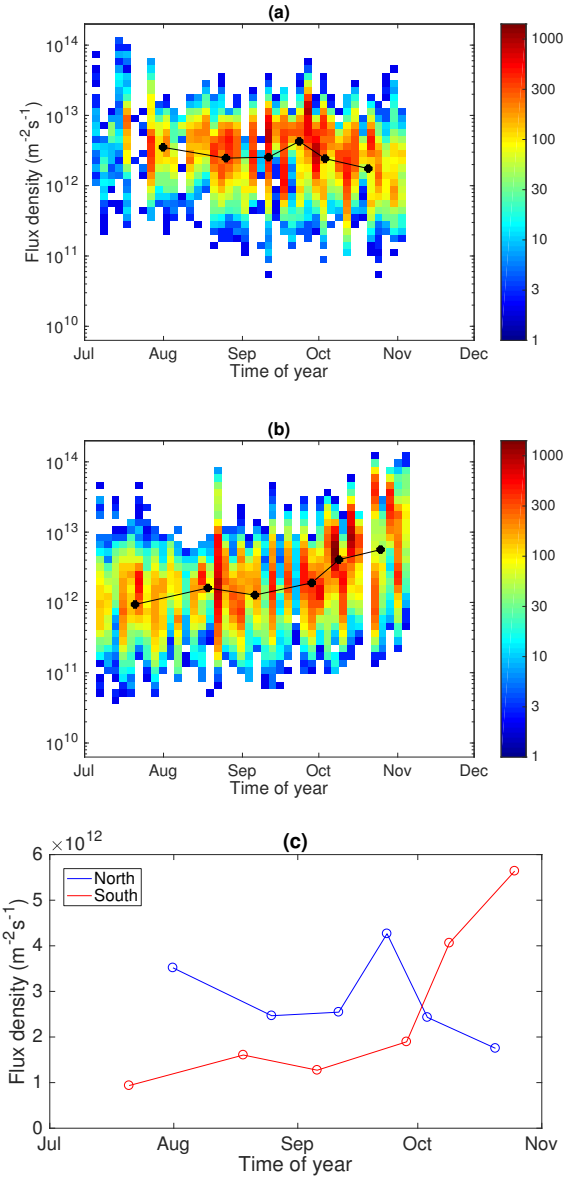

Figure 5.8: Flux density vs time. Panels **(a)** and **(b)** show the bivariate distributions of the flux density (on the y-axis) and the time of year (on the x-axis), for the northern and southern hemisphere, respectively. The black dotted line shows the average per equal amount of sorted data. Panel **(c)** shows the averages on a linear scale.

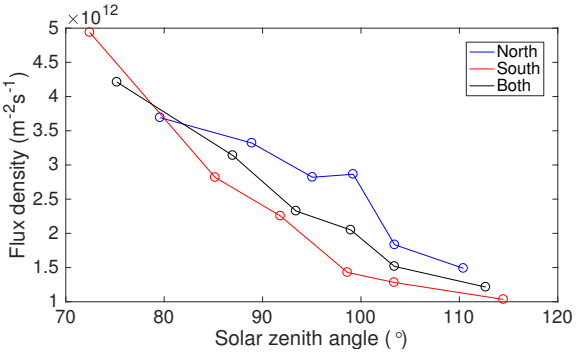

Figure 5.9: The average fluxes as in figure 5.4c, but with the passes of 23 September 2001 and 21 October 2001 eliminated.

4 Discussion

Before we draw conclusions from these results it is important to understand how biases or sampling issues in the data can affect the results shown in section 3. We discuss this in section 4.1 and continue with the interpretation of the results in section 4.2.

4.1 Effect of statistical issues

The effect one pass with many measurements can have on the statistics should not be underestimated. For example, in figure 5.4b, the red or orange patch around 95° and 4×10^{13} $m^{-2}s^{-1}$ is completely caused by one pass at 21 October 2001 of 1744 measurements. Similarly, in panel a of figure 5.4, the red bump between 94° and 99° is almost completely caused by one pass at 23 September 2001 of 3815 measurements (of which ∼2900 within the bump). To illustrate the effect passes like this can have on the averages, we show in figure 5.9 the same averages as in figure 5.4c, but without these two passes. Considering their relatively high velocity, it is not unlikely that the ions in these events are cusp outflow convected across the polar cap, rather than polar wind outflow.

This issue is even worse for the time variation, since a single pass may be spread over several SZA, but it will always be concentrated in a period of several hours. The large peak at September for the northern hemisphere is to a large extent (but not completely) caused by that same pass at 23 September 2001.

There is also an orbital bias such that there are more measurements in the later

months (Sep-Nov) from the earlier years (2001-2003) and more measurements in the earlier months (Jul-Aug) from the earlier years (2005-2007). Since the solar cycle was around its maximum in 2001-2003, and close to its minimum during the years 2005-2007, there is also some bias in F10.7. On average, the first half of the data (in day of year) has an F10.7 of almost 40 solar flux units lower than the second half. Since F10.7 has also been shown to affect the ion outflow, this may weaken the seasonal variation in the north and strengthen it in the south.

4.2 Interpretation

Figure 5.4 shows clear evidence of the importance of the solar zenith angle of the ionospheric origin for the ion flux densities in the magnetospheric lobes. This is similar to what Maes et al. [2015] find for the ion outflow above small-scale polar cap arcs, and thus seems to agree with their suggestion that the flux densities of the polar wind and of ion outflows above small-scale polar cap arcs are comparable. No dependence of the flux densities on the x_{SM}-coordinate was found, suggesting that the distance to the cusp is not an important factor.

The change of the density over the SZA evidenced in figure 5.6 is in concordance with the findings of Su et al. [1998a] with POLAR data for H^+. The velocity modulation by the SZA witnessed in figure 5.7 agrees with the observations by Akebono reported by Abe et al. [1993] and Abe et al. [2004].

The large uncertainty on the SZA due to convection may be a cause of concern. Convection can be anti-sunward, stagnant, or even sunward. We can make a rough estimate of the error due to convection. Typical convection velocities at ionospheric altitudes have an antisunward component of 250 m s^{-1}. The median altitude of all measurements is roughly 10 R_E and the median velocity 24 km s^{-1}. This gives a travel time of 44 minutes, which will change the SZA by 5.6°. So we find that convection causes a smoothing of the SZA on the order of 5°, although individual errors may be larger. This will blur the relation between the flux density and the SZA. The fact that we still see a relation, despite the error due to convection, is all the more evidence that there really is one.

A difference between our study and Maes et al. [2015] and Su et al. [1998a], is that the latter both find two regimes, i.e., outflow above a sunlit and a dark ionosphere, with a relatively small transition between both (at least for O^+). Figure 5.4c suggests more a gradual change over the SZA. However, the large uncertainty on the SZA due to convection would most likely blur any sharp transition that may be present. This is much less the case for the outflows above the small polar cap arcs, since they have been accelerated strongly by the associated electric field, which largely decreases the possible impact of

convection. Similarly, the results from Su et al. [1998a] come from measurements at $\sim$ 5000 km altitude, where convection will have had less time to play a role. Since the polar wind is dominated by H^+ ions, one may find figure 5.5 to be comparable to figure 2b in Maes et al. [2015], which also shows the distributions split up according to SZA smaller or larger than 100°. However, considering this uncertainty on the SZA, it is most likely not possible to conclude much about the nature of the transition, i.e., gradual or sharp.

The variation with the solar zenith angle is a sign that the state of the local ionosphere determines (at least in part) the outflowing flux densities. This corroborates the conclusion by André et al. [2015] that the cold ion fluxes in the magnetospheric lobes are mostly limited by the ion supply from the ionosphere.

Interestingly, though, while André et al. [2015] did find a variation of both the density and the flux density with F10.7, they reported no significant change of the velocity over different values of F10.7. We do find a variation of the velocity with the SZA. This may be of interest as to how solar illumination affects the ion outflow.

A density increase in the ion outflow may be attributed to an increase in the ionospheric density or an increased ambipolar electric field. An increase of the velocity may be due to an increased ambipolar electric field or due to additional acceleration higher up in the magnetosphere. The solar zenith angle of the ionospheric origin is unlikely to affect the energization in the magnetosphere, though, so that the former cause seems the only likely explanation. Solar illumination may alter the ambipolar electric field by increasing the ionospheric temperature and by producing hot photo-electrons. The latter is suggested by some studies to have an important effect on the ambipolar electric field [e.g., Khazanov et al., 1997; Su et al., 1998b; Glocer et al., 2012].

Despite all the statistical issues with uneven sampling and the bias in F10.7, we do also find a seasonal trend in the southern hemisphere, and a less convincing trend in the northern hemisphere. This is further evidence for the impact of solar illumination on the ion outflow via modulation of the ionosphere.

5 Conclusions

We analyzed a large dataset of ion flux densities measured at altitudes of 4 to 20 R_E in the magnetospheric lobes that uses an alternative method to measure otherwise inaccessible low energy ions. Despite the large uncertainty in determining the solar zenith angle of the ionospheric origin, we can make several conclusions:

- The flux density exhibits a dependence on the solar zenith angle.
- The density and velocity show a similar but less strong dependence and together combine to the stronger dependence of the flux density.
- Due to the correlation between solar zenith angle and the time of year we also observe a seasonal variation in the flux density.

These findings corroborate the idea that the state of the local ionosphere is the main factor determining the polar wind number flux density, and that solar illumination has an important role in this. The density of the ionosphere may be altered as well as the ambipolar electric field of the polar wind.

Contributions. L.M. designed the study, did the data analysis, interpretation, and discussion, and wrote the paper. R.M. helped with the interpretation and discussion of the results and critical revision. J.D.K. and S.H. helped with the discussion of the results and critical revision. A.E., M.A., and K.L. acquired the data and helped with discussion of the results. S.P. helped with critical revision.

Chapter 6

Conclusion

The main goal of this thesis was to study the effect of solar illumination on ionospheric outflow at high latitudes. After an introduction in chapter 1, we introduced in chapter 2 the spacecraft instruments that were used for this study, as well as the magnetic field models that were used to help interpret the measurements. In chapter 3 we therefore investigated a special type of accelerated outflow, ion outflow above small-scale polar cap arcs, and analyzed its dependence on the solar zenith angle of its ionospheric origin with the CODIF instrument on Cluster. It is clear that solar illumination is an important factor in determining the flux density of the outflow. For both H^+ and O^+ ions the flux density is lower above a dark ionosphere than above a sunlit ionosphere. The effect is stronger for the O^+ ions, and thus also the composition of the outflow changes with the solar illumination. We found that the field-aligned potential drop associated with the polar cap arcs is affected by solar illumination as well: no small potential drops were found above a dark ionosphere. This shows that the state of the ionosphere does not only affect the outflow, but also the field-aligned potential drops in the magnetosphere. Solar illumination changes the ion density and temperature, which can alter the ionospheric conductivity. Since the polar cap arc is part of a current system generated in the magnetosphere and closing in the ionosphere, the ionospheric conductivity can have an impact on this system.

In chapter 4 we applied the concept of different outflow above a sunlit ionosphere and a dark ionosphere to the polar wind to see what happens to the total flux from the polar cap when it rotates in and out of the dark. We found that there are daily and seasonal variations in the outflow from one polar cap, but also that they persist when combining the two hemispheres. Since much of the polar

wind ions probably end up in the plasma sheet, this combined flux represents a part of the ionospheric supply to the plasma sheet. Over an extended period of time, this difference in mass loading and composition may alter the dynamics of the magnetosphere in the plasma sheet. By being heavier (i.e., containing O^+ ions) and colder than typical plasma sheet plasma, the plasma of ionospheric origin could affect the reconnection processes, although this is still a hot topic, and thus geomagnetic storm and substorm activity. The seasonal maxima of the total flux turn out to occur around the same time as the two peaks in geomagnetic activity near the equinoxes. We also found that the north-south asymmetry in Earth's magnetic field may cause a north-south asymmetry in the polar wind fluxes. Haaland et al. [2017] did indeed observe a north-south asymmetry in the density in the magnetospheric lobes as estimated from the spacecraft potential. It is difficult to say, however, how much of this asymmetry can be explained by the mechanism demonstrated in chapter 4.

In chapter 5 we used a database, compiled using an alternative technique that estimates the low-energy ion fluxes far in the lobes that are otherwise inaccessible due to spacecraft charging, to analyze the solar zenith angle dependence of the polar wind. We found that, just like the outflow above polar cap arcs, the polar wind flux density depends strongly on the solar zenith angle of the ionospheric origin of the ions. This is further evidence supporting the notion that the polar wind outflow is largely controlled by the illumination state of the ionosphere. We found a correlation between the SZA and both the density and the velocity, as opposed to F10.7 for which only a clear correlation with the density was found by André et al. [2015]. We also observed a seasonal variation of the polar wind flux, confirming one of the predictions made in chapter 4. However, it is clear that this is at the limits of what is possible with this dataset, so that it is not possible to test the more interesting predictions regarding temporal variations. At the time of writing, preliminary results do show a north-south asymmetry in the flux densities, although more work is needed to confirm this.

Compared to other parameters, the influence of the solar zenith angle is not so often studied for the polar wind, and at high altitudes no other study has reported on it. The clear solar illumination dependence of both the outflow above polar cap arcs and the polar wind suggests that the state of the ionosphere strongly impacts the outflow. For the polar cap arc outflow, this would mean that the quasi-static field-aligned electric field merely accelerates the ions without changing the flux density. If that is correct, a further implication is that the polar wind flux densities are similar to the outflowing flux densities above polar cap arcs (at least up to the typical altitude of the bottom of the acceleration region of polar cap arcs, since polar wind ions may still fall back there, which does not happen for the ions above polar cap arcs). For the H^+ outflow, this is easily confirmed. When integrating the flux density over a polar cap surface

down to 70° MLAT (to make it easy to compare), we find 5.4×10^{26} s^{-1}, very similar to the 6.9×10^{26} s^{-1} we get from polar wind data or the typical values found by most studies for the flux density in the polar wind [Nagai et al., 1984; Huddleston et al., 2005; Cully et al., 2003; Engwall et al., 2009a,b; André et al., 2015].

In chapter 3 we also observe O^+ ions in the outflow above polar cap arcs. The similarity between the outflow above polar cap arcs and polar wind would suggest that there are also O^+ ions in the polar wind. This is a more controversial subject. The classical polar wind models predict that almost no O^+ ions flow out, because they are too heavy and the ambipolar electric field does not provide enough energy. Other mechanisms contribute energy, but it is not clear how efficient they are. The O^+ ions that are observed above the polar cap and in the lobes are often argued to originate in the cusp. Abe et al. [1993], however, observed O^+ ions at altitudes of 10000 km, with flux densities that lead to an O^+ flux of $\sim 10^{24}$ s^{-1}, for which they argued the ions do not originate in the cusp. This is very comparable to those we found above the polar cap arcs. It is also around these altitudes that one would expect the bottom of the acceleration region of the polar cap arcs.

An O^+ ion at 10000 km altitude has certainly not escaped Earth's gravity yet, but it has already overcome more than half of the gravitational potential from the surface. The energy needed for an O^+ ion to escape Earth from its surface is ∼10.4 eV; at 10000 km altitude this is only ∼4.3 eV. Abe et al. [1993] report typical field-aligned velocities of these O^+ of 3 - 5 km s^{-1}. This corresponds to a kinetic velocity of 0.76 - 2.1 eV. These O^+ ions have thus not escaped yet, but an energy of 2.1 eV at 10000 km will get these ions up to almost 4.5 R_E altitude without any additional energy. At that altitude, other mechanisms can become important, like centrifugal acceleration.

It is important to note that, even though the outflow may be similar, a polar cap arcs does change the situation compared to the polar wind. For example, by accelerating the ions, the electric field vacates the magnetic flux tubes and thus changes the boundary conditions significantly. On the other hand, it also reflects electrons, preventing them from escaping. It is not clear how this affects the ambipolar electric field.

It is interesting to compare the ion outflow of the polar wind with the neutral thermal outflow. If we ignore other, less important energy inputs, the only energy source for the polar wind is solar illumination, just like for thermal escape of neutral particles. The ambipolar electric field is not a field caused by some external source, but set up by the plasma itself. So, to some extent, the polar wind can be seen as the "thermal escape" of a plasma, except that for plasmas this becomes much more complex.

The estimated outflowing Jeans flux for Earth of 2×10^{26} s^{-1} mentioned in chapter 1 is for the whole surface of the Earth[1]. A magnetic polar cap going down to 70° covers only ∼3% of the Earth's surface. The Jeans escape flux from an area of this size is only 6×10^{24} s^{-1}. Despite the much higher neutral density, the ion outflow of the polar wind seems to be much larger than the neutral outflow from the same area. This would suggest that the "thermal escape" is more efficient for a plasma. This makes sense since, through the ambipolar electric field, not only the escaping electrons but also the particles that do not escape transfer a part of their energy to the ions that do escape. Additionally, the mirror force transforms the ions' perpendicular energy into parallel energy.

Heavier ions may also benefit from the ambipolar electric field. For any realistic atmospheric temperature, the Jeans flux of escaping O atoms is truly negligible compared to other outflows. If there is indeed also an O^+ flux in the polar wind of the order of 10^{23} to 10^{24} s^{-1}, then this means that the polar wind may be much more efficient for O^+ ions than Jeans escape for O atoms (keep in mind, though, that the mentioned O^+ fluxes are not necessarily above escape velocity).

Another difference for neutrals and ions is that a neutral, once above the exobase, follows a ballistic trajectory. If it is to escape, it must thus have the escape velocity as soon as it leaves the collisional atmosphere. An ion, on the other hand, can be further accelerated by electromagnetic fields. If one were to make the analogy of an atom with a cannon ball shot into space, an ion would be more like a multistage rocket. A rocket never attains the escape velocity at the surface, but it keeps adding energy while ascending.

It is clear that the escape of plasma can be much more efficient than thermal escape of neutrals, and certainly for heavier particles. So when comparing different planets, ion outflow is very important. At Earth, the outflow from the cusp and the auroral region is large due to the strong input of energy that results from the interaction of the Earth's magnetic field with the solar wind. But even with less energy input, the outflow of the polar wind is dependent on the configuration of the magnetic field. For the ambipolar field to arise, the plasma needs to be free to escape. That is why it occurs on the open magnetic field lines above the polar caps.

This makes it an interesting point regarding the question whether an intrinsic magnetic field protects the atmosphere. In an induced magnetosphere the ionopause forms a boundary and the plasma cannot simply flow out, except at the nightside. That is why much of the ion escape at non-magnetized

[1] Please bear in mind the remark made there about how large the difference can be with different temperatures.

planets depends on plasma managing to get past the ionopause (i.e. detached ionospheric clouds) or be created above it (i.e. ion pickup). On the nightside, plasma can flow out into the tail freely, and an ambipolar electric field may be set up there. However, the nightside ionosphere is dark, thus lacking the solar illumination that we have found to be so important for such outflow. On the contrary, by shielding off the solar wind, a magnetosphere caused by an intrinsic magnetic field creates a region where polar wind outflow can occur in the sunlight, and may thus promote outflow. It needs to be taken into account, however, that pressure gradients between the day- and nightside may create ion flows towards the nightside in the induced magnetosphere [Fränz et al., 2015], and also photoelectrons may end up in the tail and create a strong ambipolar electric field after all [Collinson et al., 2016].

Given the importance of solar illumination for ion outflow it would be interesting to extend the analysis of the solar zenith angle dependence to ion outflow in regions like the cusp and the auroral zone. Other processes create intense outflows there, but solar illumination may cause a background modulation of the ion outflow. Using a large amount of measurements, a statistical study might be able to find this. Cusp outflow is particularly relevant for the atmospheric erosion of O^+ ions, because the direct connection to the solar wind and the high outflowing velocity means many ions are likely to directly escape the Earth system. Cusp outflow can also end up in the plasma sheet and thus may be important for the magnetospheric dynamics as well, especially in the distant tail. The auroral oval is directly connected to the plasma sheet, so auroral outflows might be even more important for magnetospheric dynamics than cusp outflow. Since it is not clear what eventually happens to ions in the plasma sheet, auroral outflows may also contribute to atmospheric erosion to some extent.

Combining satellite observations with measurements by ground-based radars may be helpful in furthering our understanding of the acceleration processes and the altitudes at which they occur. Studies with, for example, the European Incoherent Scatter (EISCAT) radar often show ionospheric upflow at altitudes up to 1000 km [see, e.g., Moen et al., 2004; Ogawa et al., 2010], but these upflow events typically have velocities of several 100 m s^{-1}, which is not enough to lead to escape. Combining measurements of ion fluxes at different altitudes may help to understand where upflow becomes outflow. One might also compare the measured polar wind fluxes with ionospheric properties found from atmospheric or ionospheric models. Semi-empirical models can give typical values for the parameters that more directly impact polar wind fluxes but are affected by solar illumination, like exospheric temperature or electron temperature and density.

The simplicity of the model used in chapter 4 has the advantage that all the parameters can be easily adapted to represent a different situation, like Earth

		Sunlit	Dark
Above polar cap arcs:	O^+	3.3×10^{11}	4.3×10^{10}
	H^+	3.2×10^{12}	1.7×10^{12}
Polar wind:	all	5.8×10^{12}	2.3×10^{12}

Table 6.1: Overview of the flux densities (normalized at 200 km altitude) above sunlit and dark ionospheres found in chapters 3 and 5 (in $s^{-1}m^{-2}$).

		Full		Daily average	
		Max	Min	Max	Min
One hemisphere:	O^+	5.53×10^{24}	3.45×10^{24}	3.05×10^{24}	7.15×10^{23}
	H^+	2.96×10^{25}	1.57×10^{25}	2.96×10^{25}	1.74×10^{25}
Two hemispheres:	O^+	3.05×10^{24}	3.97×10^{23}	5.14×10^{24}	3.76×10^{24}
	H^+	5.62×10^{25}	4.53×10^{25}	5.41×10^{25}	4.69×10^{25}

Table 6.2: Overview of the daily variations (represented by the full variation) and seasonal variations (represented by the variation of the daily average) found in chapter 4 for a polar cap down to 75° MLAT (in s^{-1}).

at a different geological time, or even other magnetized terrestrial planets. The tilt of the rotational axis or of the magnetic axis can be easily changed, just like the orbital period or the period of the rotation. A stronger magnetic field might result in a smaller polar cap (relative to the total surface area), but may lead to a larger variation. Many other parameterizations are possible.

The preliminary north-south asymmetry found in the measurements from the wake electric field will certainly be investigated further. More work is needed to determine the significance of this asymmetry and to rule out any orbital biases as its root. Narrowing down the possible causes may be a bigger challenge.

The surprising behaviour of the autocorrelation of the flux density of some passes shown in chapter 5 in figure 5.2 and the quasi-periodicity it suggests is also interesting to explore further. It may show how the flux density and the density in the lobes are possibly affected by solar wind pressure or other phenomena like Kelvin-Helmholtz waves.

In this work we have shown that solar illumination, as parametrized by the solar zenith angle, is an important factor for outflow from the polar ionosphere. Solar illumination changes the ionospheric density and temperature as well as the presence of hot photoelectrons. This increases ionospheric outflow both above small-scale polar cap arcs and in the polar wind. As can be seen from table

6.2, the total outflow from the polar caps is on the order of 10^{25} to 10^{26} s^{-1} (depending on the size of the polar cap). This means it is not really important as a process for the erosion of the atmosphere at Earth. However, this process may be more important at other planets. As can be seen from table 6.1, we found that outflow from a sunlit ionosphere is about double that of a dark ionosphere for H^+ ions. For O^+ ions, we see that the solar illumination is even more important, since the outflow above a sunlit ionosphere is more than 7 times higher then that of above a dark ionosphere. With Earth's rotation and orbit, this cause significant daily and seasonal variations, as can be seen in table 6.2. Solar illumination also changes the ionospheric conductivity, which can affect the current system associated with the field-aligned electric fields of the polar cap arcs. Since it is possible that ionospheric outflow has an impact on magnetospheric dynamics, solar illumination may have an effect on magnetospheric processes in both a direct and indirect way.

Bibliography

Abe, T., Whalen, B. A., Yau, A. W., Horita, R. E., Watanabe, S., and Sagawa, E. (1993). EXOS D (Akebono) suprathermal mass spectrometer observations of the polar wind. *Journal of Geophysical Research*, 98:11191.

Abe, T., Yau, A. W., Watanabe, S., Yamada, M., and Sagawa, E. (2004). Long-term variation of the polar wind velocity and its implication for the ion acceleration process: Akebono/suprathermal ion mass spectrometer observations. *Journal of Geophysical Research*, 109:A09305.

Acuña, M. H., Connerney, J. E. P., Wasilewski, P., Lin, R. P., Mitchell, D., Anderson, K. A., Carlson, C. W., McFadden, J., Rème, H., Mazelle, C., Vignes, D., Bauer, S. J., Cloutier, P., and Ness, N. F. (2001). Magnetic field of Mars: Summary of results from the aerobraking and mapping orbits. *Journal of Geophysical Research*, 106:23403–23418.

Acuna, M. H., Connerney, J. E. P., Wasilewski, P., Lin, R. P., Anderson, K. A., Carlson, C. W., McFadden, J., Curtis, D. W., Mitchell, D., Reme, H., Mazelle, C., Sauvaud, J. A., D'Uston, C., Cros, A., Medale, J. L., Bauer, S. J., Cloutier, P., Mayhew, M., Winterhalter, D., and Ness, N. F. (1998). Magnetic Field and Plasma Observations at Mars: Initial Results of. *Science*, 279:1676.

Akasofu, S.-I. (1981). Auroral arcs and auroral potential structure. In Akasofu, S.-I. and Kan, J. R., editors, *Physics of Auroral Arc Formation*, pages 1–14.

Anderson, Jr., D. E. and Hord, C. W. (1977). Multidimensional radiative transfer - Applications to planetary coronae. *Planetary and Space Science*, 25:563–571.

André, M., Crew, G. B., Peterson, W. K., Persoon, A. M., and Pollock, C. J. (1990). Ion heating by broadband low-frequency waves in the cusp/cleft. *Journal of Geophysical Research*, 95:20809–20823.

André, M. and Cully, C. M. (2012). Low-energy ions: A previously hidden solar system particle population. *Geophysical Research Letters*, 39:L03101.

André, M., Li, K., and Eriksson, A. I. (2015). Outflow of low-energy ions and the solar cycle. *Journal of Geophysical Research (Space Physics)*, 120:1072–1085.

Appleton, E. V. (1927). The Existence of more than one Ionised Layer in the Upper Atmosphere. *Nature*, 120:330.

Arzner, K. and Scholer, M. (2001). Kinetic structure of the post plasmoid plasma sheet during magnetotail reconnection. *Journal of Geophysical Research*, 106:3827–3844.

Axford, W. I. (1968). The polar wind and the terrestrial helium budget. *Journal of Geophysical Research*, 73:6855–6859.

Axford, W. I., Petschek, H. E., and Siscoe, G. L. (1965). Tail of the Magnetosphere. *Journal*

of Geophysical Research, 70:1231–1236.

Bahcall, J. N., Pinsonneault, M. H., and Basu, S. (2001). Solar Models: Current Epoch and Time Dependences, Neutrinos, and Helioseismological Properties. *The Astrophysical Journal*, 555:990–1012.

Baker, D. N., Hones, Jr., E. W., Young, D. T., and Birn, J. (1982). The possible role of ionospheric oxygen in the initiation and development of plasma sheet instabilities. *Geophysical Research Letters*, 9:1337–1340.

Baker, V. R. (2001). Water and the martian landscape. *Nature*, 412:228–236.

Balogh, A. (2005). Space Physics Instrumentation and Missions. In Mártínez Pillet, V., Aparicio, A., and Sánchez, F., editors, *Payload and Mission Definition in Space Sciences*, page 233. Cambridge University Press.

Balogh, A., Dunlop, M. W., Cowley, S. W. H., Southwood, D. J., Thomlinson, J. G., Glassmeier, K. H., Musmann, G., Luhr, H., Buchert, S., Acuna, M. H., Fairfield, D. H., Slavin, J. A., Riedler, W., Schwingenschuh, K., and Kivelson, M. G. (1997). The Cluster Magnetic Field Investigation. *Space Science Reviews*, 79:65–91.

Banks, P. M. and Holzer, T. E. (1968). The polar wind. *Journal of Geophysical Research*, 73:6846–6854.

Barabash, S., Fedorov, A., Lundin, R., and Sauvaud, J.-A. (2007a). Martian Atmospheric Erosion Rates. *Science*, 315:501.

Barabash, S., Fedorov, A., Sauvaud, J. J., Lundin, R., Russell, C. T., Futaana, Y., Zhang, T. L., Andersson, H., Brinkfeldt, K., Grigoriev, A., Holmström, M., Yamauchi, M., Asamura, K., Baumjohann, W., Lammer, H., Coates, A. J., Kataria, D. O., Linder, D. R., Curtis, C. C., Hsieh, K. C., Sandel, B. R., Grande, M., Gunell, H., Koskinen, H. E. J., Kallio, E., Riihelä, P., Säles, T., Schmidt, W., Kozyra, J., Krupp, N., Fränz, M., Woch, J., Luhmann, J., McKenna-Lawlor, S., Mazelle, C., Thocaven, J.-J., Orsini, S., Cerulli-Irelli, R., Mura, M., Milillo, M., Maggi, M., Roelof, E., Brandt, P., Szego, K., Winningham, J. D., Frahm, R. A., Scherrer, J., Sharber, J. R., Wurz, P., and Bochsler, P. (2007b). The loss of ions from Venus through the plasma wake. *Nature*, 450:650–653.

Baumjohan, W. and Treumann, R. A. (1996). *Basic Space Plasma Physics*. Imperial College Press, London, 1 edition.

Berkey, F. T., Cogger, L. L., Ismail, S., and Kamide, Y. (1976). Evidence for a correlation between sun-aligned arcs and the interplanetary magnetic field direction. *Geophysical Research Letters*, 3:145–147.

Bertaux, J.-L., Leblanc, F., Witasse, O., Quemerais, E., Lilensten, J., Stern, S. A., Sandel, B., and Korablev, O. (2005). Discovery of an aurora on Mars. *Nature*, 435:790–794.

Biermann, L. (1951). Kometenschweife und solare Korpuskularstrahlung. *Zeitschrift für Astrophysik*, 29:274.

Biermann, L. (1952). Über den Schweif des Kometen Halley im Jahre 1910. *Zeitschrift für Naturforschung Teil A*, 7:127–136.

Birn, J., Yur, G., Rahman, H. U., and Minami, S. (1992). On the termination of the closed field line region of the magnetotail. *Journal of Geophysical Research*, 97:14.

Brace, L. H., Kasprzak, W. T., Taylor, H. A., Theis, R. F., Russell, C. T., Barnes, A., Mihalov, J. D., and Hunten, D. M. (1987). The ionotail of Venus - Its configuration and evidence for ion escape. *Journal ofi Geophysical Research*, 92:15–26.

Brain, D. A. and Jakosky, B. M. (1998). Atmospheric loss since the onset of the Martian geologic record: Combined role of impact erosion and sputtering. *Journal of Geophysical Research*, 103:22689–22694.

Brain, D. A., McFadden, J. P., Halekas, J. S., Connerney, J. E. P., Bougher, S. W., Curry, S., Dong, C. F., Dong, Y., Eparvier, F., Fang, X., Fortier, K., Hara, T., Harada, Y., Jakosky, B. M., Lillis, R. J., Livi, R., Luhmann, J. G., Ma, Y., Modolo, R., and Seki, K. (2015). The spatial distribution of planetary ion fluxes near Mars observed by MAVEN. *Geophysical Research Letters*, 42:9142–9148.

Brambles, O. J., Lotko, W., Damiano, P. A., Zhang, B., Wiltberger, M., and Lyon, J. (2010). Effects of causally driven cusp O^+ outflow on the storm time magnetosphere-ionosphere system using a multifluid global simulation. *Journal of Geophysical Research (Space Physics)*, 115:A00J04.

Brambles, O. J., Lotko, W., Zhang, B., Wiltberger, M., Lyon, J., and Strangeway, R. J. (2011). Magnetosphere Sawtooth Oscillations Induced by Ionospheric Outflow. *Science*, 332:1183.

Brinton, H. C., Grebowsky, J. M., and Mayr, H. G. (1971). Altitude variation of ion composition in the midlatitude trough region: Evidence for upward plasma flow. *Journal of Geophysical Research*, 76:3738–3745.

Cahill, L. J. and Amazeen, P. G. (1963). The Boundary of the Geomagnetic Field. *Journal of Geophysical Research*, 68:1835–1843.

Cai, L., Aikio, A. T., and Nygrén, T. (2013). Height-dependent energy exchange rates in the high-latitude E region ionosphere. *Journal of Geophysical Research*, 118:7369–7383.

Candidi, M., Orsini, S., and Formisano, V. (1982). The properties of ionospheric O+ ions as observed in the magnetotail boundary layer and northern plasma lobe. *Journal of Geophysical Research*, 87:9097–9106.

Candidi, M., Orsini, S., and Ghielmetti, A. G. (1984). Observations of multiple ion beams in the magnetotail Evidence for a double proton population. *Journal of Geophysical Research*, 89:2180–2184.

Carpenter, D. L. (1966). Whistler studies of the plasmapause in the magnetosphere: 1. Temporal variations in the position of the knee and some evidence on plasma motions near the knee. *Journal of Geophysical Research*, 71:693–709.

Cassen, P., Reynolds, R. T., and Peale, S. J. (1979). Is there liquid water on Europa. *Geophysical Research Letters*, 6:731–734.

Cattell, C., Dombeck, J., Carlson, C., and McFadden, J. (2006). FAST observations of the solar illumination dependence of downgoing auroral electron beams: Relationship to electron energy flux. *Journal of Geophysical Research*, 111:2201.

Chandler, M. O., Fuselier, S. A., Lockwood, M., and Moore, T. E. (1999). Evidence of component merging equatorward of the cusp. *Journal of Geophysical Research*, 104:22623–22634.

Chandler, M. O., Moore, T. E., and Waite, Jr., J. H. (1991). Observations of polar ion outflows. *Journal of Geophysical Research*, 96:1421–1428.

Chappell, C. R., Moore, T. E., and Waite, Jr., J. H. (1987). The ionosphere as a fully adequate source of plasma for the earth's magnetosphere. *Journal of Geophysical Research*, 92:5896–5910.

Chassefière, E. and Leblanc, F. (2004). Mars atmospheric escape and evolution; interaction with the solar wind. *Planetary and Space Science*, 52:1039–1058.

Cladis, J. B. (1986). Parallel acceleration and transport of ions from polar ionosphere to plasma sheet. *Geophysical Research Letters*, 13:893–896.

Cladis, J. B. and Francis, W. E. (1992). Distribution in magnetotail of O(+) ions from cusp/cleft ionosphere - A possible substorm trigger. *Journal of Geophysical Research*,

97:123–130.

Cleland, C. E. and Chyba, C. F. (2002). Defining 'Life'. *Origins of Life and Evolution of the Biosphere*, 32:387–393.

Cliver, E. W., Kamide, Y., and Ling, A. G. (2000). Mountains versus valleys: Semiannual variation of geomagnetic activity. *Journal of Geophysical Research*, 105:2413–2424.

Cole, K. D. (1962). Joule Heating of the Upper Atmosphere. *Australian Journal of Physics*, 15:223.

Collinson, G. A., Frahm, R. A., Glocer, A., Coates, A. J., Grebowsky, J. M., Barabash, S., Domagal-Goldman, S. D., Fedorov, A., Futaana, Y., Gilbert, L. K., Khazanov, G., Nordheim, T. A., Mitchell, D., Moore, T. E., Peterson, W. K., Winningham, J. D., and Zhang, T. L. (2016). The electric wind of Venus: A global and persistent "polar wind"-like ambipolar electric field sufficient for the direct escape of heavy ionospheric ions. *Geophysical Research Letters*, 43:5926–5934.

Colpitts, C. A. (2015). Investigations of the Many Distinct Types of Auroras. In Zhang, Y. and Paxton, L. J., editors, *Auroral Dynamics and Space Weather*, pages 1–18. American Geophysical Union, Washington DC.

Connerney, J. E. P., Acuña, M. H., Wasilewski, P. J., Kletetschka, G., Ness, N. F., Rème, H., Lin, R. P., and Mitchell, D. L. (2001). The global magnetic field of Mars and implications for crustal evolution. *Geophysical Research Letters*, 28:4015–4018.

Cowley, S. W. H. (1995). Theoretical Perspectives of the Magnetopause: A Tutorial Review. *Washington DC American Geophysical Union Geophysical Monograph Series*, 90:29.

Cowley, S. W. H. (2000). TUTORIAL: Magnetosphere-Ionosphere Interactions: A Tutorial Review. In Ohtani, S.-I., Fujii, R., Hesse, M., and Lysak, R. L., editors, *Magnetospheric Current Systems*. American Geophysical Union Geophysical Monograph Series, Washington DC.

Crosby, N. B., Aschwanden, M. J., and Dennis, B. R. (1993). Frequency distributions and correlations of solar X-ray flare parameters. *Solar Physics*, 143:275–299.

Cully, C. M., Donovan, E. F., Yau, A. W., and Arkos, G. G. (2003). Akebono/Suprathermal Mass Spectrometer observations of low-energy ion outflow: Dependence on magnetic activity and solar wind conditions. *Journal of Geophysical Research*, 108:1093.

Daglis, I. A. and Axford, W. I. (1996). Fast ionospheric response to enhanced activity in geospace: Ion feeding of the inner magnetotail. *Journal of Geophysical Research*, 101:5047–5066.

Daglis, I. A., Thorne, R. M., Baumjohann, W., and Orsini, S. (1999). The terrestrial ring current: Origin, formation, and decay. *Reviews of Geophysics*, 37:407–438.

Daly, P. W. (1986). Structure of the distant terrestrial magnetotail. *Advances in Space Research*, 6:245–257.

Dandouras, I. (2013). Detection of a plasmaspheric wind in the Earth's magnetosphere by the Cluster spacecraft. *Annales Geophysicae*, 31:1143–1153.

Darrouzet, F., de Keyser, J., and Pierrard, V. (2009). *The Earth's Plasmasphere*. Springer.

Davis, T. N. (1963). Negative Correlation between Polar-Cap Visual Aurora and Magnetic Activity. *Journal of Geophysical Research*, 68:4447.

De Keyser, J. and Echim, M. (2010). Auroral and sub-auroral phenomena: an electrostatic picture. *Annales Geophysicae*, 28:633–650.

De Keyser, J., Maes, L., Maggiolo, R., and Haaland, S. (2017). Magnetopause thickness at the dawn and dusk flanks. In Haaland, S., Runov, A., and Forsyth, C., editors, *Dawn-*

Dusk Asymmetries in Planetary Plasma Environments. American Geophysical Union, Washington DC (in print).

Delcourt, D. C., Moore, T. E., and Chappell, C. R. (1994). Contribution of low-energy ionospheric protons to the plasma sheet. *Journal of Geophysical Research*, 99:5681–5689.

Dessler, A. J. and Cloutier, P. A. (1969). Discussion of letter by Peter M. Banks and Thomas E. Holzer, "The polar wind". *Journal of Geophysical Research*, 74:3730–3733.

Dessler, A. J. and Juday, R. D. (1965). Configuration of auroral radiation in space. *Planetary and Space Science*, 13:63–72.

Dessler, A. J. and Michel, F. C. (1966). Plasma in the geomagnetic tail. *Journal of Geophysical Research*, 71:1421–1426.

Du, A. M., Nakamura, R., Zhang, T. L., Panov, E. V., Baumjohann, W., Luo, H., Xu, W. Y., Lu, Q. M., Volwerk, M., Retinò, A., Zieger, B., Angelopoulos, V., Glassmeier, K.-H., McFadden, J. P., and Larson, D. (2011). Fast tailward flows in the plasma sheet boundary layer during a substorm on 9 March 2008: THEMIS observations. *Journal of Geophysical Research*, 116:A03216.

Dubinin, E., Fraenz, M., Fedorov, A., Lundin, R., Edberg, N., Duru, F., and Vaisberg, O. (2011). Ion Energization and Escape on Mars and Venus. *Space Science Reviews*, 162:173–211.

Dungey, J. W. (1961). Interplanetary Magnetic Field and the Auroral Zones. *Physical Review Letters*, 6:47–48.

Ebihara, Y., Kistler, L. M., and Eliasson, L. (2008). Imaging cold ions in the plasma sheet from the Equator-S satellite. *Geophysical Research Letters*, 35:L15103.

Ebihara, Y., Yamada, M., Watanabe, S., and Ejiri, M. (2006). Fate of outflowing suprathermal oxygen ions that originate in the polar ionosphere. *Journal of Geophysical Research (Space Physics)*, 111:A04219.

Echer, E., Gonzalez, W. D., and Tsurutani, B. T. (2011). Statistical studies of geomagnetic storms with peak Dst<-50 nT from 1957 to 2008. *Journal of Atmospheric and Solar-Terrestrial Physics*, 73:1454–1459.

Emmert, J. T., Richmond, A. D., and Drob, D. P. (2010). A computationally compact representation of Magnetic-Apex and Quasi-Dipole coordinates with smooth base vectors. *Journal of Geophysical Research (Space Physics)*, 115:A08322.

Engwall, E., Eriksson, A. I., André, M., Dandouras, I., Paschmann, G., Quinn, J., and Torkar, K. (2006). Low-energy (order 10 eV) ion flow in the magnetotail lobes inferred from spacecraft wake observations. *Geophysical Research Letters*, 33:L06110.

Engwall, E., Eriksson, A. I., Cully, C. M., André, M., Puhl-Quinn, P. A., Vaith, H., and Torbert, R. (2009a). Survey of cold ionospheric outflows in the magnetotail. *Annales Geophysicae*, 27:3185–3201.

Engwall, E., Eriksson, A. I., Cully, C. M., André, M., Torbert, R., and Vaith, H. (2009b). Earth's ionospheric outflow dominated by hidden cold plasma. *Nature Geoscience*, 2:24–27.

Ergun, R. E., Carlson, C. W., McFadden, J. P., Mozer, F. S., Delory, G. T., Peria, W., Chaston, C. C., Temerin, M., Elphic, R., Strangeway, R., Pfaff, R., Cattell, C. A., Klumpar, D., Shelley, E., Peterson, W., Moebius, E., and Kistler, L. (1998). FAST satellite observations of electric field structures in the auroral zone. *Geophysical research Letters*, 25:2025–2028.

Eriksson, A. I., André, M., Klecker, B., Laakso, H., Lindqvist, P.-A., Mozer, F., Paschmann, G., Pedersen, A., Quinn, J., Torbert, R., Torkar, K., and Vaith, H. (2006). Electric field measurements on Cluster: comparing the double-probe and electron drift techniques. *Annales Geophysicae*, 24:275–289.

Escoubet, C. P., Berchem, J., Bosqued, J. M., Trattner, K. J., Taylor, M. G. G. T., Pitout, F., Laakso, H., Masson, A., Dunlop, M., Dandouras, I., Reme, H., Fazakerley, A. N., and Daly, P. (2008). Effect of a northward turning of the interplanetary magnetic field on cusp precipitation as observed by Cluster. *Journal of Geophysical Research*, 113:A07S13.

Escoubet, C. P., Fehringer, M., and Goldstein, M. (2001). Introduction: The Cluster mission. *Annales Geophysicae*, 19:1197–1200.

Escoubet, C. P., Schmidt, R., and Goldstein, M. L. (1997). Cluster - Science and Mission Overview. *Space Science Reviews*, 79:11–32.

Fairfield, D. H. and Scudder, J. D. (1985). Polar rain - Solar coronal electrons in the earth's magnetosphere. *Journal of Geophysical Research*, 90:4055–4068.

Fear, R. C. and Milan, S. E. (2012a). Ionospheric flows relating to transpolar arc formation. *Journal of Geophysical Research*, 117:A09230.

Fear, R. C. and Milan, S. E. (2012b). The IMF dependence of the local time of transpolar arcs: Implications for formation mechanism. *Journal of Geophysical Research*, 117:A03213.

Fear, R. C., Milan, S. E., Maggiolo, R., Fazakerley, A. N., Dandouras, I., and Mende, S. B. (2014). Direct observation of closed magnetic flux trapped in the high-latitude magnetosphere. *Science*, 346:1506–1510.

Fedorov, A., Barabash, S., Sauvaud, J.-A., Futaana, Y., Zhang, T. L., Lundin, R., and Ferrier, C. (2011). Measurements of the ion escape rates from Venus for solar minimum. *Journal of Geophysical Research*, 116:A07220.

Feldman, U., Landi, E., and Schwadron, N. A. (2005). On the sources of fast and slow solar wind. *Journal of Geophysical Research (Space Physics)*, 110:A07109.

Förster, M. and Cnossen, I. (2013). Upper atmosphere differences between northern and southern high latitudes: The role of magnetic field asymmetry. *Journal of Geophysical Research (Space Physics)*, 118:5951–5966.

Förster, M., Paschmann, G., Haaland, S. E., Quinn, J. M., Torbert, R. B., Vaith, H., and Kletzing, C. A. (2007). High-latitude plasma convection from Cluster EDI: variances and solar wind correlations. *Annales Geophysicae*, 25:1691–1707.

Förster, M., Rentz, S., Köhler, W., Liu, H., and Haaland, S. E. (2008). IMF dependence of high-latitude thermospheric wind pattern derived from CHAMP cross-track measurements. *Annales Geophysicae*, 26:1581–1595.

Frank, L. A., Craven, J. D., Burch, J. L., and Winningham, J. D. (1982). Polar views of the earth's aurora with Dynamics Explorer. *Geophysical Research Letters*, 9:1001–1004.

Fränz, M., Dubinin, E., Andrews, D., Barabash, S., Nilsson, H., and Fedorov, A. (2015). Cold ion escape from the Martian ionosphere. *Planetary Space Science*, 119:92–102.

Gary, S. P. (1991). Electromagnetic ion/ion instabilities and their consequences in space plasmas - A review. *Space Science Reviews*, 56:373–415.

Glocer, A., Kitamura, N., Toth, G., and Gombosi, T. (2012). Modeling solar zenith angle effects on the polar wind. *Journal of Geophysical Research*, 117:4318.

Goldstein, J. and Sandel, B. R. (2013). The Global Pattern of Evolution of Plasmaspheric Drainage Plumes. In Burch, J. L., Schulz, M., and Spence, H., editors, *Inner Magnetosphere Interactions: New Perspectives from Imaging*, pages 1–22. American Geophysical Union.

Gomes, R., Levison, H. F., Tsiganis, K., and Morbidelli, A. (2005). Origin of the cataclysmic Late Heavy Bombardment period of the terrestrial planets. *Nature*, 435:466–469.

Green, J. L. and Waite, Jr., J. H. (1985). On the origin of polar ion streams. *Geophysical Research Letters*, 12:149–152.

Grigorenko, E. E., Hoshino, M., Hirai, M., Mukai, T., and Zelenyi, L. M. (2009). "Geography" of ion acceleration in the magnetotail: X-line versus current sheet effects. *Journal of Geophysical Research*, 114:A03203.

Gringauz, K. I. (1963). The structure of the ionized gas envelope of earth from direct measurements in the U.S.S.R. of local charged particle concentrations. *Planetary and Space Science*, 11:281–296.

Gunell, H., De Keyser, J., Gamby, E., and Mann, I. (2013). Vlasov simulations of parallel potential drops. *Annales Geophysicae*, 31:1227–1240.

Gurgiolo, C. and Burch, J. L. (1982). DE-1 observations of the polar wind - A heated and an unheated component. *Geophysical Research Letters*, 9:945–948.

Gustafsson, G., Bostrom, R., Holback, B., Holmgren, G., Lundgren, A., Stasiewicz, K., Ahlen, L., Mozer, F. S., Pankow, D., Harvey, P., Berg, P., Ulrich, R., Pedersen, A., Schmidt, R., Butler, A., Fransen, A. W. C., Klinge, D., Thomsen, M., Falthammar, C.-G., Lindqvist, P.-A., Christenson, S., Holtet, J., Lybekk, B., Sten, T. A., Tanskanen, P., Lappalainen, K., and Wygant, J. (1997). The Electric Field and Wave Experiment for the Cluster Mission. *Space Science Reviews*, 79:137–156.

Haaland, S., André, M., Eriksson, A., Li, K., Nilsson, H., Baddeley, L., Johnsen, C., Maes, L., Lybekk, B., and Pedersen, A. (2016). *Low-energy Ion Outflow Observed by Cluster*, pages 33–47. John Wiley & Sons, Inc.

Haaland, S., Eriksson, A., André, M., Maes, L., Baddeley, L., Barakat, A., Chappell, R., Eccles, V., Johnsen, C., Lybekk, B., Li, K., Pedersen, A., Schunk, R., and Welling, D. (2015). Estimation of cold plasma outflow during geomagnetic storms. *Journal of Geophysical Research (Space Physics)*, 120:10.

Haaland, S., Eriksson, A., Engwall, E., Lybekk, B., Nilsson, H., Pedersen, A., Svenes, K., André, M., Förster, M., Li, K., Johnsen, C., and Østgaard, N. (2012). Estimating the capture and loss of cold plasma from ionospheric outflow. *Journal of Geophysical Research*, 117:7311.

Haaland, S., Hasegawa, H., De Keyser, J., and Maes, L. (2017). Dawn-dusk asymmetries at the terrestrial magnetopause: Observations. In Haaland, S., Runov, A., and Forsyth, C., editors, *Dawn-Dusk Asymmetries in Planetary Plasma Environments*. American Geophysical Union, Washington DC (in print).

Haaland, S., Lybekk, B., Maes, L., Laundal, K., Pedersen, A., Tenfjord, P., Ohma, A., Østgaard, N., Reistad, J., and Snekvik, K. (2017). North-south asymmetries in cold plasma density in the magnetotail lobes: Cluster observations. *Journal of Geophysical Research: Space Physics*, 122(1):136–149. 2016JA023404.

Haaland, S., Reistad, J., Tenfjord, P., Gjerloev, J., Maes, L., DeKeyser, J., Maggiolo, R., Anekallu, C., and Dorville, N. (2014). Characteristics of the flank magnetopause: Cluster observations. *Journal of Geophysical Research (Space Physics)*, 119:9019–9037.

Haerendel, G., Olipitz, B. U., Buchert, S., Bauer, O. H., Rieger, E., and La Hoz, C. (1996). Optical and radar observations of auroral arcs with emphasis on small-scale structures. *Journal of Atmospheric and Terrestrial Physics*, 58:71–83.

Hansen, A. M., Bahnsen, A., and Dangelo, N. (1976). The cusp-magnetosheath interface. *Journal of Geophysical Research*, 81:556–561.

Hartle, R. E. and Grebowsky, J. M. (1990). Upward ion flow in ionospheric holes on Venus. *Journal of Geophysical Research*, 95:31–37.

Hartle, R. E. and Grebowsky, J. M. (1993). Light ion flow in the nightside ionosphere of Venus. *Journal of Geophysical Research*, 98:7437–7445.

Hartle, R. E. and Grebowsky, J. M. (1995). Planetary loss from light ion escape on Venus. *Advances in Space Research*, 15.

Heikkila, W. J. and Winningham, J. D. (1971). Penetration of magnetosheath plasma to low altitudes through the dayside magnetospheric cusps. *Journal of Geophysical Research*, 76:883.

Hoffman, J. H. (1970). Studies of the composition of the ionosphere with a magnetic deflection mass spectrometer. *International Journal of Mass Spectrometry and Ion Processes*, 4:315–322.

Hoffman, J. H. and Dodson, W. H. (1980). Light ion concentrations and fluxes in the polar regions during magnetically quiet times. *Journal of Geophysical Research*, 85:626–632.

Hoffman, J. H., Dodson, W. H., Lippincott, C. R., and Hammack, H. D. (1974). Initial ion composition results from the Isis 2 satellite. *Journal of Geophysical Research*, 79:4246–4251.

Hones, Jr., E. W. (1979). Transient phenomena in the magnetotail and their relation to substorms. *Space Science Reviews*, 23:393–410.

Horne, R. B., Glauert, S. A., and Thorne, R. M. (2003). Resonant diffusion of radiation belt electrons by whistler-mode chorus. *Geophysical Research Letters*, 30:46–1.

Huddleston, M. M., Chappell, C. R., Delcourt, D. C., Moore, T. E., Giles, B. L., and Chandler, M. O. (2005). An examination of the process and magnitude of ionospheric plasma supply to the magnetosphere. *Journal of Geophysical Research*, 110:A12202.

Hultqvist, B. (1999). Introduction. In Hultqvist, B., Øieroset, M., Paschmann, G., and Treumann, R., editors, *Magnetospheric Plasma Sources and Losses*, volume 88, chapter 1, pages 1–5. Space Science Reviews.

Hunten, D. M. (1982). Thermal and nonthermal escape mechanisms for terrestrial bodies. *Planetary Space Science*, 30:773–783.

Iijima, T. and Potemra, T. A. (1976). Field-aligned currents in the dayside cusp observed by Triad. *Journal of Geophysical Research*, 81:5971–5979.

Imber, S. M., Slavin, J. A., Auster, H. U., and Angelopoulos, V. (2011). A THEMIS survey of flux ropes and traveling compression regions: Location of the near-Earth reconnection site during solar minimum. *Journal of Geophysical Research*, 116:A02201.

Ingersoll, A. P. (1969). The Runaway Greenhouse: A History of Water on Venus. *Journal of Atmospheric Sciences*, 26:1191–1198.

Jeans, J. H. (1925). *The dynamical theory of gases*. Cambridge University Press, Cambridge, 4 edition.

Johnson, F. S. (1960). The Ion Distribution above the F_2 Maximum. *Journal of Geophysical Research*, 65:577.

Karlsson, T. (2012). The Acceleration Region of Stable Auroral Arcs. *Washington DC American Geophysical Union Geophysical Monograph Series*, 197:227–239.

Kelley, M. C. (2009). *High-Latitude Electrodynamics*, volume 96 of *International Geophysics*, chapter 8, pages 379 – 431. Academic Press.

Kennel, C. F. and Petschek, H. E. (1966). Limit on Stably Trapped Particle Fluxes. *Journal of Geophysical Research*, 71:1.

Kessel, R. L., Chen, S.-H., Green, J. L., Fung, S. F., Boardsen, S. A., Tan, L. C., Eastman, T. E., Craven, J. D., and Frank, L. A. (1996). Evidence of high-latitude reconnecting during northward IMF: Hawkeye observations. *Geophysical Research Letters*, 23:583–586.

Khazanov, G. V., Liemohn, M. W., and Moore, T. E. (1997). Photoelectron effects on the

self-consistent potential in the collisionless polar wind. *Journal of Geophysical Research*, 102:7509–7522.

Killeen, T. L., Won, Y.-I., Niciejewski, R. J., and Burns, A. G. (1995). Upper thermosphere winds and temperatures in the geomagnetic polar cap: Solar cycle, geomagnetic activity, and interplanetary magnetic field dependencies. *Journal of Geophysical Research*, 100:21327–21342.

Kistler, L. M., Mouikis, C. G., Cao, X., Frey, H., Klecker, B., Dandouras, I., Korth, A., Marcucci, M. F., Lundin, R., McCarthy, M., Friedel, R., and Lucek, E. (2006). Ion composition and pressure changes in storm time and nonstorm substorms in the vicinity of the near-Earth neutral line. *Journal of Geophysical Research (Space Physics)*, 111:A11222.

Kronberg, E. A., Ashour-Abdalla, M., Dandouras, I., Delcourt, D. C., Grigorenko, E. E., Kistler, L. M., Kuzichev, I. V., Liao, J., Maggiolo, R., Malova, H. V., Orlova, K. G., Peroomian, V., Shklyar, D. R., Shprits, Y. Y., Welling, D. T., and Zelenyi, L. M. (2014). Circulation of Heavy Ions and Their Dynamical Effects in the Magnetosphere: Recent Observations and Models. *Space Science Reviews*, 184:173–235.

Kucharek, H., Möbius, E., Mouikis, C., Lee, M., Liu, Y., Miao, B., and Scholer, M. (2008). On the physics of collisionless shocks: Cluster investigations and simulations. *Journal of Atmospheric and Solar-Terrestrial Physics*, 70:316–324.

Kullen, A., Brittnacher, M., Cumnock, J. A., and Blomberg, L. G. (2002). Solar wind dependence of the occurrence and motion of polar auroral arcs: A statistical study. *Journal of Geophysical Research*, 107:1362.

Kurosawa, K. (2015). Impact-driven planetary desiccation: The origin of the dry Venus. *Earth and Planetary Science Letters*, 429:181–190.

Lammer, H. (2013a). *Escape of Planetary Atmospheres*, pages 25–74. Springer Berlin Heidelberg, Berlin.

Lammer, H. (2013b). *Evolution of the Solar/Stellar Radiation and Plasma Environment*, pages 15–24. Springer Berlin Heidelberg, Berlin.

Lammer, H., Lichtenegger, H. I. M., Biernat, H. K., Erkaev, N. V., Arshukova, I. L., Kolb, C., Gunell, H., Lukyanov, A., Holmstrom, M., Barabash, S., Zhang, T. L., and Baumjohann, W. (2006). Loss of hydrogen and oxygen from the upper atmosphere of Venus. *Planet. Space Sci*, 54:1445–1456.

Lammer, H., Lichtenegger, H. I. M., Kolb, C., Ribas, I., Guinan, E. F., Abart, R., and Bauer, S. J. (2003). Loss of water from Mars:. Implications for the oxidation of the soil. *Icarus*, 165:9–25.

Lemaire, J. (2000). The formation plasmaspheric tails. *Physics and Chemistry of the Earth C*, 25:9–17.

Lemaire, J. and Scherer, M. (1969). Le champ électrique de polarisation dans l'exosphère ionique polaire. *Comptes Rendus de l'Academie des Sciences, Série B*, 269:666–669.

Lemaire, J. and Scherer, M. (1970). Model of the polar ion-exosphere. *Planetary and Space Science*, 18:103–120.

Lemaire, J. and Scherer, M. (1972). Ion-Exosphere with Asymmetric Velocity Distribution. *Physics of Fluids*, 15:760–766.

Lemaire, J. and Scherer, M. (1973). Kinetic models of the solar and polar winds. *Reviews of Geophysics and Space Physics*, 11:427–468.

Lemaire, J. and Schunk, R. W. (1992). Plasmaspheric wind. *Journal of Atmospheric and Terrestrial Physics*, 54:467–477.

Li, K., Haaland, S., Eriksson, A., André, M., Engwall, E., Wei, Y., Kronberg, E. A., Fränz, M., Daly, P. W., Zhao, H., and Ren, Q. Y. (2012). On the ionospheric source region of cold ion outflow. *Geophysical Research Letters*, 39:L18102.

Li, K., Haaland, S., Eriksson, A., André, M., Engwall, E., Wei, Y., Kronberg, E. A., Fränz, M., Daly, P. W., Zhao, H., and Ren, Q. Y. (2013). Transport of cold ions from the polar ionosphere to the plasma sheet. *Journal of Geophysical Research (Space Physics)*, 118:5467–5477.

Liao, J., Cai, X., Kistler, L. M., Clauer, C. R., Mouikis, C. G., Klecker, B., and Dandouras, I. (2014). The relationship between sawtooth events and O^+ in the plasma sheet. *Journal of Geophysical Research (Space Physics)*, 119:1572–1586.

Liou, K., Zhang, Y.-L., Newell, P. T., Paxton, L. J., and Carbary, J. F. (2011). TIMED/GUVI observation of solar illumination effect on auroral energy deposition. *Journal of Geophysical Research*, 116:9305.

Liou, K. N. (2002). *An introduction to atmospheric radiation*, volume 84. Academic press, San Diego.

Lockwood, M., Waite, Jr., J. H., Moore, T. E., Chappell, C. R., and Chandler, M. O. (1985). The cleft ion fountain. *Journal of Geophysical Research*, 90:9736–9748.

Lotko, W. (2007). The magnetosphere ionosphere system from the perspective of plasma circulation: A tutorial. *Journal of Atmospheric and Solar-Terrestrial Physics*, 69:191–211.

Luhmann, J. G. and Kozyra, J. U. (1991). Dayside pickup oxygen ion precipitation at Venus and Mars - Spatial distributions, energy deposition and consequences. *Journal of Geophycial Research*, 96:5457–5467.

Lundin, R., Barabash, S., Holmström, M., Nilsson, H., Futaana, Y., Ramstad, R., Yamauchi, M., Dubinin, E., and Fraenz, M. (2013). Solar cycle effects on the ion escape from Mars. *Geophysical Research Letters*, 40:6028–6032.

Lundin, R., Barabash, S., Holmström, M., Nilsson, H., Yamauchi, M., Dubinin, E. M., and Fraenz, M. (2009). Atmospheric origin of cold ion escape from Mars. *Geophysical Research Letters*, 36:L17202.

Lundin, R., Barabash, S., Holmström, M., Nilsson, H., Yamauchi, M., Fraenz, M., and Dubinin, E. M. (2008). A comet-like escape of ionospheric plasma from Mars. *Geophysical Research Letters*, 35:L18203.

Lundin, R., Zakharov, A., Pellinen, R., Barabasj, S. W., Borg, H., Dubinin, E. M., Hultqvist, B., Koskinen, H., Liede, I., and Pissarenko, N. (1990). ASPERA/Phobos measurements of the ion outflow from the Martian ionosphere. *Geophysical Research Letters*, 17:873–876.

Lybekk, B., Pedersen, A., Haaland, S., Svenes, K., Fazakerley, A. N., Masson, A., Taylor, M. G. G. T., and Trotignon, J.-G. (2012). Solar cycle variations of the Cluster spacecraft potential and its use for electron density estimations. *Journal of Geophysical Research (Space Physics)*, 117:A01217.

Lyons, L. R. (1980). Generation of large-scale regions of auroral currents, electric potentials, and precipitation by the divergence of the convection electric field. *Journal of Geophysical Research*, 85:17–24.

Lyons, L. R. (1981). Discrete aurora as the direct result of an inferred high-altitude generating potential distribution. *Journal of Geophysical Research*, 86:1–8.

Lyons, L. R., Evans, D. S., and Lundin, R. (1979). An observed relation between magnetic field aligned electric fields and downward electron energy fluxes in the vicinity of auroral forms. *Journal of Geophysical Research*, 84:457–461.

Maes, L., Maggiolo, R., De Keyser, J., Dandouras, I., Fear, R. C., Fontaine, D., and Haaland, S.

(2015). Solar illumination control of ionospheric outflow above polar cap arcs. *Geophysical Research Letters*, 42:1304–1311.

Maggiolo, R. (2015). Auroral Arcs and Ion Outflow. In Zhang, Y. and Paxton, L. J., editors, *Auroral Dynamics and Space Weather*, pages 39–58. American Geophysical Union, Washington DC.

Maggiolo, R., Echim, M., de Keyser, J., Fontaine, D., Jacquey, C., and Dandouras, I. (2011). Polar cap ion beams during periods of northward IMF: Cluster statistical results. *Annales Geophysicae*, 29:771–787.

Maggiolo, R., Echim, M., Wedlund, C. S., Zhang, Y., Fontaine, D., Lointier, G., and Trotignon, J.-G. (2012). Polar cap arcs from the magnetosphere to the ionosphere: kinetic modelling and observations by Cluster and TIMED. *Annales Geophysicae*, 30:283–302.

Maggiolo, R. and Kistler, L. M. (2014). Spatial variation in the plasma sheet composition: Dependence on geomagnetic and solar activity. *Journal of Geophysical Research (Space Physics)*, 119:2836–2857.

Maggiolo, R., Sauvaud, J. A., Fontaine, D., Teste, A., Grigorenko, E., Balogh, A., Fazakerley, A., Paschmann, G., Delcourt, D., and Rème, H. (2006). A multi-satellite study of accelerated ionospheric ion beams above the polar cap. *Annales Geophysicae*, 24:1665–1684.

Marklund, G. T., Sadeghi, S., Karlsson, T., Lindqvist, P.-A., Nilsson, H., Forsyth, C., Fazakerley, A., Lucek, E. A., and Pickett, J. (2011). Altitude Distribution of the Auroral Acceleration Potential Determined from Cluster Satellite Data at Different Heights. *Physical Review Letters*, 106(5):055002.

Martyn, D. F. (1947). Location of the Currents Causing the Solar and Lunar Diurnal Magnetic Variations. *Nature*, 160:535–537.

Mawson, D. (1925). Records of the Aurora Polaris, Australasian Antarctic expedition 1911-1914. *Scientific Reports*, B:11.

McKay, C. P. and Stoker, C. R. (1989). The Early Environment and its Evolution on Mars: Implications for Life. *Reviews of Geophysics*, 27.

Meredith, N. P., Horne, R. B., Thorne, R. M., and Anderson, R. R. (2009). Survey of upper band chorus and ECH waves: Implications for the diffuse aurora. *Journal of Geophysical Research (Space Physics)*, 114:A07218.

Meyer-Vernet, N. (2007). The wind from the sun: an introduction. In *Basics of the Solar Wind:*, pages 1–40. Cambridge University Press, Cambridge.

Milan, S. E., Hubert, B., and Grocott, A. (2005). Formation and motion of a transpolar arc in response to dayside and nightside reconnection. *Journal of Geophysical Research*, 110:A01212.

Milan, S. E., Hutchinson, J., Boakes, P. D., and Hubert, B. (2009). Influences on the radius of the auroral oval. *Annales Geophysicae*, 27:2913–2924.

Miyashita, Y., Ieda, A., Kamide, Y., Machida, S., Mukai, T., Saito, Y., Liou, K., Meng, C.-I., Parks, G. K., McEntire, R. W., Nishitani, N., Lester, M., Sofko, G. J., and Villain, J.-P. (2005a). Plasmoids observed in the near-Earth magnetotail at X $\sim$-7 R_E. *Journal of Geophysical Research*, 110:A12214.

Miyashita, Y., Miyoshi, Y., Matsumoto, Y., Ieda, A., Kamide, Y., Nosé, M., Machida, S., Hayakawa, H., McEntire, R. W., Christon, S. P., Evans, D. S., and Troshichev, O. A. (2005b). Geotail observations of signatures in the near-Earth magnetotail for the extremely intense substorms of the 30 October 2003 storm. *Journal of Geophysical Research*, 110:A09S25.

Moen, J., Oksavik, K., and Carlson, H. C. (2004). On the relationship between ion upflow events and cusp auroral transients. *Geophysical Research Letters*, 31:L11808.

Moore, T. E., Chappell, C. R., Chandler, M. O., Craven, P. D., Giles, B. L., Pollock, C. J., Burch, J. L., Young, D. T., Waite, Jr., J. H., Nordholt, J. E., Thomsen, M. F., McComas, D. J., Berthelier, J. J., Williamson, W. S., Robson, R., and Mozer, F. S. (1997). High-altitude observations of the polar wind. *Science*, 277:349–351.

Moore, T. E. and Khazanov, G. V. (2010). Mechanisms of ionospheric mass escape. *Journal of Geophysical Research (Space Physics)*, 115:A00J13.

Moore, T. E., Lundin, R., Alcayde, D., André, M., Ganguli, S. B., Temerin, M., and Yau, A. (1999). Source Processes in the High-Latitude Ionosphere. In Hultqvist, B., Øieroset, M., Paschmann, G., and Treumann, R., editors, *Magnetospheric Plasma Sources and Losses*, volume 88, chapter 2, pages 7–84. Space Science Reviews.

Möstl, U. V., Erkaev, N. V., Zellinger, M., Lammer, H., Gröller, H., Biernat, H. K., and Korovinskiy, D. (2011). The Kelvin-Helmholtz instability at Venus: What is the unstable boundary? *Icarus*, 216:476–484.

Nagai, T., Nakamura, R., Mukai, T., Yamamoto, T., Nishida, A., and Kokubun, S. (1997). Substorms, tail flows and plasmoids. *Advances in Space Research*, 20:961–971.

Nagai, T., Waite, Jr., J. H., Green, J. L., Chappell, C. R., Olsen, R. C., and Comfort, R. H. (1984). First measurements of supersonic polar wind in the polar magnetosphere. *Geophysical Research Letters*, 11:669–672.

Nagy, A. F., Cravens, T. E., Yee, J.-H., and Stewart, A. I. F. (1981). Hot oxygen atoms in the upper atmosphere of Venus. *Geophysical Research Letters*, 8:629–632.

Ness, N. F. (1965). The Earth's Magnetic Tail. *Journal of Geophysical Research*, 70:2989–3005.

Ness, N. F., Scearce, C. S., and Seek, J. B. (1964). Initial Results of the Imp 1 Magnetic Field Experiment. *Journal of Geophysical Research*, 69:3531–3569.

Newell, P. T., Liou, K., and Wilson, G. R. (2009). Polar cap particle precipitation and aurora: Review and commentary. *Journal of Atmospheric and Solar-Terrestrial Physics*, 71:199–215.

Newell, P. T., Meng, C.-I., and Lyons, K. M. (1996). Suppression of discrete aurorae by sunlight. *Nature*, 381:766–767.

Newell, P. T., Sotirelis, T., and Wing, S. (2010). Seasonal variations in diffuse, monoenergetic, and broadband aurora. *Journal of Geophysical Research*, 115:3216.

Nicolet, M. and Aikin, A. C. (1960). The Formation of the D Region of the Ionosphere. *Journal of Geophysical Research*, 65:1469.

Nilsson, H., Barghouthi, I. A., Slapak, R., Eriksson, A. I., and André, M. (2012). Hot and cold ion outflow: Spatial distribution of ion heating. *Journal of Geophysical Research*, 117:11201.

Nilsson, H., Edberg, N. J. T., Stenberg, G., Barabash, S., Holmström, M., Futaana, Y., Lundin, R., and Fedorov, A. (2011). Heavy ion escape from Mars, influence from solar wind conditions and crustal magnetic fields. *Icarus*, 215:475–484.

Nilsson, H., Engwall, E., Eriksson, A., Puhl-Quinn, P. A., and Arvelius, S. (2010). Centrifugal acceleration in the magnetotail lobes. *Annales Geophysicae*, 28:569–576.

Nilsson, H., Waara, M., Marghitu, O., Yamauchi, M., Lundin, R., Rème, H., Sauvaud, J.-A., Dandouras, I., Lucek, E., Kistler, L. M., Klecker, B., Carlson, C. W., Bavassano-Cattaneo, M. B., and Korth, A. (2008). An assessment of the role of the centrifugal acceleration mechanism in high altitude polar cap oxygen ion outflow. *Annales Geophysicae*, 26:145–157.

Nilsson, H., Yamauchi, M., Eliasson, L., Norberg, O., and Clemmons, J. (1996). Ionospheric signature of the cusp as seen by incoherent scatter radar. *Journal of Geophysical Research*,

101:10947–10964.

Nishida, A. (1966). Formation of plasmapause, or magnetospheric plasma knee, by the combined action of magnetospheric convection and plasma escape from the tail. *Journal of Geophysical Research*, 71:5669–5679.

Nishimura, Y., Bortnik, J., Li, W., Thorne, R. M., Ni, B., Lyons, L. R., Angelopoulos, V., Ebihara, Y., Bonnell, J. W., Le Contel, O., and Auster, U. (2013). Structures of dayside whistler-mode waves deduced from conjugate diffuse aurora. *Journal of Geophysical Research (Space Physics)*, 118:664–673.

Ogawa, Y., Buchert, S. C., Sakurai, A., Nozawa, S., and Fujii, R. (2010). Solar activity dependence of ion upflow in the polar ionosphere observed with the European Incoherent Scatter (EISCAT) Tromsø UHF radar. *Journal of Geophysical Research*, 115:A07310.

Ouellette, J. E., Brambles, O. J., Lyon, J. G., Lotko, W., and Rogers, B. N. (2013). Properties of outflow-driven sawtooth substorms. *Journal of Geophysical Research (Space Physics)*, 118:3223–3232.

Pannekoek, A. (1922). Ionization in stellar atmospheres (Errata: 2 24). *Bulletin of the Astronomical Institutes of the Netherlands*, 1:107.

Parker, E. N. (1958). Dynamics of the Interplanetary Gas and Magnetic Fields. *Astrophysical Journal*, 128:664.

Parks, G. K. (1991). *Physics of space plasmas - an introduction*. Addison-Wesley Publishing Co., Redwood City, CA.

Partamies, N., Donovan, E., and Knudsen, D. (2008). Statistical study of inverted-V structures in FAST data. *Annales Geophysicae*, 26:1439–1449.

Paschmann, G., Melzner, F., Frenzel, R., Vaith, H., Parigger, P., Pagel, U., Bauer, O. H., Haerendel, G., Baumjohann, W., Scopke, N., Torbert, R. B., Briggs, B., Chan, J., Lynch, K., Morey, K., Quinn, J. M., Simpson, D., Young, C., McIlwain, C. E., Fillius, W., Kerr, S. S., Mahieu, R., and Whipple, E. C. (1997). The Electron Drift Instrument for Cluster. *Space Science Reviews*, 79:233–269.

Pedersen, A., Décréau, P., Escoubet, C.-P., Gustafsson, G., Laakso, H., Lindqvist, P.-A., Lybekk, B., Masson, A., Mozer, F., and Vaivads, A. (2001). Four-point high time resolution information on electron densities by the electric field experiments (EFW) on Cluster. *Annales Geophysicae*, 19:1483–1489.

Pedersen, A., Lybekk, B., André, M., Eriksson, A., Masson, A., Mozer, F. S., Lindqvist, P.-A., DéCréAu, P. M. E., Dandouras, I., Sauvaud, J.-A., Fazakerley, A., Taylor, M., Paschmann, G., Svenes, K. R., Torkar, K., and Whipple, E. (2008). Electron density estimations derived from spacecraft potential measurements on Cluster in tenuous plasma regions. *Journal of Geophysical Research (Space Physics)*, 113:A07S33.

Peterson, W. K. (2002). Ionospheric Influence on Substorm Development. *Proceedings of the Sixth International Conference on Substorms, University of Washington*, page 143.

Peterson, W. K., Sharp, R. D., Shelley, E. G., Johnson, R. G., and Balsiger, H. (1981). Energetic ion composition of the plasma sheet. *Journal of Geophysical Research*, 86:761–767.

Phan, T. D. and Paschmann, G. (1996). Low-latitude dayside magnetopause and boundary layer for high magnetic shear 1. Structure and motion. *Journal of Geophysical Research*, 101:7801–7816.

Plane, J. M. C. (2012). Cosmic dust in the earth's atmosphere. *Chemical Society Reviews*, 41:6507–6518.

Pollock, C. J., Chandler, M. O., Moore, T. E., Chappell, C. R., and Waite, Jr., J. H.

(1990). A survey of upwelling ion event characteristics. *Journal of Geophysical Research*, 95:18969–18980.

Potemra, T. A. (1984). Magnetospheric Currents. *Washington DC American Geophysical Union Geophysical Monograph Series*, 28.

Rème, H., Aoustin, C., Bosqued, J. M., Dandouras, I., Lavraud, B., Sauvaud, J. A., Barthe, A., Bouyssou, J., Camus, T., Coeur-Joly, O., Cros, A., Cuvilo, J., Ducay, F., Garbarowitz, Y., Medale, J. L., Penou, E., Perrier, H., Romefort, D., Rouzaud, J., Vallat, C., Alcaydé, D., Jacquey, C., Mazelle, C., D'Uston, C., Möbius, E., Kistler, L. M., Crocker, K., Granoff, M., Mouikis, C., Popecki, M., Vosbury, M., Klecker, B., Hovestadt, D., Kucharek, H., Kuenneth, E., Paschmann, G., Scholer, M., Sckopke, N., Seidenschwang, E., Carlson, C. W., Curtis, D. W., Ingraham, C., Lin, R. P., McFadden, J. P., Parks, G. K., Phan, T., Formisano, V., Amata, E., Bavassano-Cattaneo, M. B., Baldetti, P., Bruno, R., Chionchio, G., di Lellis, A., Marcucci, M. F., Pallocchia, G., Korth, A., Daly, P. W., Graeve, B., Rosenbauer, H., Vasyliunas, V., McCarthy, M., Wilber, M., Eliasson, L., Lundin, R., Olsen, S., Shelley, E. G., Fuselier, S., Ghielmetti, A. G., Lennartsson, W., Escoubet, C. P., Balsiger, H., Friedel, R., Cao, J.-B., Kovrazhkin, R. A., Papamastorakis, I., Pellat, R., Scudder, J., and Sonnerup, B. (2001). First multispacecraft ion measurements in and near the Earth's magnetosphere with the identical Cluster ion spectrometry (CIS) experiment. *Annales Geophysicae*, 19:1303–1354.

Rème, H., Bosqued, J. M., Sauvaud, J. A., Cros, A., Dandouras, J., Aoustin, C., Bouyssou, J., Camus, T., Cuvilo, J., Martz, C., Medale, J. L., Perrier, H., Romefort, D., Rouzaud, J., D'Uston, C., Mobius, E., Crocker, K., Granoff, M., Kistler, L. M., Popecki, M., Hovestadt, D., Klecker, B., Paschmann, G., Scholer, M., Carlson, C. W., Curtis, D. W., Lin, R. P., McFadden, J. P., Formisano, V., Amata, E., Bavassano-Cattaneo, M. B., Baldetti, P., Belluci, G., Bruno, R., Chionchio, G., di Lellis, A., Shelley, E. G., Ghielmetti, A. G., Lennartsson, W., Korth, A., Rosenbauer, H., Lundin, R., Olsen, S., Parks, G. K., McCarthy, M., and Balsiger, H. (1997). The Cluster Ion Spectrometry (cis) Experiment. *Space Science Reviews*, 79:303–350.

Richmond, A. D. (1987). The ionosphere. In Akasofu, S.-I. and Kamide, Y., editors, *The Solar Wind and the Earth*, pages 123–140. Terra Scientific Publishing Company, Tokyo.

Roble, R. G., Ridley, E. C., and Dickinson, R. E. (1987). On the global mean structure of the thermosphere. *Journal of Geophysical Research*, 92:8745–8758.

Rosseland, S. (1924). Electrical state of a star. *Monthly Notices of the Royal Astronomical Society*, 84:720–728.

Russell, C. T. and Elphic, R. C. (1978). Initial ISEE magnetometer results - Magnetopause observations. *Space Science Reviews*, 22:681–715.

Russell, C. T. and McPherron, R. L. (1973). Semiannual variation of geomagnetic activity. *Journal of Geophysical Research*, 78:92.

Sabine, E. (1856). On Periodical Laws Discoverable in the Mean Effects of the Larger Magnetic Disturbances. No. III. *Philosophical Transactions of the Royal Society of London Series I*, 146:357–374.

Schunk, R. and Nagy, A. (2000). *Ionospheres: Physics, Plasma Physics, and Chemistry*. Cambridge University Press, Cambridge, 1 edition.

Schunk, R. W. and Nagy, A. F. (1978). Electron temperatures in the F region of the ionosphere - Theory and observations. *Reviews of Geophysics and Space Physics*, 16:355–399.

Schwabe, M. (1844). Sonnenbeobachtungen im Jahre 1843. Von Herrn Hofrath Schwabe in Dessau. *Astronomische Nachrichten*, 21:233.

Seki, K., Elphic, R. C., Hirahara, M., Terasawa, T., and Mukai, T. (2001). On Atmospheric

Loss of Oxygen Ions from Earth Through Magnetospheric Processes. *Science*, 291:1939–1941.

Seki, K., Hirahara, M., Hoshino, M., Terasawa, T., Elphic, R. C., Saito, Y., Mukai, T., Hayakawa, H., Kojima, H., and Matsumoto, H. (2003). Cold ions in the hot plasma sheet of Earth's magnetotail. *Nature*, 422:589–592.

Seki, K., Hirahara, M., Terasawa, T., Mukai, T., Saito, Y., Machida, S., Yamamoto, T., and Kokubun, S. (1998). Statistical properties and possible supply mechanisms of tailward cold O^+ beams in the lobe/mantle regions. *Journal of Geophysical Research*, 103:4477–4490.

Seo, Y., Horwitz, J. L., and Caton, R. (1997). Statistical relationships between high-latitude ionospheric F region/topside upflows and their drivers: DE 2 observations. *Journal of Geophysical Research*, 102:7493–7500.

Sharp, R. D., Carr, D. L., Peterson, W. K., and Shelley, E. G. (1981). Ion streams in the magnetotail. *Journal of Geophysical Research*, 86:4639–4648.

Shay, M. A. and Swisdak, M. (2004). Three-Species Collisionless Reconnection: Effect of O^+ on Magnetotail Reconnection. *Physical Review Letters*, 93(17):175001.

Slapak, R., Nilsson, H., Westerberg, L. G., and Larsson, R. (2015). O^+ transport in the dayside magnetosheath and its dependence on the IMF direction. *Annales Geophysicae*, 33:301–307.

Slavin, J. A., Baker, D. N., Fairfield, D. H., Craven, J. D., Frank, L. A., Elphic, R. C., Galvin, A. B., Hughes, W. J., Manka, R. H., and Smith, E. J. (1989). CDAW 8 observations of plasmoid signatures in the geomagnetic tail - An assessment. *Journal of Geophysical Research*, 94:15153–15175.

Slavin, J. A., Hesse, M., Owen, C. J., Taguchi, S., Fairfield, D. H., Lepping, R. P., Kokubun, S., Mukai, T., Lui, A. T. Y., Anderson, R. R., Matsumoto, H., and Sutcliffe, P. R. (1999). Dual spacecraft observations of lobe magnetic field perturbations before, during and after plasmoid release. *Geophysical Research Letters*, 26:2897–2900.

Spohn, T., Acuña, M. H., Breuer, D., Golombek, M., Greeley, R., Halliday, A., Hauber, E., Jaumann, R., and Sohl, F. (2001). Geophysical Constraints on the Evolution of Mars. *Space Science Reviews*, 96:231–262.

Spohn, T. and Schubert, G. (2003). Oceans in the icy Galilean satellites of Jupiter? *Icarus*, 161:456–467.

Strangeway, R. J., Ergun, R. E., Su, Y.-J., Carlson, C. W., and Elphic, R. C. (2005). Factors controlling ionospheric outflows as observed at intermediate altitudes. *Journal of Geophysical Research (Space Physics)*, 110:A03221.

Strangeway, R. J., Russell, C. T., and Luhmann, J. G. (2010). Comparative Planetology: How Effective is an Intrinsic Magnetic Field in Shielding a Planetary Atmosphere? In *European Planetary Science Congress 2010*, page 334.

Su, Y.-J., Horwitz, J. L., Moore, T. E., Giles, B. L., Chandler, M. O., Craven, P. D., Hirahara, M., and Pollock, C. J. (1998a). Polar wind survey with the Thermal Ion Dynamics Experiment/Plasma Source Instrument suite aboard POLAR. *Journal of Geophysical Research*, 103:29305–29338.

Su, Y.-J., Horwitz, J. L., Wilson, G. R., Richards, P. G., Brown, D. G., and Ho, C. W. (1998b). Self-consistent simulation of the photoelectron-driven polar wind from 120 km to 9 R_E altitude. *Journal of Geophysical Research*, 103:2279–2296.

Tam, S. W. Y., Chang, T., and Pierrard, V. (2007). Kinetic modeling of the polar wind. *Journal of Atmospheric and Solar-Terrestrial Physics*, 69:1984–2027.

Tam, S. W. Y., Yasseen, F., and Chang, T. (1998). Further development in theory/data

closure of the photoelectron-driven polar wind and day-night transition of the outflow. *Annales Geophysicae*, 16:948–968.

Tam, S. W. Y., Yasseen, F., Chang, T., and Ganguli, S. B. (1995). Self-consistent kinetic photoelectron effects on the polar wind. *Geophysical research Letters*, 22:2107–2110.

Taylor, M. G. G. T., Escoubet, C. P., Laakso, H., Masson, A., and Goldstein, M. L. (2010). The Cluster Mission: Space Plasma in Three Dimensions. *Astrophysics and Space Science Proceedings*, 11:309–330.

Terada, N., Machida, S., and Shinagawa, H. (2002). Global hybrid simulation of the Kelvin-Helmholtz instability at the Venus ionopause. *Journal of Geophysical Research (Space Physics)*, 107:1471.

Thébault, E., Finlay, C. C., Beggan, C. D., Alken, P., Aubert, J., Barrois, O., Bertrand, F., Bondar, T., Boness, A., Brocco, L., Canet, E., Chambodut, A., Chulliat, A., Coïsson, P., Civet, F., Du, A., Fournier, A., Fratter, I., Gillet, N., Hamilton, B., Hamoudi, M., Hulot, G., Jager, T., Korte, M., Kuang, W., Lalanne, X., Langlais, B., Léger, J.-M., Lesur, V., Lowes, F. J., Macmillan, S., Mandea, M., Manoj, C., Maus, S., Olsen, N., Petrov, V., Ridley, V., Rother, M., Sabaka, T. J., Saturnino, D., Schachtschneider, R., Sirol, O., Tangborn, A., Thomson, A., Tøffner-Clausen, L., Vigneron, P., Wardinski, I., and Zvereva, T. (2015). International Geomagnetic Reference Field: the 12th generation. *Earth, Planets, and Space*, 67:79.

Thomas, P., Tajeddine, R., Tiscareno, M., Burns, J., Joseph, J., Loredo, T., Helfenstein, P., and Porco, C. (2016). Enceladus's measured physical libration requires a global subsurface ocean. *Icarus*, 264:37 – 47.

Thorne, R. M., Ni, B., Tao, X., Horne, R. B., and Meredith, N. P. (2010). Scattering by chorus waves as the dominant cause of diffuse auroral precipitation. *Nature*, 467:943–946.

Toledo-Redondo, S., Vaivads, A., André, M., and Khotyaintsev, Y. V. (2015). Modification of the Hall physics in magnetic reconnection due to cold ions at the Earth's magnetopause. *Geophysical Research Letters*, 42:6146–6154.

Trenberth, K. E. and Smith, L. (2005). The Mass of the Atmosphere: A Constraint on Global Analyses. *Journal of Climate*, 18:864–875.

Tsurutani, B. T. and Gonzalez, W. D. (1995). The future of geomagnetic storm predictions: implications from recent solar and interplanetary observations. *Journal of Atmospheric and Terrestrial Physics*, 57:1369–1384.

Tsyganenko, N. A. (1987). Global quantitative models of the geomagnetic field in the cislunar magnetosphere for different disturbance levels. *Planetary and Space Science*, 35:1347–1358.

Tsyganenko, N. A. (1989). A magnetospheric magnetic field model with a warped tail current sheet. *Planetary and Space Science*, 37:5–20.

Tsyganenko, N. A. (1996). Effects of the solar wind conditions in the global magnetospheric configurations as deduced from data-based field models (Invited). In Rolfe, E. J. and Kaldeich, B., editors, *International Conference on Substorms*, volume 389 of *ESA Special Publication*, page 181.

Tsyganenko, N. A. and Usmanov, A. V. (1982). Determination of the magnetospheric current system parameters and development of experimental geomagnetic field models based on data from IMP and HEOS satellites. *Planetary and Space Science*, 30:985–998.

Tu, J., Song, P., Reinisch, B. W., and Green, J. L. (2007). Smooth electron density transition from plasmasphere to the subauroral region. *Journal of Geophysical Research*, 112:A05227.

Verigin, M. I., Shutte, N. M., Galeev, A. A., Gringauz, K. I., Kotova, G. A., Remizov, A. P., Rosenbauer, H., Hemmerich, P., Livi, S., Richter, A. K., Apathy, I., Szego, K., Riedler, W.,

Schwingenschuh, K., Steller, M., and Yeroshenko, Y. G. (1991). Ions of planetary origin in the Martian magnetosphere (Phobos 2/TAUS experiment). *Planetary Space Science*, 39:131–137.

Volkov, A. N., Johnson, R. E., Tucker, O. J., and Erwin, J. T. (2011). Thermally Driven Atmospheric Escape: Transition from Hydrodynamic to Jeans Escape. *Astrophysical Journal Letters*, 729:L24.

Waara, M., Slapak, R., Nilsson, H., Stenberg, G., André, M., and Barghouthi, I. A. (2011). Statistical evidence for O^+ energization and outflow caused by wave-particle interaction in the high altitude cusp and mantle. *Annales Geophysicae*, 29:945–954.

Wahlund, J.-E., Opgenoorth, H. J., Haggstrom, I., Winser, K. J., and Jones, G. O. L. (1992). EISCAT observations of topside ionospheric ion outflows during auroral activity - Revisited. *Journal of Geophysical Research*, 97:3019–3037.

Waite, Jr., J. H., Chappell, C. R., Nagai, T., Johnson, J. F. E., Burch, J. L., Killeen, T. L., Hays, P. B., Carignan, G. R., Peterson, W. K., and Shelley, E. G. (1985). Escape of suprathermal O(+) ions in the polar cap. *Journal of Geophysical Research*, 90:1619–1630.

Walsh, B. M., Sibeck, D. G., Wang, Y., and Fairfield, D. H. (2012). Dawn-dusk asymmetries in the Earth's magnetosheath. *Journal of Geophysical Research (Space Physics)*, 117:A12211.

Webb, D. F. and Howard, R. A. (1994). The solar cycle variation of coronal mass ejections and the solar wind mass flux. *Journal of Geophysical Research*, 99:4201–4220.

Wetherill, G. W. (1975). Late heavy bombardment of the moon and terrestrial planets. In *Lunar and Planetary Science Conference Proceedings*, volume 6 of *Lunar and Planetary Science Conference Proceedings*, pages 1539–1561.

Wood, B. E. (2006). The Solar Wind and the Sun in the Past. *Space Science Reviews*, 126:3–14.

Yau, A. W., Abe, T., and Peterson, W. K. (2007). The polar wind: Recent observations. *Journal of Atmospheric and Solar-Terrestrial Physics*, 69:1936–1983.

Yau, A. W. and André, M. (1997). Sources of Ion Outflow in the High Latitude Ionosphere. *Space Science Reviews*, 80:1–25.

Yau, A. W., Peterson, W. K., and Shelley, E. G. (1988). Quantitative parametrization of energetic ionospheric ion outflow. *Washington DC American Geophysical Union Geophysical Monograph Series*, 44:211–217.

Yau, A. W., Whalen, B. A., and Sagawa, E. (1991). Minor ion composition in the polar ionosphere. *Geophysical Research Letters*, 18:345–348.

Yoshikawa, I., Yamazaki, A., Yamashita, K., Takizawa, Y., and Nakamura, M. (2003). Which is a significant contributor for outside of the plasmapause, an ionospheric filling or a leakage of plasmaspheric materials?: Comparison of He II (304 Å) images. *Journal of Geophysical Research*, 108:1080.

Yu, Y. and Ridley, A. J. (2013). Exploring the influence of ionospheric O^+ outflow on magnetospheric dynamics: dependence on the source location. *Journal of Geophysical Research (Space Physics)*, 118:1711–1722.

Zhang, Y., Paxton, L. J., Zhang, Q., and Xing, Z. (2016). Polar cap arcs: Sun-aligned or cusp-aligned? *Journal of Atmospheric and Solar-Terrestrial Physics*, 146:123–128.

Zheng, Y., Moore, T. E., Mozer, F. S., Russell, C. T., and Strangeway, R. J. (2005). Polar study of ionospheric ion outflow versus energy input. *Journal of Geophysical Research (Space Physics)*, 110:A07210.

Zhu, L., Schunk, R. W., and Sojka, J. J. (1997). Polar cap arcs: a review. *Journal of Atmospheric and Solar-Terrestrial Physics*, 59:1087–1126.

Publications

Publications (main author)

***Maes, L.**, Maggiolo, R., De Keyser, J., Dandouras, I., Fear, R. C., Fontaine, D. and Haaland, S. (2015), Solar illumination control of ionospheric outflow above polar cap arcs. Geophys. Res. Lett., 42: 1304–1311. doi: 10.1002/2014GL062972.*

***Maes, L.**, Maggiolo, R., and De Keyser, J. (2016), Seasonal variations and north–south asymmetries in polar wind outflow due to solar illumination. Ann. Geophys., 34, 961-974, doi:10.5194/angeo-34-961-2016.*

***Maes, L.**, Maggiolo, R., De Keyser, J., André, M., Li, K., Eriksson, A. I. , Haaland, S., Solar illumination control of the polar wind.* (in preparation)

Publications (co-author)

*Haaland, S., B. Lybekk, **Maes, L.**, Laundal,K., Pedersen, A., Tenfjord, P., Ohma, A., Østgaard, N., Reistad, J., Snekvik, K. (2017), North-south asymmetries in cold plasma density in the magnetospheric lobes: Cluster observations, Journal of Geophysical Research.*

*Haaland, S., André, M., Eriksson, A., Li, K., Nilsson, H., Baddeley, L., Johnsen, C., **Maes, L.**, Lybekk, B., Pedersen, A. (2016), Low-energy ion outflow observed by Cluster: Utilizing the spacecraft potential. In: C. R. Chappell (ed.) Magnetosphere-Ionosphere Coupling in the Solar System. American Geophysical Union, 33-49.*

*De Keyser, J., **Maes, L.**, Maggiolo, R., S. Haaland (2017), Magnetopause thickness at the dawn and dusk flanks. In: S. Haaland (ed.) Dawn-Dusk*

Asymmetries in Planetary Plasma Environments, American Geophysical Union. (in print)

Haaland, S., H. Hasegawa, De Keyser, J., ***Maes, L.*** *(2017), Dawn-dusk asymmetries at the terrestrial magnetopause: Observations. In: S. Haaland (ed.) Dawn-Dusk Asymmetries in Planetary Plasma Environments, American Geophysical Union.* (in print)

Maggiolo, R., Hamrin, M., Pitkänen, T., Cessateur, G., Gunell, H., ***Maes, L.****, De Keyser, J., The delayed time response of geomagnetic activity to the solar wind, Journal of Geophysical Research.* (submitted)

Maggiolo, R., Fontaine, D., Hosakawa, K., ***Maes, L.****, The connection between small scale polar cap arcs and the Low Latitude Boundary Layer.* (in preparation)

FACULTY OF SCIENCE
DEPARTMENT OF MATHEMATICS
PLASMA ASTROPHYSICS
Celestijnenlaan 200B box 2400
B-3001 Leuven
http://wis.kuleuven.be/CmPA